2009

Hyperfine structure and hyperfine transitions of helium-3

Qixue Wu
University of Windsor

Hyperfine Structure and Hyperfine Transitions of ^{3}He

by
Qixue Wu

A Dissertation
Submitted to the Faculty of Graduate Studies
through the Department of Physics
in Partial Fulfilment of the Requirements for
the Degree of Doctor of Philosophy at the
University of Windsor

Windsor, Ontario, Canada

2009

Your file Votre référence
ISBN: 978-0-494-57573-4
Our file Notre référence
ISBN: 978-0-494-57573-4

Declaration of Previous Publication

I. Declaration of Previous Publication

This thesis references two original papers that have been previously published/submitted for publication in peer reviewed journals, as follows:

Thesis Section	Publication title/full citation	Publication status*
Section 3	*Hyperfine structure in 2P state of helium-3 with and without external magnetic field*	*published*
Section 4.4	*Hyperfine suppression of 2S-3P transitions in he-3*	*published*

This inclusion of the above material is within the bounds of fair dealing within the meaning of the Canada Copying Act. I certify that the above material describes work completed during my registration as graduate student at the University of Windsor.

I declare that, to the best of my knowledge, my thesis does not infringe upon anyone's copyright nor violate any proprietary rights and that any ideas, techniques, quotations, or any other material from the work of other people included in my thesis, published or otherwise, are fully acknowledged in accordance with the standard referencing practices.

I declare that this is a true copy of my thesis, including any final revisions, as approved by my thesis committee and the Graduate Studies office, and that this thesis has not been submitted for a higher degree to any other University of Institution.

Abstract

The hyperfine structure of ^{3}He with an external magnetic field is precisely calculated by using double basis set wave functions. The comparison with available experiments effectively tests the theory of hyperfine structure.

An exact diagonalization provides a comprehensive interpretation of the results across the complete range of hyperfine coupling strengths of ^{3}He. The theoretical investigation shows that suppression of the hyperfine transitions is caused mainly by strong hyperfine mixing and accidental cancellation between two hyperfine states. An IS coupling model can also qualitatively interpret the suppression of the hyperfine transitions. However, this work has shown that the IS model will become more accurate as the hyperfine transitions occur between $2\,^3S_1$ and $n\,^3P_J$ states with higher values of principal quantum number n.

An unexpected result of this work is that even for the low-Z isotope ^{3}He, hyperfine-induced transitions are still important. This originates from strong hyperfine mixing between singlet and triplet states.

for Jenny, Kaiyi, and Leah

Acknowledgements

Without the guidance and expertise of my supervisor Dr. Gordon Drake, this project would not have been completed. For this I express my sincere gratitude.

Thanks go to the Department of Physics at the University of Windsor and Dr. Gordon Drake for their financial support throughout my graduate studies. Thanks also go to four-year Ontario Graduate Scholarship.

I would also like to thank Dr. Tim Reddish, Dr. William Baylis, Dr. Eugene Kim, Dr. Mordechay Schlesinger, Dr. Chitra Rangan, Dr. Brian Atkinson, Dr. Roman Maev, Dr. Elena Mavea, Dr. Wladyslaw Kedzierski for their great help in my graduate studies.

Finally, I wish to thank Zheng Zhong, Atef Suleiman Titi, Houfar Daneshvar Hosseini, Paul Moffatt, Rida El-wazni, Eva Schulhoff, and Mike Busuttil for discussing problems of mutual interest.

Contents

List of Tables

List of Figures

1 Introduction

Helium is the simplest multielectron atom and thus well suited for the study of electron-electron interactions. Moreover, ^{3}He is the simplest three-body system in which all three bodies have spin. Hence, ^{4}He and ^{3}He are excellent testing grounds for the approximation methods of quantum mechanics. Historically, the helium atom has been the subject of considerable experimental and theoretical interest in atomic physics for several reasons. First, because of its simplicity of two electrons only, the helium atom can be solved with very high accuracy in the nonrelativistic limit. For example, the nonrelativistic energy for the ground state of helium has been calculated precisely by Drake *et al.* [7] with the value of -2.903 724 377 034 119 598 311(1) in atomic units. In addition, there is a systematic procedure for calculating the relativistic and higher-order quantum electrodynamics (QED) corrections as perturbations. According to Drake [8], accurate calculations of the Bethe logarithm term in QED are now available and the theoretical energy levels are complete up to and including terms of order α^3 Ry. Second, comparisons between precise theory and experiment provide an important test of the theory of QED and lead to a determination of fundamental physical quantities, such as the fine structure constant α with high accuracy [9, 10]. Finally, a combination of accurate theoretical isotope shift with experimental measurements provides a precise determination of the nuclear charge radius. This provides an especially valuable method for short-lived halo nucleus such as ^{6}He [11] and ^{8}He [12], and opens up a new area of study at the interface between atomic physics and nuclear physics. In astrophysics, ^{4}He is important because it is the second most abundant element in the universe. Its spectrum is prominent whenever the temperature is hot enough to excite the transitions. The rare ^{3}He is also interesting because its spectral lines can be comparable in strength with ^{4}He in certain peculiar stars [13]. However, a comprehensive listing of precise energy levels and transitions of ^{3}He and ^{4}He are not available in the literature until recently, when

Morton, Wu, and Drake [14] published energy levels of the two isotopes , and Drake and Morton [15] published transition rates of ^{4}He for $n = 1$ to 10 and $L = 0$ to 7. It is desirable to supplement the table of transition rates of ^{4}He with those of ^{3}He.

This thesis is divided into six major sections. Section 2 briefly summarizes precise nonrelativistic calculations of atomic energies and relativistic and QED corrections. Section 3 contains the hyperfine structure theory, especially with its application to the hyperfine structure of the 2P state of ^{3}He in an external magnetic field. The resulting Zeeman shift in the hyperfine energy levels causes some of them to cross at particular values of the magnetic field strength. A comparison with experiment provides a sensitive test of the theory. Section 4 presents a study of hyperfine suppression (anomalously weak hyperfine transition) of the 2 ^{3}S$_1$ to 3 ^{3}P$_J$ radiative transition in ^{3}He. The IS coupling model explains qualitatively the recent experimental measurement by Sulai *et al.*[5]. However, the exact diagonalization we propose is able to account for the deviation between the IS coupling model and experiment and leads to an excellent agreement between theory and experiment. Section 5 investigates the hyperfine-induced transition (HFI) for ^{1,3}D to ^{1,3}P, which supplements the study of HFI for high-Z ions in the literature. Section 6 contains results and conclusions. Finally, the extensively calculated electric dipole transitions of all possibilities for 2S to nP and 2P to nD of ^{3}He are compiled in Appendix A, and Appendix B, respectively, which supplements Drake and Morton's work [15]. Appendix C is a general integral needed for this work, and Appendix D contains detailed list of common transition factors $|\langle 2\ ^{1,3}S\|r_1{}^{(1)}+r_2{}^{(1)}\|n\ ^{1,3}P\rangle|^2 (n = 2-10)$ and $|\langle 2\ ^{1,3}P\|r_1{}^{(1)}+r_2{}^{(1)}\|n\ ^{1,3}D\rangle|^2 (n = 3-10)$.

2 Heliumlike Atomic System and Its Description

2.1 Nonrelativistic Description

The Schrödinger equation for two-electron atomic systems is based on the knowledge of all the energy interaction in this system. The Hamiltonian of this work may be defined by

$$H = H_{\rm NR} + H_{\rm Rel} + H_{\rm QED} + H_{\rm hfs} \tag{1}$$

where $H_{\rm NR}$ is the nonrelativistic Hamiltonian, $H_{\rm Rel}$ represents the relativistic correction of lowest order, $H_{\rm QED}$ stands for all higher-order effective relativistic and quantum electrodynamic (QED) corrections, and $H_{\rm hfs}$ is the hyperfine interaction between electrons and nucleus for the case where the nuclear spin is nonzero (hyperfine structure will be discussed in Section 3) .

The approach followed is first to solve the Schrödinger equation to obtain sufficiently accurate wave functions, then treating $H_{\rm Rel}$, $H_{\rm QED}$, $H_{\rm hfs}$ as corrections by means of perturbation theory.

The Schrödinger equation for the heliumlike two-electron atomic system is defined by

$$H_{\rm NR}\psi = E_{\rm NR}\psi, \tag{2}$$

The nonrelativistic Hamiltonian is

$$\begin{aligned} H_{\rm NR} \;=\; & -\frac{\hbar^2}{2M}\nabla_R^2 - \frac{\hbar^2}{2m}\nabla_{R_1}^2 - \frac{\hbar^2}{2m}\nabla_{R_2}^2 - \frac{Ze^2}{|\vec{R}-\vec{R}_1|} - \frac{Ze^2}{|\vec{R}-\vec{R}_2|} \\ & + \frac{e^2}{|\vec{R}_1-\vec{R}_2|} \end{aligned} \tag{3}$$

where $\hbar$ is the Planck constant, e is the electronic charge, $\vec{R}$ is the position vector of the nucleus of mass M, $\vec{R}_1$ and $\vec{R}_2$ are the position vectors of the two electrons with mass m as shown in Figure 1.

Figure 1: Helium atom in fixed-origin coordinate system.

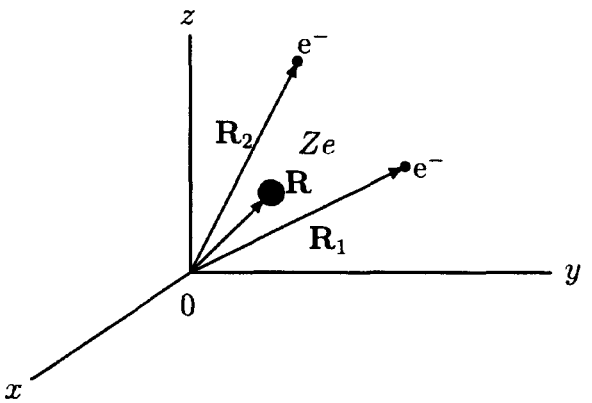

We now make the standard transformation to scaled center-of-mass and relative coordinates defined by

$$\vec{X} = \frac{M\vec{R} + m\vec{R}_1 + m\vec{R}_2}{(M+2m)a_\mu} \tag{4}$$

$$\vec{r_1} = \frac{\vec{R}_1 - \vec{R}}{a_\mu} \tag{5}$$

$$\vec{r_2} = \frac{\vec{R}_2 - \vec{R}}{a_\mu} \tag{6}$$

where $a_\mu = \frac{m}{\mu}a_0$ is the reduced Bohr radius, $\mu = \frac{mM}{m+M}$ is the reduced electron mass, and $a_0 = \frac{\hbar^2}{me^2}$ is the Bohr radius ($4\pi\varepsilon_0 = 1$ through out this thesis). The

Figure 2: Helium atom in center-of-mass coordinate system.

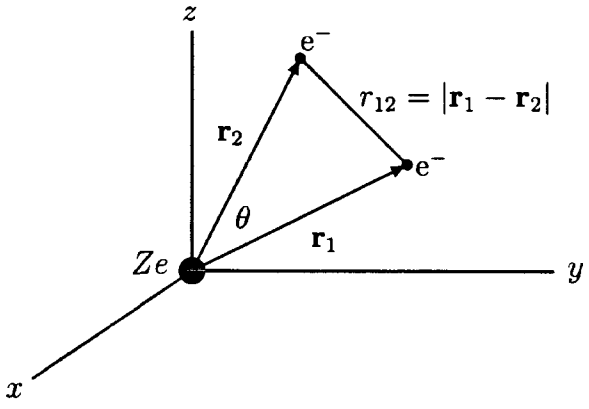

center-of-mass $\vec{X}$ is an ignorable coordinate and the Schrödinger equation reduces to the dimensionless form

$$\left[-\frac{1}{2}\nabla_1^2 - \frac{1}{2}\nabla_2^2 - \frac{\mu}{M}\vec{\nabla}_1 \cdot \vec{\nabla}_2 - \frac{Z}{r_1} - \frac{Z}{r_2} + \frac{1}{r_{12}}\right]\psi(r_1, r_2) = E\psi(r_1, r_2), \tag{7}$$

where $r_{12} = |\vec{r_1} - \vec{r_2}|$, $E_{\mathrm{NR}} = \frac{e^2}{a_\mu}E$ is the nonrelativistic energy. The unit of energy is $\frac{e^2}{a_\mu} = 2R_M$, where $R_M = \frac{\mu}{m}R_\infty$ is the reduced-mass Rydberg, and $\frac{e^2}{a_0} = 2R_\infty$ is the atomic unit of energy. Figure 2 shows the helium atom in the center-of-mass system.

The mass polarization term $-\frac{\mu}{M}\vec{\nabla}_1 \cdot \vec{\nabla}_2$ in Equation (7) produces the state-dependent special isotope shift. If $\frac{\mu}{M} \ll 1$, then this term can be dropped to a first approximation. In this approximation, we obtain the Schrödinger equation for infinite nuclear mass

$$\left[-\frac{1}{2}\nabla_1^2 - \frac{1}{2}\nabla_2^2 - \frac{Z}{r_1} - \frac{Z}{r_2} + \frac{1}{r_{12}}\right]\psi(r_1, r_2) = E\psi(r_1, r_2) \tag{8}$$

In practical calculations, Z-scaled coordinates $\rho = Zr$ are introduced. Equation (8) then becomes

$$\left[-\frac{1}{2}\nabla_{\rho_1}^2 - \frac{1}{2}\nabla_{\rho_2}^2 - \frac{1}{\rho_1} - \frac{1}{\rho_2} + \frac{Z^{-1}}{\rho_{12}}\right]\psi(\rho_1,\rho_2) = E'\psi(\rho_1,\rho_2) \tag{9}$$

where $E = Z^2E'$, and $E_{NR} = Z^2\frac{e^2}{a_\mu}E'$. The advantage is that the Schrödinger equation becomes independent of Z in the limit $Z \to \infty$. Because of the Coulomb interaction term $\frac{Z^{-1}}{\rho_{12}}$ between the two electrons, the exact wave function $\psi(\rho_1,\rho_2)$ cannot be written as a simple product of one-electron functions. The practical calculation is to to find a trial wave function $|\psi\rangle = |\psi_{\rm tr}\rangle$ expressed in terms of linear variational coefficients a_i as

$$|\psi_{\rm tr}\rangle = \sum_{i=1}^{N} a_i|\phi_i\rangle \tag{10}$$

where $|\phi_i\rangle$ denote the members of a basis set, and the linear coefficients are determined by

$$\frac{\partial}{\partial a_i}\frac{\langle\psi_{\rm tr}|H|\psi_{\rm tr}\rangle}{\langle\psi_{\rm tr}|\psi_{\rm tr}\rangle} = 0, \quad i = 1,2,3...N \tag{11}$$

which is equivalent to the matrix equation

$$\tilde{H}\tilde{a} = E\tilde{O}\tilde{a} \tag{12}$$

where $\tilde{H}$ is a matrix with matrix element $H_{ij} = \langle\phi_i|H|\phi_j\rangle$, $\tilde{O}$ is a matrix with matrix element $O_{ij} = \langle\phi_i|\phi_j\rangle$, and $\tilde{a}$ is a column vector with element a_i.

Solving the generalized eigenvalue problem will yield N eigenvalues and corresponding N sets of coefficients a_i, which represents the trial wave function in the chosen basis set. For any approximate wave function, the computed energy is an upper bound to the exact lowest eigenvalue. For excited states, the Hylleraas-Undheim-Macdonald theorem states that the computed energies are also upper

bounds to the corresponding exact eigenenergy [16, 17], provided only the correct number of states lies below. Hylleraas [18] was the first to include r_{12} dependence in the trial wave function for the ground state of helium in the form

$$\psi_{\rm tr}(r_1, r_2, r_{12}) = \sum_{ijk} a_{ijk} r_1^i r_2^j r_{12}^k e^{-\alpha r_1 - \beta r_2} \tag{13}$$

where the a_{ijk} are liner variational coefficients, α and β are nonlinear parameters. The same trial function is often expressed in terms of the equivalent variables

$$s = r_1 + r_2 \qquad t = r_1 - r_2 \qquad u = r_{12}$$

The Hylleraas method has been applied with great success by many authors to the low-lying states of helium and heliumlike ions, especially in the early 1970's, in calculations by Pekeris and co-workers [19]. However, the two problems of linear dependence and loss of accuracy for high-lying states have to be solved. Drake [20] has proposed a new variational approach. This approach relies on including the screened hydrogenic wave function for two electrons in the trial function and doubling the remaining correlated part of the wave function

$$\begin{aligned} \psi_{\rm tr}(r_1, r_2, r_{12}) &= a_0 \psi_0(1s, nl) + \sum_{ijk} [a_{ijk} \chi_{ijk}(\alpha_1, \beta_1) + b_{ijk} \chi_{ijk}(\alpha_2, \beta_2)] \\ &\quad \times Y^M_{l_1, l_2, L}(\vec{r_1}, \vec{r_2}) \pm \text{exchange}, \end{aligned} \tag{14}$$

where $\psi_0(1s, nl)$ denotes the screened hydrogenic wave function defined by

$$\psi_0(1s, nl) = \varphi_{1s}(\vec{r}_1, Z) \varphi_{nl}(\vec{r}_2, Z-1), \tag{15}$$

where $\varphi_{1s}(\vec{r}_1, Z)$ and $\varphi_{nl}(\vec{r}_2, Z-1)$ are hydrogenic wave function for nuclear charge Z and $Z-1$ respectively. $\chi_{ijk}(\alpha, \beta)$ are the correlated basis function of the form

$$\chi_{ijk}(\alpha, \beta) = r_1^i r_2^j r_{12}^k e^{-\alpha r_1 - \beta r_2}, \tag{16}$$

the angular function $Y^M_{l_1,l_2,L}(\vec{r}_1,\vec{r}_2)$ denotes a vector product of solid spherical harmonics for the two electrons to form a state of total angular momentum L

$$Y^M_{l_1 l_2 L}(\vec{r}_1,\vec{r}_2) = r_1^{l_1} r_2^{l_2} \sum_{m_1,m_2} \langle l_1 l_2 m_1 m_2 | LM \rangle Y^{m_1}_{l_1}(\vec{r_1}) Y^{m_2}_{l_2}(\vec{r_2}) \tag{17}$$

The double basis set method includes each combination of powers i, j, k with two different pairs of nonlinear parameters (α_1, β_1) and (α_2, β_2). This has the effect of naturally dividing the basis set into two sectors with quite different distance scales–an asymptotic scale with α_1 and β_1 close to their screened hydrogenic values $\alpha_1 \simeq Z$ and $\beta_1 \simeq (Z-1)/n$, and inner correlation scale with much larger α_2 and β_2. Thus linear dependence is avoided as the two pairs of nonlinear parameters will be sufficiently different. In addition, two different pairs of nonlinear parameters (α_1, β_1) and (α_2, β_2) are optimized completely to make the calculated eigenenergy as low as possible

$$\frac{\partial E}{\partial \alpha_i} = 0, \quad i = 1, 2 \tag{18}$$

$$\frac{\partial E}{\partial \beta_i} = 0, \quad i = 1, 2 \tag{19}$$

This new variational approach has proved to be very successful in improving the precision of calculated energy eigenvalues. For example, Drake, Cassar, and Nistor [7] has calculated the ground state energy of helium with the extrapolated value (in atomic units) of $-2.903\,724\,377\,034\,119\,598\,311(1)$. A detailed list of high precision variational energy eigenvalues for all states of helium up to $n = 10$ and $L = 7$ and their comparison with other calculations can be found in Drake [20, 21].

2.2 Finite Nuclear Mass Correction

As pointed on previously, Equation (7) includes the mass polarization term $-\frac{\mu}{M}\vec{\nabla}_1 \cdot \vec{\nabla}_2$ which was dropped in Equation (8). The correction coming from this mass polarization term can be treated by expanding in powers of $\frac{\mu}{M}$ according to perturbation theory

$$\psi_M = \psi_\infty + \frac{\mu}{M}\psi^{(1)} + \left(\frac{\mu}{M}\right)^2 \psi^{(2)} + \dots \tag{20}$$

$$E_M = E_\infty + \frac{\mu}{M}\varepsilon_M^{(1)} + (\frac{\mu}{M})^2\varepsilon_M^{(2)} + \dots \tag{21}$$

in units of $\frac{e^2}{a_\mu} = 2R_M$, where

$$\varepsilon_M^{(1)} = -\langle\psi(n)_\infty|\vec{\nabla}_1 \cdot \vec{\nabla}_2|\psi(n)_\infty\rangle \tag{22}$$

$$\varepsilon_M^{(2)} = \sum_{l\neq n} \frac{\langle\psi(n)_\infty|\vec{\nabla}_1 \cdot \vec{\nabla}_2|\psi(l)_\infty\rangle\langle\psi(l)_\infty|\vec{\nabla}_1 \cdot \vec{\nabla}_2|\psi(n)_\infty\rangle}{E_n - E_l} \tag{23}$$

and E_∞ and $\psi(n)_\infty$ are the nth solution to the infinite mass problem. Instead of calculating $\varepsilon_M^{(2)}$ directly, the coefficient of the quadratic term can be extracted from two calculations: one for infinite mass energy E_∞ and one for a particular finite mass energy E_M, and subtracting the first order correction $\frac{\mu}{M}\varepsilon_M^{(1)}$ calculated by Equation (22). Then Equation (21) will be used for isotopes with different nuclear mass, for example, ^{3}He, ^{4}He, ^{6}He, and ^{8}He.

2.3 Lowest-Order Relativistic Corrections

Relativistic corrections of the lowest order $O(\alpha^2)$ are calculated with respect to ψ_∞ satisfying the nonrelativistic Schrodinger for infinite nuclear mass (in atomic units)

$$\Delta E_{\rm rel} = \langle \psi_\infty | H_{\rm rel} | \psi_\infty \rangle \tag{24}$$

where $H_{\rm rel} = \sum_{i=1}^{6} B_i$, and $\{B_i\}$ are Breit operators [22]

$$B_1 = -\frac{\alpha^2}{8}(\nabla_1^4 + \nabla_2^4) \tag{25}$$

$$B_2 = \frac{\alpha^2}{2}\left[\frac{1}{r_{12}}\vec{\nabla}_1 \cdot \vec{\nabla}_2 + \frac{1}{r_{12}^3}\vec{r_{12}}(\vec{r_{12}} \cdot \vec{\nabla}_1)\vec{\nabla}_2\right] \tag{26}$$

$$\begin{aligned} B_3 \;=\; & \frac{\alpha^2}{2r_{12}^3}\left[(\vec{r_2} - \vec{r_1}) \times \vec{p_1} \cdot (\vec{s_1} + 2\vec{s_2}) + (\vec{r_1} - \vec{r_2}) \times \vec{p_2} \cdot (\vec{s_2} + 2\vec{s_1})\right] \\ & + \frac{Z\alpha^2}{2}\left[\frac{1}{r_1^3}\vec{r_1} \times \vec{p_1} \cdot \vec{s_1} + \frac{1}{r_2^3}\vec{r_2} \times \vec{p_2} \cdot \vec{s_2}\right] \end{aligned} \tag{27}$$

$$B_4 = \frac{1}{2}\pi\alpha^2 Z\left[\delta(\vec{r_1}) + \delta(\vec{r_2})\right] \tag{28}$$

$$B_5 = \alpha^2\left[\frac{1}{r_{12}^3}\vec{s_1} \cdot \vec{s_2} - \frac{3}{r_{12}^5}(\vec{s_1} \cdot \vec{r_{12}})(\vec{s_2} \cdot \vec{r_{12}})\right] \tag{29}$$

$$B_6 = -\frac{8}{3}\pi\alpha^2\delta(\vec{r_{12}})\vec{s_1} \cdot \vec{s_2} \tag{30}$$

where B_1 is the relativistic correction due to the variation of mass with velocity. B_2 corresponds to the classical relativistic orbit-orbit interaction between the electrons. B_3 describes the spin-orbit interaction and spin-other-orbit interaction between the two electrons. B_4 represents the contact terms. B_5 represents the interaction between the spin magnetic dipole moments of the two electrons. B_6 stands for the spin-spin contact term which accounts for the interaction of the spin magnetic moments of two electrons.

2.4 Relativistic Reduced Mass and Recoil Corrections

The relativistic reduced mass correction comes from the reduced mass scaling of the above B_i terms upon the replacement $r \to \frac{m}{\mu} r$ together with additional terms $\triangle_2$ and $\triangle_3$, generated by the transformation of the Breit interaction to center-of-mass and relative coordinates [23, 24].

$$\langle \triangle E_{RR} \rangle_M = \sum_{i=1}^{6} \langle B_i^M \rangle \tag{31}$$

in units of $\frac{e^2}{a_\mu}$, where

$$B_1^M = -3\frac{\mu}{M} B_1 \tag{32}$$

$$B_2^M = -2\frac{\mu}{M} B_2 + \triangle_2 \tag{33}$$

$$B_3^M = -2\frac{\mu}{M} B_{3e} + \triangle_3 \tag{34}$$

$$B_{3e} = \frac{\alpha^2}{2r_{12}^3} \left[(\vec{r_2} - \vec{r_1}) \times \vec{p_1} \cdot (\vec{s_1} + 2\vec{s_2}) + (\vec{r_1} - \vec{r_2}) \times \vec{p_2} \cdot (\vec{s_2} + 2\vec{s_1}) \right] \tag{35}$$

$$B_i^M = -2\frac{\mu}{M} B_i, \quad i = 4, 5, 6 \tag{36}$$

$$\begin{aligned} \triangle_2 \;=\; & \frac{1}{2} Z\alpha^2 \frac{\mu}{M} \sum_{j=1}^{2} \left\{ \frac{1}{r_j^3} \vec{r_j} \cdot \left[\vec{r_j} \cdot (\vec{\nabla}_1 + \vec{\nabla}_2) \vec{\nabla}_j \right] \right\} \\ & + \frac{1}{2} Z\alpha^2 \frac{\mu}{M} \sum_{j=1}^{2} \left\{ \frac{1}{r_j} (\vec{\nabla}_1 + \vec{\nabla}_2) \cdot \vec{\nabla}_j \right\} \end{aligned} \tag{37}$$

$$\triangle_3 = Z\alpha^2 \frac{\mu}{M} \left[\frac{1}{r_1^3} \vec{r_1} \times \vec{p_2} \cdot \vec{s_1} + \frac{1}{r_2^3} \vec{r_2} \times \vec{p_1} \cdot \vec{s_2} \right] \tag{38}$$

The recoil correction arises from second-order cross terms between the B_i and the mass polarization operator $-\frac{\mu}{M}\nabla \cdot \nabla$ denoted by

$$\langle \triangle E_{RR} \rangle_X = \sum_{i=1}^{6} \langle B_i^X \rangle \tag{39}$$

where

$$\langle B_i^X \rangle = -2\frac{\mu}{M} \sum_{k \neq n} \frac{\langle \psi_\infty^{(n)} | \vec{\nabla}_1 \cdot \vec{\nabla}_2 | \psi_\infty^{(k)} \rangle \langle \psi_\infty^{(k)} | B_i | \psi_\infty^{(n)} \rangle}{E_n - E_k} \tag{40}$$

2.5 Spin-Dependent Anomalous Magnetic Moment Corrections

The spin-dependent parts of the anomalous magnetic moment correction to B_i can be included by replacing each spin factor s_i by $\frac{1}{2} g_i s_i$, where $g_i \simeq 2(1 + \frac{\alpha}{2\pi})$. The result is expressed as

$$\langle \triangle E_{\text{anom}} \rangle = \langle B_3^A \rangle + \langle B_5^A \rangle + \langle B_6^A \rangle \tag{41}$$

where

$$B_3^A = \frac{\alpha}{2\pi} B_3 \tag{42}$$

$$B_5^A = \frac{\alpha}{2\pi} B_5 \tag{43}$$

$$B_6^A = \frac{\alpha}{\pi} B_6 \tag{44}$$

2.6 Quantum Electrodynamics Corrections

Two kinds of QED corrections are considered, which are the electron-nucleus correction and the electron-electron correction.

2.6.1 Electron-Nucleus QED Correction

As derived by Kabir and Salpeter [25], the general form of the electron-nucleus part denoted as $\triangle E_{L,1}$ for helium is simply obtained from the corresponding hydrogenic case by inserting the correct electron density at the nucleus in place of the hydrogenic quantity $\delta(\vec{r}) = \frac{Z^3}{(\pi n^3)}$, and the correct two-electron value of the Bethe logarithm. The lowest-order QED shift is

$$\triangle E_{L,1} = \frac{4\alpha^3 Z}{3}\langle\delta(\vec{r_1}) + \delta(\vec{r_2})\rangle\left[\ln(Z\alpha^2)^{-2} + 19/30 - \beta(1snl)\right], \tag{45}$$

where $\beta(nls)$ is the two-electron Bethe logarithm term defined by

$$\beta(1snl) = \frac{\sum_{i\neq 0}|\langle\psi_\infty^{(0)}|\vec{p_1} + \vec{p_2}|\psi^{(i)}\rangle|^2(E_i - E_0)\ln|\mathrm{E_i} - \mathrm{E_0}|}{\sum_{i\neq 0}|\langle\psi_\infty^{(0)}|\vec{p_1} + \vec{p_2}|\psi^{(i)}\rangle|^2(E_i - E_0)} \tag{46}$$

2.6.2 Electron-Electron QED Correction

Araki and Sucher [26] derived the electron-electron QED shift as

$$\triangle E_{L,2} = \alpha^3\left[\frac{14}{3}\ln(\alpha) + \frac{164}{15}\right]\langle\delta(\vec{r_{12}})\rangle - \frac{14}{3}\alpha^3 Q, \tag{47}$$

where

$$Q = \frac{1}{4\pi} \lim_{\varepsilon \to 0} \langle r_{12}^{-3}(\varepsilon) + 4\pi(\gamma + \ln(\varepsilon))\delta(\mathrm{r}_{12}) \rangle \tag{48}$$

γ is Euler's constant, and ε is the radius of a sphere centered about r_{12} that is excluded from the range of integration.

2.7 Correction Due to Finite Nuclear Size

The lowest-order correction due to finite nuclear size is

$$\triangle E_{\mathrm{nuc}} = \frac{2\pi Z}{3} \left(\frac{R}{a_0} \right)^2 \langle \delta(\vec{r_1}) + \delta(\vec{r_2}) \rangle, \tag{49}$$

where R is the root-mean-square (rms) radius of the nuclear charge distribution and a_0 is the Bohr radius. This equation is very important in determining the rms nuclear radius of ^{3}He [27] , ^{6}He [28], and ^{8}He [29], experimentally by the atomic isotope shift method.

2.8 Total Energy

Accounting for the relativistic corrections and QED corrections, the total energy for state $^{2S+1}L_J$ may be expressed as

$$\begin{aligned} E_{\mathrm{tot}} \;=\; & E_{\mathrm{NR}} + \triangle E_M^{(1)} + \triangle E_M^{(2)} + \triangle E_{\mathrm{rel}} + (\triangle E_{RR})_M + (\triangle E_{RR})_X + \\ & \triangle E_{\mathrm{anom}} + \triangle E_{L,1} + \triangle E_{L,2} + \triangle E_{\mathrm{nuc}} + \triangle E_{\mathrm{ST}}, \end{aligned} \tag{50}$$

where

$$\triangle E_M^{(1)} = -\frac{\mu}{M} \varepsilon_M^{(1)} \tag{51}$$

$$\triangle E_M^{(2)} = (\frac{\mu}{M})^2 \varepsilon_M^{(2)}. \tag{52}$$

$\triangle E_{\rm ST}$ is due to the singlet-triplet mixing caused by the spin-dependent Breit operators, the anomalous magnetic moment, and finite mass corrections providing off-diagonal singlet-triplet coupling terms. It is the difference between the energies of state $n\,^1L_J$ before diagonalization and after diagonalization of the Hamiltonian matrix in the two-dimensional basis sets of LS-coupled states with the same n, L, and J. Other terms have been described previously.

3 Hyperfine Structure of the $2\,^3P$ State of ^3He with External Magnetic Field

The Zeeman effect, the study of the behavior of atoms in the presence of a magnetic field, is a long and well established branch of spectroscopy. If the theory of the Zeeman effect is sufficiently well understood, then it can be used to extrapolate precise measurements for the fine structure or the hyperfine structure in the presence of magnetic fields to zero-field strength. Experimentally, level-crossing has been used to investigate the fine structure and the hyperfine structure of the excited states of atoms, such as ^4He [31, 32, 33, 34], and ^3He [2, 35, 36, 37]. As a two-electron atomic system, helium has been the object of extensive investigation for many years. ^3He, one of the isotopes of helium, has hyperfine structure because of its nonzero nuclear spin ($I = 1/2$). The splitting of the hyperfine structure levels of ^3He with and without an applied magnetic field has been studied in many theoretical and experimental works [1, 3, 14, 38, 39, 40, 41, 42, 43]. This section summarizes the general description of the hyperfine structure of $2\,^3P$ state of ^3He. The hyperfine structure in the $2\,^3P$ state of ^3He with an external magnetic field is presented. The high precision values of field strengths where magnetic sublevels cross are predicted. The crossings are compared with available experimental data.

3.1 Hyperfine Structure $2\,^3P$ State of ^3He

The total Hamiltonian in the absence of external fields is

$$H = H_{\rm NR} + H_{\rm Rel} + H_{\rm QED} + H_{\rm hfs} \tag{53}$$

where each term in the above equation has the same significance as in Section 2. The spin-dependent operators in $H_{\rm Rel}$ and $H_{\rm QED}$ are responsible for the fine structure for helium as described by many authors (see Drake [23, 24] for a review).

Following the notation of Hinds, Prestage and Pichanick [39], the fine structure parameters needed to diagonalize the total Hamiltonian matrix in the finite subset of states were previously calculated by Morton, Wu and Drake [14] and listed in the Table 1. In this work, instead of using directly the theoretical fine structure energies for ^{3}He, we combined the theoretical isotope shifts for ^{3}He relative to ^{4}He with the best experimental ionization energies for ^{4}He, as recently measured by, for example, Zelevinsky *et al.* [44]. This gives higher accuracy because, due to cancellations of the mass-independent QED uncertainties, the calculated isotope shifts are considerably more accurate than the total ionization energies. This higher accuracy (better than ± 100 kHz in the isotope shift) has been used to deduce nuclear charge radii for light isotopes and halo nuclei [20, 45, 46, 47, 27]. $H_{\rm hfs}$, the hyperfine interaction term coming from the magnetic interaction between electrons and the nuclear spin for ^{3}He, leads to each fine structure energy level being split into several sublevels with total quantum numbers from $F = |J - I|$ to $F = J + I$. Since the interaction for the higher-order multipoles (such as magnetic octupole) vanish for $I = 1/2$, we need only consider the magnetic dipole contribution. According to Bethe and Salpeter [22], the magnetic dipole hyperfine interaction for a two-electron atomic system can be written as

$$H_{\rm hfs} = -2\mu_0 \sum_{i=1}^{2} \left\{ \frac{-8\pi}{3}(\vec{s}_i \cdot \vec{\mu})\delta(\vec{r}_i) - \frac{1}{r_i^3}(\vec{l}_i \cdot \vec{\mu}) + \frac{1}{r_i^3}\left[(\vec{s}_i \cdot \vec{\mu}) - \frac{3}{r_i^2}(\vec{s}_i \cdot \vec{r}_i)(\vec{\mu} \cdot \vec{r}_i)\right] \right\} \tag{54}$$

where $\vec{\mu} = -\mu_0 g_I \vec{I}$ is the nuclear magnetic moment, $\mu_0 = 13.996\,246\,04(35) \times 10^3$MHz/T (CODATA 2006 adjustment values) the Bohr magneton, $g_I = 2.317\,4824(7) \times 10^{-3}$ the nuclear g factor for ^{3}He [39], and $\vec{r}_i$, $\vec{s}_i$, $\vec{l}_i$ the position vector, spin and orbital angular momentum of the ith electron, respectively.

Hyperfine structure can be treated as a small perturbation relative to the large electrostatic splitting between states with different principal quantum number n, but it cannot be treated as a small perturbation relative to the fine structure splitting since the hyperfine splittings are in fact comparable in size to the fine structure splittings. The principle of the calculation is to carry out an exact diagonalization of the fine and hyperfine interaction matrix together within each manifold of states with the same n. The most important interactions are within the manifold of fine structure states with the same L, S, and F, but different J; but there are also significant off-diagonal mixings between singlet and triplet states.

With the definitions

$$W^{I,F}_{J,J'}(1) = (-1)^{J+I+F}[(2J+1)(2J'+1)]^{1/2}\frac{\left\{\begin{array}{ccc} F & I & J' \\ 1 & J & I \end{array}\right\}}{\left(\begin{array}{ccc} I & 1 & I \\ -I & 0 & I \end{array}\right)} \tag{55}$$

$$X_{S,S'} = -[(2S+1)(2S'+1)]^{1/2}\left\{\begin{array}{ccc} 1/2 & S' & 1/2 \\ S & 1/2 & 1 \end{array}\right\} \tag{56}$$

then the hyperfine interaction matrix element in the coupled representation $|LSJIF\rangle$ is expressed as

$$\langle LS'J'IF|H_{\rm hfs}|LSJIF\rangle = W^{I,F}_{J,J'}(1)I\Bigg[\, C_{S',S}\sqrt{6}(-1)^{L+J'}X_{S,S'}\begin{Bmatrix} S' & J' & L \\ J & S & 1 \end{Bmatrix}$$
$$- D_S\delta_{S,S'}(-1)^{J+S+M}\begin{Bmatrix} L & J' & S \\ J & L & 1 \end{Bmatrix}\Bigg/\begin{pmatrix} L & 1 & L \\ -M & 0 & M \end{pmatrix}$$
$$+E_{S',S}\frac{12}{\sqrt{5}}(-1)^{S'-L+M}X_{S,S'}\begin{Bmatrix} L & L & 2 \\ S' & S & 1 \\ J' & J & 1 \end{Bmatrix}\Bigg/\begin{pmatrix} L & 2 & L \\ -M & 0 & M \end{pmatrix}\Bigg] \tag{57}$$

The three hyperfine structure parameters [39, 40], extended to include off-diagonal matrix elements, are defined by

$$C_{S',S} = -\frac{8\pi}{3}g_I\mu_0^2\langle\, {}^{2S'+1}LM \mid \delta(\vec{r}_1) + (-1)^{S'-S}\delta(\vec{r}_2) \mid {}^{2S+1}LM\rangle \tag{58}$$

$$D_S = -2g_I\mu_0^2\langle\, {}^{2S+1}LM \mid l_{1,z}r_1^{-3} + l_{2,z}r_2^{-3} \mid {}^{2S+1}LM\rangle \tag{59}$$

$$E_{S',S} = -\frac{5}{2}g_I\mu_0^2\langle\, {}^{2S'+1}LM \mid (-1)^{S'-S}C_2^0(\hat{\vec{r}}_1)r_1^{-3} + C_2^0(\hat{\vec{r}}_2)r_2^{-3} \mid {}^{2S+1}LM\rangle \tag{60}$$

evaluated with $M = L$ throughout Eqs. (57– 60). Here, $C_2^0(\hat{r}) = \sqrt{4\pi/5}\,Y_2^0(\hat{r})$, and the conversion factor from atomic units to MHz is $g_I\mu_0^2 = 202.998\,180(61)$ MHz [14].

High precision values for all the hyperfine structure parameters in Equations (58) to (60) can be calculated by using the double basis set wave functions in Hylleraas co-ordinates with and without the mass polarization correction. The details are described in full by Drake [20, 21]. Thus the linear mass polarization coefficient $\delta_{\rm MP}$ can be deduced and applied to any helium isotope. The final expression, including the linear mass polarization $\delta_{\rm MP}$, reduced mass correction and higher

order relativistic, QED, and finite nuclear size corrections are [48]

$$C_{S',S} = C^{(0)}_{S',S}[1 + (\delta^C_{\rm MP} - 3)\mu/M + \alpha/2\pi + \delta^C_{\rm ho}] \quad (61)$$

$$D_S = D^{(0)}_S[1 + (\delta^D_{\rm MP} - 3)\mu/M + \delta^D_{\rm ho}] \quad (62)$$

$$E_{S',S} = E^{(0)}_{S',S}[1 + (\delta^E_{\rm MP} - 3)\mu/M + \alpha/2\pi + \delta^E_{\rm ho}] \quad (63)$$

where the ratio of reduced mass to nuclear mass (from CODATA 2006 adjustment values) is $\mu/M = 1.819\,212\,062(2) \times 10^{-4}$, and the fine structure constant $\alpha = 7.297\,352\,537\,6(50) \times 10^{-3}$. In order to achieve higher accuracy for the hyperfine structure, it is necessary to estimate $\delta^C_{\rm ho}$ in Equation (61) for the dominant Fermi contact term C_{11}. As suggested by Hambro [40], Hinds [39], and the detailed comparison in Table V of Riis *et al.* [48], we assume $\delta^C_{\rm ho} = 0.000\,507(4)$ for the 2 P states with the uncertainty of 0.000 004 being the difference of $\delta^C_{\rm ho}$ between He($1s2s$) and He$^+$($1s$). The calculated values for all hyperfine structure parameters are listed in Table 1 as well.

Finally, once the fine structure parameters and the hyperfine structure parameters are available, the hyperfine energy structure can be obtained by diagonalizing the complete 11×11 matrix of the Hamiltonian operator in the coupled representation $|LSJIF\rangle$. Since the Hamiltonian in Equation (53) is rotationally invariant, the dependence on the associated magnetic quantum number M_F can be dropped. Table 2 tabulates our hyperfine splittings in the 2 ^{3}P state of ^{3}He, and compares them with other theoretical works. The comparison shows that our results are in good agreement with other calculations, but with higher accuracy.

Table 1: Δ, E_0, and E_1 are the $2\,^1P_1$–$2\,^3P_2$, $2\,^3P_0$–$2\,^3P_2$ and $2\,^3P_1$–$2\,^3P_2$ energy level separation, respectively. E_M, is the off-diagonal matrix element being used by Morton, Wu, and Drake [14]. Δ' and E_1' are the corresponding quantities before diagonalization. $C_{S,S'}$, D_S, and $E_{S,S'}$ are the hyperfine structure parameters. The uncertainty of $C_{1,1}$ comes from $\delta_{\rm ho}^C$. Units are MHz.

Fine structure parameters		Hyperfine structure parameters	
Δ	614 312 86.5(2) [14]	C_{11}	−4283.850(15)
Δ'	614 312 81.8(2)	C_{10}	−4285.830
E_0	31908.83978(94)	D_1	−28.145
E_1	2292.16359(51)	D_0	−15.547
E_1'	2296.91553(51)	E_{11}	7.126
E_2	0.	E_{10}	5.597
E_M	−17085.289		

Table 2: The hyperfine splitting of 2 ^{3}P state of ^{3}He . The quoted errors of the calculated quantities in the present work reflect the contribution from $\delta^c_{\rm ho}$. Units are MHz.

Hyperfine splitting				
$(J,F)-(J',F')$	Present work	Other theory		
$(0,1/2)-(2,3/2)$	27 424.837(12)	27 426[a]	27 424.8[b]	27 413.5(1.0)[c]
$(2,3/2)-(1,1/2)$	668.033(9)	668[a]	668.0[b]	668.2(1.0)[c]
$(1,1/2)-(1,3/2)$	4512.191(12)	4510[a]	4512.2[b]	4512.2(1.0)[c]
$(1,3/2)-(2,5/2)$	1780.880(1)	1780[a]	1780.9[b]	1781.0(1.0)[c]

[a]Johnson *et al.* [43]
[b]Hinds *et al.* [39]
[c]Hijikata and Ohtsuki [42]

3.2 Hyperfine Structure With External Magnetic Field

The total Hamiltonian of the ^{3}He atom in an applied magnetic field is

$$H = H_{\rm NR} + H_{\rm Rel} + H_{\rm QED} + H_{\rm hfs} + H_{\rm Z}, \tag{64}$$

where each term in Equation (64) has the same significance as before, except for the Zeeman term $H_{\rm Z}$ representing the interaction between the atom (electrons and nuclear spin) with external magnetic field.

In order to obtain Zeeman sublevels with higher accuracy, we follow the formalism of Yan and Drake [49, 51], in which the Zeeman interaction (between electrons and magnetic field) includes the linear terms, diamagnetic terms, and α^2 relativistic correction terms. The general form of the Zeeman interaction between the atom and magnetic field was derived from the Breit interaction by Perl and Hughes [52], later by Lewis, Pichanick and Hughes [53] and by Lewis and Hughes [54]. In Ref. [49], Yan and Drake published a detailed description of the evaluation of the various terms using their double basis set variational technique for the states of $2\,^3{\rm P}_J$, $2\,^1{\rm P}_1$, $2\,^3{\rm S}_1$, $3\,^3{\rm P}_J$ of ^{4}He. All the matrix elements corrected to order α^2 in their work are considered to be very precise and were cited by many authors such as Zelevinsky *et al.* [44] and Courtade *et al.* [41].

The total Zeeman Hamiltonian (electrons and nuclear spin included) can be expressed as

$$H_{\rm Z} = \sum_{i=0}^{7} H_i, \tag{65}$$

where

$$H_0 = \mu_B \vec{B} \cdot (g_L \vec{L} + g_S \vec{S}) \tag{66}$$

$$H_1 = -\frac{1}{2}\alpha^2\mu_B\vec{B}\cdot\sum_j \nabla_j^2(i\vec{r}_j\times\nabla_j) + \alpha^2\mu_B\vec{B}\cdot\sum_j \vec{s}_j\nabla_j^2 \tag{67}$$

$$H_2 = \frac{Z}{2}\alpha^2\mu_B\vec{B}\cdot\sum_j[\frac{2\vec{s}_j}{3r_j} + \frac{1}{3r_j}(\vec{s}_j - \frac{3\vec{r}_j(\vec{r}_j\cdot\vec{s}_j)}{r_j^2})] \tag{68}$$

$$H_3 = \frac{1}{2}\alpha^2\mu_B\vec{B}\cdot\sum_{j\neq k}\frac{1}{r_{jk}^3}[(\vec{s}_j + 2\vec{s}_k)\times\vec{r}_{jk}]\times\vec{r}_j \tag{69}$$

$$\begin{aligned} H_4 \;=\; & \frac{1}{2}\alpha^2\mu_B\vec{B}\cdot\sum_{k>j}\left[\frac{i}{r_{jk}}(\vec{r}_j\times\nabla_k + \vec{r}_k\times\nabla_j)\right] - \\ & \frac{1}{2}\alpha^2\mu_B\vec{B}\cdot\sum_{k>j}\left[\frac{i}{r_{jk}}(\vec{r}_j\times\vec{r}_k)\vec{r}_{jk}\times(\nabla_j + \nabla_k)\right] \end{aligned} \tag{70}$$

$$H_5 = \frac{m}{M}\mu_B\vec{B}\cdot\sum_{j\neq k}(i\vec{r}_j\times\nabla_k) \tag{71}$$

$$H_6 = \frac{1}{3}(\mu_B B_Z)^2\sum_j r_j^2[1 - C_2^0(\hat{r}_j)] \tag{72}$$

$$H_7 = -\mu_B g_I(\vec{B}\cdot\vec{I}) \tag{73}$$

Using standard angular momentum theory, the matrix element of H_Z in the coupled representation $|LSJIFM_F\rangle$ can be written in the form

$$\langle LSJ'IF'M_F'|H_Z|LSJIFM_F\rangle = H_Z(1) + H_Z(2) + H_Z(3) + H_Z(4), \tag{74}$$

where

$$H_Z(1) = (-1)^{F'+F+I-M_F+J'}[6(2F'+1)(2F+1)(2J'+1)(2J+1)]^{1/2}$$
$$\left[(-1)^{J+L+S} g'_L \left\{ \begin{array}{ccc} L & J' & S \\ J & L & 1 \end{array} \right\} + (-1)^{L+S-J'} g'_S \left\{ \begin{array}{ccc} J & J' & 1 \\ S & S & L \end{array} \right\} \right.$$
$$\left. + g_x \left\{ \begin{array}{ccc} L & L & 2 \\ S' & S & 1 \\ J' & J & 1 \end{array} \right\} \right] \left(\begin{array}{ccc} F' & 1 & F \\ -M_F & 0 & M_F \end{array} \right)$$
$$\left\{ \begin{array}{ccc} J' & F' & I \\ F & J & 1 \end{array} \right\} \delta_{M_{F'},M_F}(\mu_0 B) \tag{75}$$

$$H_Z(2) = (-1)^{2F+I-M_F+2J+L+S}[(2F+1)(2J+1)] \left(\begin{array}{ccc} F & 0 & F \\ -M_F & 0 & M_F \end{array} \right)$$
$$\left\{ \begin{array}{ccc} J & F & I \\ F & J & 0 \end{array} \right\} \left\{ \begin{array}{ccc} L & J & S \\ J & L & 0 \end{array} \right\} \delta_{F',F}\delta_{M_{F'},M_F}$$
$$\delta_{J',J} \frac{(\mu_0 B)^2}{3} \frac{g_{Q_1}}{R_\infty} \tag{76}$$

$$H_Z(3) = (-1)^{F'+F+I-M_F+J+J'+L+S+1} \left(\begin{array}{ccc} F' & 2 & F \\ -M_F & 0 & M_F \end{array} \right)$$
$$\left\{ \begin{array}{ccc} J' & F' & I \\ F & J & 2 \end{array} \right\} [(2F'+1)(2F+1)(2J'+1)(2J+1)]^{\frac{1}{2}}$$
$$\left\{ \begin{array}{ccc} L & J' & S \\ J & L & 2 \end{array} \right\} \delta_{M_{F'},M_F} \frac{(\mu_0 B)^2}{3} \frac{g_{Q_2}}{R_\infty} \tag{77}$$

$$H_Z(4) = (-1)^{2F'-M_F+I+J}[(2F'+1)(2F+1)(2I+1)(I+1)I]^{\frac{1}{2}}$$
$$\left(\begin{array}{ccc} F' & 1 & F \\ -M_F & 0 & M_F \end{array} \right) \left\{ \begin{array}{ccc} I & F' & J \\ F & I & 1 \end{array} \right\} \delta_{M_{F'},M_F}\delta_{J',J}(\mu_0 B) g_I, \tag{78}$$

where B is the external magnetic field strength, and $R_\infty = 3.289\,841\,960\,360(22) \times 10^9$(MHz) is the Rydberg constant. The physical origin of these terms is as follows. The linear term $H_Z(1)$ consists of the lowest-order Zeeman effect (g_L and g_S term), the correction for the motion of the center of mass (m/M term), and the relativistic corrections (α^2 term). $H_Z(2)$ and $H_Z(3)$ arise from the scalar quantity $\frac{1}{3}(\mu_0 B)^2 \sum_{i=1}^{2} r_i^2[1 - C_2^0(\hat{r}_i)]$ due to the diamagnetic magnetic field effect. The last term $H_Z(4)$ represents the linear interaction between the nuclear spin and the

external magnetic field. The various g factors are defined as

$$g'_L = \sqrt{\frac{(2L+1)L(L+1)}{6}} g_L + \frac{2}{\sqrt{6}} \frac{m}{M} F_1 + \frac{\alpha^2}{\sqrt{6}} (F_2 + F_3 - F_4) \tag{79}$$

$$\begin{aligned} g'_S &= \sqrt{\frac{(2S+1)S(S+1)}{6}} g_S + \alpha^2 (-1) \frac{(2S+1)}{\sqrt{2L+1}} \left\{ \begin{array}{ccc} 1/2 & S & 1/2 \\ S & 1/2 & 1 \end{array} \right\} \\ &\quad \times \left(F_5 + \frac{Z}{3} F_6 - \frac{1}{2} F_7 \right) \end{aligned} \tag{80}$$

$$g_x = \alpha^2 (-1)^S (2S+1) \left\{ \begin{array}{ccc} 1/2 & S & 1/2 \\ S & 1/2 & 1 \end{array} \right\} \sqrt{\frac{5}{6}} \left(-Z F_8 + \frac{3}{2} F_9 \right) \tag{81}$$

with [55, 56]

$$g_{Q_1} = F_{10} \tag{82}$$

$$g_{Q_2} = F_{11} \tag{83}$$

$$g_L = 1 - \frac{m}{M} \tag{84}$$

$$g_s = 2 \left[1 + \frac{\alpha}{2\pi} - 0.328\,478\,965 \left(\frac{\alpha}{\pi} \right)^2 + 1.176\,11 \left(\frac{\alpha}{\pi} \right)^3 + \cdots \right] \tag{85}$$

$m/M = 1.819\,543\,075(2) \times 10^{-4}$ is the ratio of the electron mass to the nuclear mass for ^{3}He, α is the fine structure constant as previously, $F_i (i = 1-11)$ represent the deduced matrix elements defined as follows, and $Z = 2$ is the atomic number of helium.

By the Wigner-Eckart theorem, the relation between the matrix element and the reduced matrix element is

$$\langle LM | O^k_q | L'M' \rangle = (-1)^{L-M} \left(\begin{array}{ccc} L & k & L' \\ -M & q & M' \end{array} \right) \langle L \| O^k \| L' \rangle \tag{86}$$

where O_q^k is a spherical tensor operator. All the reduced matrix elements are to be calculated with respect to the nonrelativistic wave function of helium.

$$F_1 =< L\|i(\vec{r}_1 \times \nabla_2)\|L > \tag{87}$$

$$F_2 =< L\|i\frac{1}{r_{12}}(\vec{r}_1 \times \nabla_2)\|L > \tag{88}$$

$$F_3 =< L\| - i\nabla_1^2(\vec{r}_1 \times \nabla_1)\|L > \tag{89}$$

$$F_4 =< L\|i\frac{1}{r_{12}^3}(\vec{r}_1 \times \vec{r}_2)(\vec{r}_{12} \cdot \nabla_2)\|L > \tag{90}$$

$$F_5 =< L\|\nabla_1^2\|L > \tag{91}$$

$$F_6 =< L\|\frac{1}{r_1}\|L > \tag{92}$$

$$F_7 =< L\|\frac{1}{r_{12}}\|L > \tag{93}$$

$$F_8 =< L\|\frac{1}{r_1}C_2(r_1)\|L > \tag{94}$$

$$F_9 =< L\|\frac{1}{r_{12}}C_2(r_{12})\|L > \tag{95}$$

$$F_{10} =< L\|r_1^2\|L > \tag{96}$$

$$F_{11} =< L\|r_1^2C_2(r_1)\|L > \tag{97}$$

All the matrix elements F_i in Equations (87) to (97) for ^{3}He can be directly derived from those of ^{4}He by means of the following expansion, for each F_i of ^{4}He is available from the work of Yan and Drake [49]

$$< F_i >= \left(\frac{m}{\mu}\right)^n \left[\langle F_i^{\infty}\rangle + \delta^i_{\rm MP}\left(\frac{\mu}{M}\right)\right], \tag{98}$$

where $\langle F_i\rangle$ represents the matrix element for the finite nuclear mass case (including mass polarization via the $\delta^i_{\rm MP}$ term), and F_i^{∞} is the matrix element for infinite nuclear mass. Also, n is the degree of homogeneity with respect to r for each operator. For example, $n = 1$ for F_6.

The derived values of F_i for the 2 ^{3}P and 2 ^{1}P states of ^{3}He are tabulated in Table 3. All reduced g values are summarized in Table 4.

Table 3: The derived matrix element F_i in 2P state of ^{3}He. Units are atomic units.

Term	$2\,^3P_J$	$2\,^1P_1$
F_1	0.157 572 048(12)	−0.079 995 675 82(29)
F_2	0.064 728 895 998 8(61)	−0.047 076 820 946(16)
F_3	−0.385 681 226 510 79(95)	−0.295 614 066 179 7(12)
F_4	−0.003 064 538 914 974(73)	0.018 276 650 484 6(12)
F_5	−3.693 445 280 159 661(98)	
F_6	1.962 501 026 331 505(35)	
F_7	0.461 810 189 574 096(48)	
F_8	−0.153 716 797 823(19)	
F_9	−0.287 899 246 328 34(58)	
F_{10}	22.887 028 979 21(20)	27.321 297 504 07(84)
F_{11}	−14.057 589 603 46(12)	−16.863 541 757 87(54)

Table 4: Derived g factors in the 2P states. Units are atomic units.

Term	Derived value ($2\,^1$P)	Derived value ($2\,^3$P)
$10^6\delta g_L$	−19.731 916 04(6)	16.498 893 49(45)
$10^6\delta g_S$		−80.428 595 9(6)
$10^6 g_x$		−5.391 770 42(4)
g_{Q_1}	27.321 297 504 07(84)	22.887 028 979 21(20)
g_{Q_2}	−16.863 541 757 87(54)	−14.057 589 603 46(12)
g'_L	0.999 798 313 776 14(7)	0.999 834 544 585 67(5)
g'_S		2.002 238 875 776(8)

Using the tabulated values for the parameters and matrix elements, the energies of Zeeman sublevels of the hyperfine structure of ^{3}He are then obtained as a function of the applied magnetic field strength by diagonalizing the complete 24×24 matrix of the Hamiltonian in the coupled representation $|LSJIFM_F\rangle$, including all basis states of a given L, n, and spin multiplicity. Figures 3 and Figure 4 illustrate the behavior of the $2\,^3$P state as the magnetic field strength is varied from 0 to 10 000 gauss, where each sublevel is labeled by the three quantum numbers J, F, M_F.

Figure 3: Zeeman sublevel of hyperfine 2 ^{3}P state of ^{3}He with magnetic field strength up to 2000 gauss.

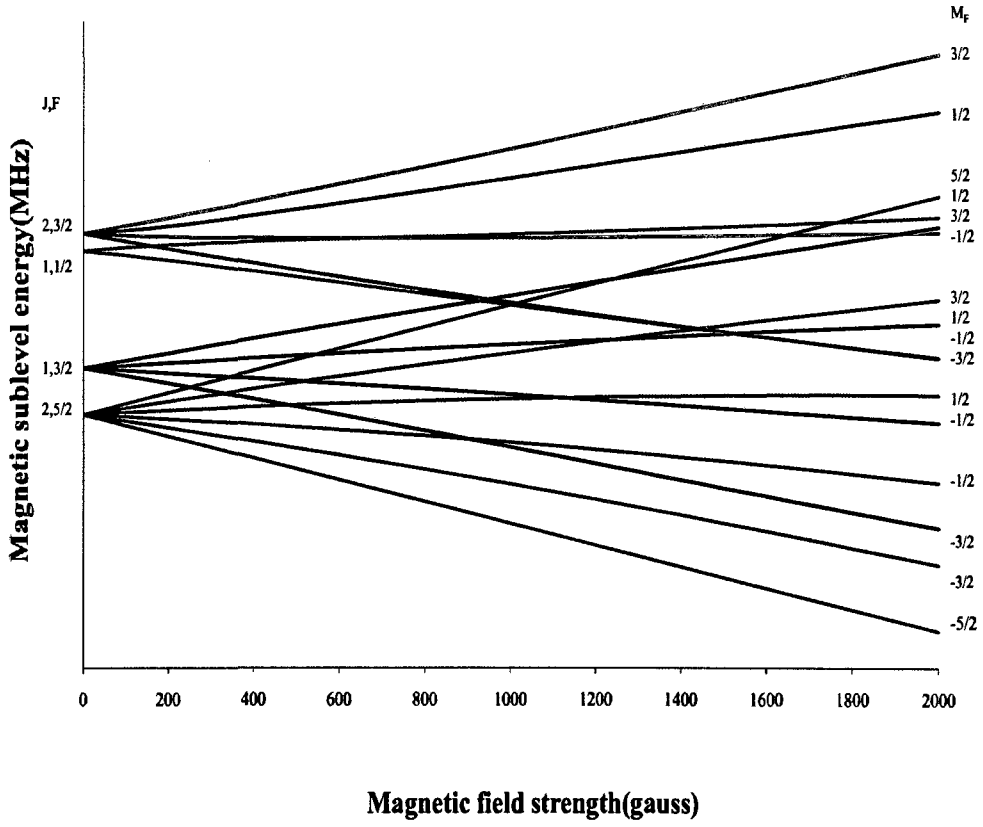

Figure 4: Zeeman sublevel of hyperfine 2 ^{3}P state of ^{3}He with magnetic field strength up to 10000 gauss.

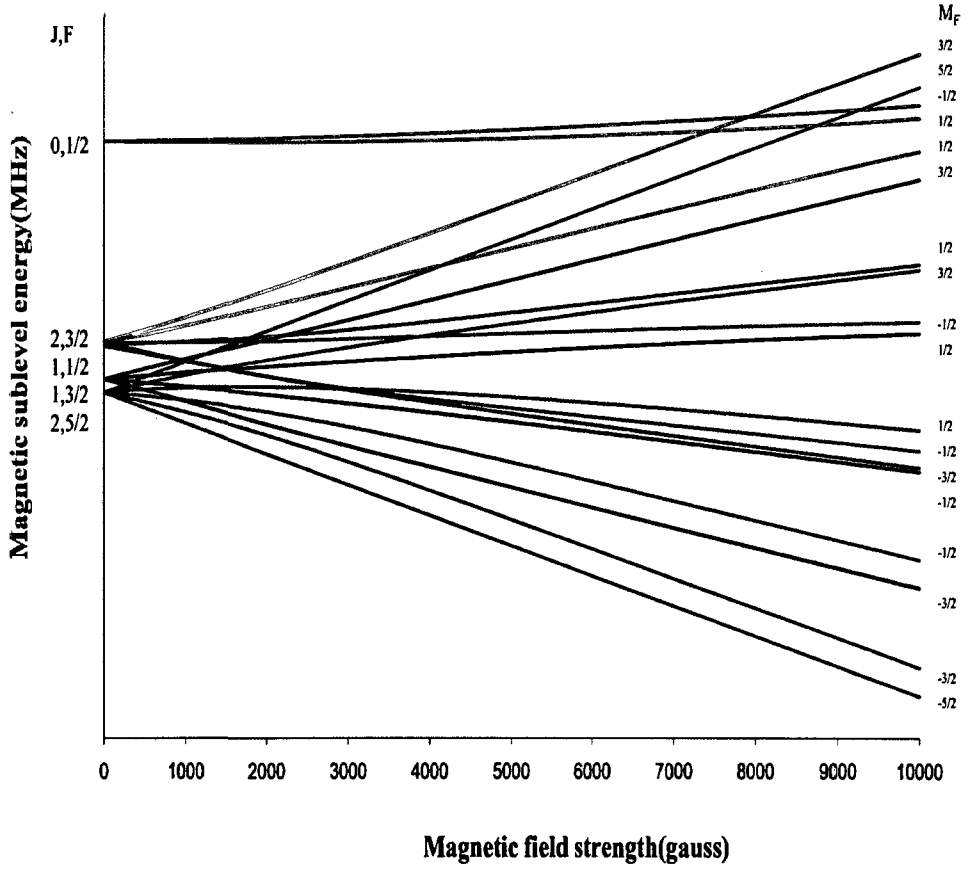

3.3 Zeeman Sublevel Crossings

The calculation of Zeeman sublevels of the hyperfine structure carried out above allows us to determinate the sublevel crossing points. The level crossing is referred to a situation when sublevel energies coincide. Numerical studies of the Zeeman pattern in the region of magnetic field strengths up to 10 000 gauss show that the total number of crossings of magnetic sublevels in the 2 ^{3}P state of ^{3}He is 32. The details are clearly demonstrated in Table 5, where the available experimental values of the crossing field are also tabulated for comparison.

What is particularly noteworthy in Table 5 is that half of the calculated field strengths for the crossings show significant disagreements with the 18 values that have been measured [37]. Most of the discrepancies involve the 2 ^{3}P state with $J' = 2$ and $F' = 5/2$. However, there is no particular reason why the calculated crossings for this state should be less accurate than for the others, and the discrepancies in some cases are much larger than what can be accounted for theoretically. It would be interesting to repeat the 1967 measurements reported in Ref. [37] since some of these older measurements may be in error. On the one hand, new theoretical formulations are needed, such as suggested by Pachucki [58] who considered the relativistic and the second order contributions to the hyperfine structure of the 2 $^3S_1$ state of ^{3}He. An extension of his work to higher angular momentum states would be helpful in further investigations of the hyperfine structure, and work on this is still in progress. On the other hand, the refined experiments on the hyperfine structure of this isotope will be useful to provide further comparison between theory and measurement.

Table 5: Field for crossing of magnetic sublevels. The quoted errors of the calculated quantities in the present work reflect the contribution from δ^{c}_{ho}. Significant differences between theory and experiment are indicated by an asterisk (*). Units are gauss.

	Crossing					
	(J, F, M_F)	–	(J', F', M'_F)	Present work	Experiment [37]	Difference
1	$(2, 3/2, -3/2)$	–	$(1, 1/2, 1/2)$	160.8422(20)	160.831(2)	0.011(3) *
2	$(1, 3/2, -3/2)$	–	$(2, 5/2, 5/2)$	249.262(1)		
3	$(1, 3/2, -3/2)$	–	$(2, 5/2, 3/2)$	328.3754(3)		
4	$(1, 3/2, -1/2)$	–	$(2, 5/2, 5/2)$	343.102(1)		
5	$(1, 3/2, -3/2)$	–	$(2, 5/2, 1/2)$	480.9610(7)	480.963(2)	–0.002(2)
6	$(1, 3/2, -1/2)$	–	$(2, 5/2, 3/2)$	518.2855(4)	518.285(2)	0.000(2)
7	$(1, 3/2, 1/2)$	–	$(2, 5/2, 5/2)$	544.7925(5)	544.793(2)	–0.000(2)
8	$(2, 3/2, -1/2)$	–	$(1, 1/2, 1/2)$	647.7145(4)	647.852(647)	–0.14(65)
9	$(1, 3/2, -3/2)$	–	$(2, 5/2, -1/2)$	900.728(3)	900.765(5)	–0.037(6) *
10	$(1, 1/2, -1/2)$	–	$(1, 3/2, 3/2)$	925.3176(29)	925.323(9)	–0.005(10)
11	$(1, 3/2, 3/2)$	–	$(2, 3/2, -3/2)$	947.4447(38)		
12	$(2, 5/2, 5/2)$	–	$(1, 1/2, -1/2)$	998.9944(26)		
13	$(2, 5/2, 5/2)$	–	$(2, 3/2, -3/2)$	1013.5076(50)		
14	$(1, 3/2, -1/2)$	–	$(2, 5/2, 1/2)$	1111.987(4)	1112.042(4)	–0.055(6) *
15	$(1, 3/2, 3/2)$	–	$(2, 5/2, 5/2)$	1233.584(3)	1233.566(16)	0.018(16)
16	$(1, 1/2, -1/2)$	–	$(2, 5/2, 3/2)$	1434.0633(4)	1434.081(4)	–0.018(4) *
17	$(2, 5/2, 3/2)$	–	$(2, 3/2, -3/2)$	1438.823(9)		
18	$(1, 3/2, 1/2)$	–	$(1, 1/2, -1/2)$	1520.682(9)		
19	$(2, 3/2, -3/2)$	–	$(1, 3/2, 1/2)$	1523.7742(88)	1523.780(15)	–0.006(16)
20	$(2, 3/2, -3/2)$	–	$(1, 1/2, -1/2)$	1595.704(28)	1595.695(800)	0.009(800)
21	$(2, 5/2, 5/2)$	–	$(2, 3/2, -1/2)$	1644.203(7)		
22	$(1, 1/2, 1/2)$	–	$(2, 5/2, 5/2)$	1763.790(5)	1763.803(3)	–0.013(6) *
23	$(1, 3/2, 3/2)$	–	$(2, 3/2, -1/2)$	1907.107(6)		
24	$(1, 1/2, 1/2)$	–	$(1, 3/2, 3/2)$	2205.307(11)	2205.220(44)	0.087(45)*
25	$(2, 5/2, 1/2)$	–	$(2, 3/2, -3/2)$	2859.490(8)		
26	$(1, 1/2, -1/2)$	–	$(2, 5/2, 1/2)$	3001.283(5)	3001.414(30)	–0.131(30) *
27	$(2, 5/2, 3/2)$	–	$(2, 3/2, -1/2)$	3841.227(9)		
28	$(2, 3/2, 1/2)$	–	$(2, 5/2, 5/2)$	4137.720(11)	4137.743(21)	–0.023(24)
29	$(2, 3/2, 3/2)$	–	$(0, 1/2, 1/2)$	7436.796(3)		
30	$(0, 1/2, -1/2)$	–	$(2, 3/2, 3/2)$	7903.917(4)	7903.978(8)	–0.061(9) *
31	$(0, 1/2, 1/2)$	–	$(2, 5/2, 5/2)$	8747.236(3)	8747.303(17)	–0.067(17)*
32	$(2, 5/2, 5/2)$	–	$(0, 1/2, -1/2)$	9262.1496(44)		

4 Hyperfine Suppression of $2\,^3S_1$ to $n\,^3P_J$ Radiative Transitions in ^3He

4.1 Experimental Observation of Hyperfine Suppression of $2\,^3S_1$ to $3\,^3P_J$ Radiative Transition in ^3He

Recently, Sulai *et al.* [5] have investigated hyperfine transitions in ^3He that have anomalous line strengths when compared with estimates from a pure LSJ coupling model. The transitions are those between the $2\,^3S_1$, F and $3\,^3P_J$, F manifolds. They surprisingly observed that the strength of two allowed transitions, $2\,^3S_1(F = \frac{3}{2}) - 3\,^3P_1(F = \frac{3}{2})$ and $2\,^3S_1(F = \frac{1}{2}) - 3\,^3P_2(F = \frac{3}{2})$ are 1000 times weaker than that of the strongest transition $2\,^3S_1(F = \frac{3}{2}) - 3\,^3P_2(F = \frac{5}{2})$. The level scheme showing these transitions is presented in Figure 5. Their final measured results, along with estimated uncertainties are given in Table 6.

Figure 5: Level scheme of ^{3}He showing the levels investigated, with the red arrows indicating the suppressed transitions observed. The dark arrow is used as reference. The levels are designated by the familiar term symbols, with $\vec{J} = \vec{L} + \vec{S}$, $\vec{F} = \vec{J} + \vec{I}$ on the left. The level are labeled on the right using $\vec{K} = \vec{I} + \vec{S}$ and $\vec{F} = \vec{K} + \vec{L}$. The level position is not drawn to scale.

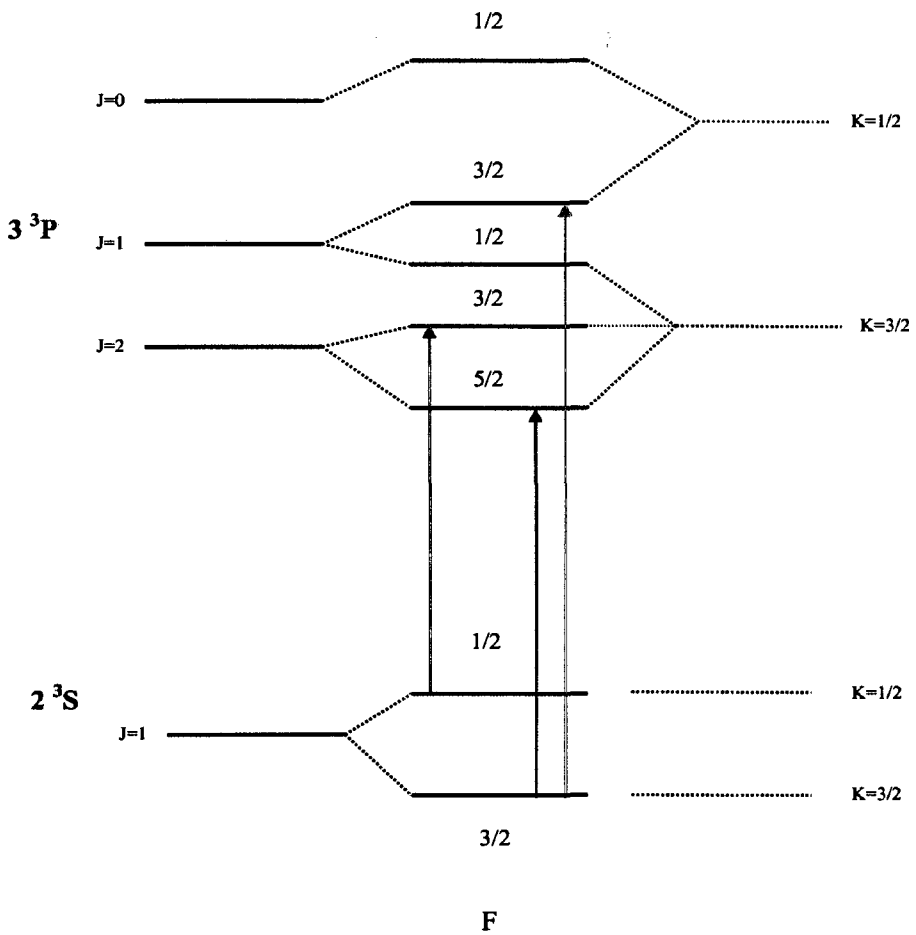

Table 6: Relative transition strengths for all E1 allowed transitions between the 2^3S_1 and 3^3P_J manifolds. All values are normalized with respect to the $2^3S_1, F = \frac{3}{2} \rightarrow 3^3P_2, F = \frac{5}{2}$. Values in red indicate suppressed transitions.

Initial state (J, F) 2^3S_J	Final state (J, F) 3^3P_J	Experiment
(1,3/2)	(2,5/2)	1
	(2,3/2)	0.693(42)
	(1,1/2)	0.267(44)
	(1,3/2)	0.0012(6)
	(0,1/2)	0.098(59)
(1,1/2)	(2,3/2)	0.0011(4)
	(1,1/2)	0.088(28)
	(1,3/2)	0.654(40)
	(0,1/2)	0.276(45)

4.2 Pure LSJ Coupling Model

The line strength of electric dipole transition between two hyperfine states $|\gamma LSJIF\rangle$ and $|\gamma' L'S'J'IF'\rangle$ is the form:

$$S = |\langle \gamma LSJIF \| \vec{r_1} + \vec{r_2} \| \gamma' L'S'J'IF' \rangle|^2 \tag{99}$$

which can be reduced to the following expression in term of the standard angular momentum theory:

$$S = [(2J+1)(2J'+1)(2F+1)(2F'+1)] \left\{ \begin{array}{ccc} J & F & I \\ F' & J' & 1 \end{array} \right\}^2 \left\{ \begin{array}{ccc} L & J & S \\ J' & L' & 1 \end{array} \right\}^2 \delta_{S,S'} |\langle \gamma L \| \vec{r_1} + \vec{r_2} \| \gamma' L' \rangle|^2 \tag{100}$$

As a result, the selection rules for electric dipole transitions are thus:

$$\Delta S = 0 \tag{101}$$

$$\Delta L = \pm 1 \tag{102}$$

$$\Delta J = 0, \pm 1 (J = 0 \rightarrow J' = 0 \text{ forbidden}) \tag{103}$$

$$\Delta F = 0, \pm 1 (F = 0 \rightarrow F' = 0 \text{ forbidden}) \tag{104}$$

For transitions between $|^3\mathrm{S}_1\, 3/2\rangle$ and $|^3\mathrm{P}_J\, F\rangle$, all the line strengths are expressed as:

$$\begin{aligned} S_1 &= |\langle {}^3\mathrm{S}_1, 3/2 \| \vec{r_1} + \vec{r_2} \| {}^3\mathrm{P}_0, 1/2 \rangle|^2 \\ &= \frac{4}{9} |\langle {}^3\mathrm{S} \| \vec{r_1} + \vec{r_2} \| {}^3\mathrm{P} \rangle|^2 \end{aligned} \tag{105}$$

$$
\begin{aligned}
S_2 &= |\langle {}^3\mathrm{S}_1, 3/2 \| \vec{r_1} + \vec{r_2} \| {}^3\mathrm{P}_1, 1/2 \rangle|^2 \\
&= \frac{2}{9} |\langle {}^3\mathrm{S} \| \vec{r_1} + \vec{r_2} \| {}^3\mathrm{P} \rangle|^2 \qquad (106)
\end{aligned}
$$

$$
\begin{aligned}
S_3 &= |\langle {}^3\mathrm{S}_1, 3/2 \| \vec{r_1} + \vec{r_2} \| {}^3\mathrm{P}_1, 3/2 \rangle|^2 \\
&= \frac{10}{9} |\langle {}^3\mathrm{S} \| \vec{r_1} + \vec{r_2} \| {}^3\mathrm{P} \rangle|^2 \qquad (107)
\end{aligned}
$$

$$
\begin{aligned}
S_4 &= |\langle {}^3\mathrm{S}_1, 3/2 \| \vec{r_1} + \vec{r_2} \| {}^3\mathrm{P}_2, 3/2 \rangle|^2 \\
&= \frac{2}{9} |\langle {}^3\mathrm{S} \| \vec{r_1} + \vec{r_2} \| {}^3\mathrm{P} \rangle|^2 \qquad (108)
\end{aligned}
$$

$$
\begin{aligned}
S_5 &= |\langle {}^3\mathrm{S}_1, 3/2 \| \vec{r_1} + \vec{r_2} \| {}^3\mathrm{P}_2, 5/2 \rangle|^2 \\
&= 2 |\langle {}^3\mathrm{S} \| \vec{r_1} + \vec{r_2} \| {}^3\mathrm{P} \rangle|^2 \qquad (109) \\
& \qquad (110)
\end{aligned}
$$

Alternatively, for transitions between $|{}^3\mathrm{S}_1\, 1/2\rangle$ and $|{}^3\mathrm{P}_J\, F\rangle$, all the line strengths are expressed as:

$$
\begin{aligned}
S_1' &= |\langle {}^3\mathrm{S}_1, 1/2 \| \vec{r_1} + \vec{r_2} \| {}^3\mathrm{P}_0, 1/2 \rangle|^2 \\
&= \frac{2}{9} |\langle {}^3\mathrm{S} \| \vec{r_1} + \vec{r_2} \| {}^3\mathrm{P} \rangle|^2 \qquad (111)
\end{aligned}
$$

$$
\begin{aligned}
S_2' &= |\langle {}^3\mathrm{S}_1, 1/2 \| \vec{r_1} + \vec{r_2} \| {}^3\mathrm{P}_1, 1/2 \rangle|^2 \\
&= \frac{4}{9} |\langle {}^3\mathrm{S} \| \vec{r_1} + \vec{r_2} \| {}^3\mathrm{P} \rangle|^2 \qquad (112)
\end{aligned}
$$

$$
\begin{aligned}
S_3' &= |\langle {}^3\mathrm{S}_1, 1/2 \| \vec{r_1} + \vec{r_2} \| {}^3\mathrm{P}_1, 3/2 \rangle|^2 \\
&= \frac{2}{9} |\langle {}^3\mathrm{S} \| \vec{r_1} + \vec{r_2} \| {}^3\mathrm{P} \rangle|^2 \qquad (113)
\end{aligned}
$$

$$
\begin{aligned}
S'_4 &= |\langle {}^3\mathrm{S}_1, 1/2 \| \vec{r_1} + \vec{r_2} \| {}^3\mathrm{P}_2, 3/2 \rangle|^2 \\
&= \frac{10}{9} |\langle {}^3\mathrm{S} \| \vec{r_1} + \vec{r_2} \| {}^3\mathrm{P} \rangle|^2
\end{aligned} \tag{114}
$$

$$
\begin{aligned}
S'_5 &= |\langle {}^3\mathrm{S}_1, 1/2 \| \vec{r_1} + \vec{r_2} \| {}^3\mathrm{P}_2, 5/2 \rangle|^2 \\
&= 0
\end{aligned} \tag{115}
$$

Relative transition line strengths are shown in Table 7. It is obvious that there is not even qualitative agreement between experiment and theory based on the Pure LSJ model. It is thus concluded that the simple pure LSJ model is no longer applicable to hyperfine transition of ^{3}He.

Table 7: Relative transitions strengths for all E1 allowed transitions between the 2^3S_1 and 3^3P_J manifolds. All values are normalized with respect to the $2^3S_1, F = \frac{3}{2} \rightarrow 3^3P_2, F = \frac{5}{2}$. Values in red indicate suppressed transitions.

Initial state (J, F) 2^3S_J	Final state (J, F) 3^3P_J	Experiment [5]	Pure LSJ
(1,3/2)	(2,5/2)	1	1
	(2,3/2)	0.693(42)	0.1111
	(1,1/2)	0.267(44)	0.1111
	(1,3/2)	0.0012(6)	0.5555
	(0,1/2)	0.098(59)	0.2222
(1,1/2)	(2,3/2)	0.0011(4)	0.5555
	(1,1/2)	0.088(28)	0.2222
	(1,3/2)	0.654(40)	0.1111
	(0,1/2)	0.276(45)	0.1111

4.3 IS Coupling Model

Recently, Santra in Reference [5] suggested an IS coupling model to understand Sulai's experiment. The basic idea underlying the IS coupling model is that the electrostatic exchange interaction between the two electrons preserves total spin S, the hyperfine interaction couples S and nuclear spin I to form a new intermediate angular momentum K, and the total angular momentum of the atom F is then obtained by coupling K and total orbital angular momentum L. In this picture, the ^{3}He eigenstates of relevance here are not labeled in terms of $|\gamma LSJIF\rangle$, but in terms of $|\gamma ISKLF\rangle$. Santra diagonalized the contact hyperfine operator plus the spin-orbit operator in the subspace of the $3\,^3$P states.

$$|KM_K\rangle = (-1)^{I-S-M_K}\sqrt{2K+1}\sum \begin{pmatrix} S & I & K \\ -M_S & M_I & -M_K \end{pmatrix} |IM_I\rangle|SM_S\rangle \tag{116}$$

$$|FM_F\rangle = (-1)^{L-K-M_F}\sqrt{2F+1}\sum \begin{pmatrix} K & L & F \\ M_K & M_L & -M_F \end{pmatrix} |KM_K\rangle|LM_L\rangle \tag{117}$$

The dipole matrix elements are of the form:

$$\langle F'M'_F|\vec{r}_1+\vec{r}_2|FM_F\rangle = (-1)^{L-K-M_F+L'-K'-M'_F}\sqrt{(2F+1)(2F'+1)}\sum \begin{pmatrix} K & L & F \\ M_K & M_L & -M_F \end{pmatrix}\begin{pmatrix} K' & L' & F' \\ M'_K & M'_L & -M'_F \end{pmatrix} \langle KM'_K|KM_K\rangle\langle L'M'_L|\vec{r}_1+\vec{r}_2|LM_L\rangle \tag{118}$$

resulting in the selection rule $\triangle K = 0$.

Since all transitions are from the $2S(L = M = 0)$ level, the final expression for the square of matrix elements is reduced to:

$$\langle F' M'_F | \vec{r}_1 + \vec{r}_2 | F M_F \rangle^2 = \frac{2F'+1}{9(2F+1)} \begin{pmatrix} K' & 1 & F' \\ M'_F & q & -M'_F \end{pmatrix} \langle \gamma' L' = 1 || \vec{r}_1 + \vec{r}_2 || \gamma L = 0 \rangle^2 \quad (119)$$

Equation (119) along with the selection rule $\Delta K = 0$ is used to calculate the relative strength for the transitions here. The final results are shown in Table 8. Obviously, there is good qualitative agreement between experiment and the IS coupling model. For instance, within the IS coupling model, the suppression of the transition from $2\,^3\mathrm{S}_1, F = \frac{3}{2}\,(K = \frac{3}{2})$ to $3\,^3\mathrm{P}_1, F = \frac{3}{2}\,(K = \frac{1}{2})$ follows from the K-selection rule for electric dipole transitions. On the other hand, according to experiment, the transition from $2\,^3\mathrm{S}_1, F = \frac{3}{2}\,(K = \frac{3}{2})$ to $3\,^3\mathrm{P}_0, F = \frac{1}{2}\,(K = \frac{1}{2})$ is weakly allowed, in slight deviation from the K-selection rule in electric dipole transitions. In order to characterize the nature of the perturbation to the IS coupling model for ^{3}He, and to account for the slight deviation, an exact diagonalization must be performed. This is discussed in the following section.

Table 8: Relative transitions strengths for all E1 allowed transitions between the 2^3S_1 and 3^3P_J manifolds. All values are normalized with respect to the $2^3S_1, F = \frac{3}{2} \rightarrow 3^3P_2, F = \frac{5}{2}$. Values in red indicate suppressed transitions.

Initial state (J,F) 2^3S_J	Final state (J,F) 3^3P_J	Experiment [5]	Pure LSJ	IS
(1,3/2)	(2,5/2)	1	1	1
	(2,3/2)	0.693(42)	0.1111	0.6666
	(1,1/2)	0.267(44)	0.1111	0.3333
	(1,3/2)	0.0012(6)	0.5555	0
	(0,1/2)	0.098(59)	0.2222	0
(1,1/2)	(2,3/2)	0.0011(4)	0.5555	0
	(1,1/2)	0.088(28)	0.2222	0
	(1,3/2)	0.654(40)	0.1111	0.6666
	(0,1/2)	0.276(45)	0.1111	0.3333

4.4 Exact Diagonalization

The total Hamiltonian of the ^{3}He atom is

$$H = H_{\rm NR} + H_{\rm Rel} + H_{\rm QED} + H_{\rm hfs}, \tag{120}$$

where $H_{\rm NR}$, $H_{\rm Rel}$, $H_{\rm QED}$ and $H_{\rm hfs}$ have the same significance as in Section 3. High precision values for all the hyperfine structure parameters can be calculated by using the double basis set wave functions in Hylleraas co-ordinates developed by Drake [20, 21]. The final hyperfine structure parameters, including the linear mass polarization $\delta_{\rm MP}$, reduced-mass correction and estimated higher-order relativistic, QED, and finite nuclear size corrections for dominate Fermi contact parameter are also listed in Table 9.

Table 9: Δ, E_0, and E_1 are the $3\ ^1P_1$–$3\ ^3P_2$, $3\ ^3P_0$–$3\ ^3P_2$ and $3\ ^3P_1$–$3\ ^3P_2$ energy level separation, respectively. E_M is the off-diagonal matrix element. Δ' and E_1' are the corresponding quantity before diagonalization. $C_{S,S'}$, D_S, and $E_{S,S'}$ are the hyperfine structure parameters. Units are MHz.

fine structure parameters		hyperfine structure parameters	
Δ'	193 395 51.5	C_{11}	−4318.803
Δ	193 395 51.8	C_{10}	−4287.381
E_0	8772.537(33)	D_1	−8.162
E_1	659.077(18)	D_0	−4.261
E_1'	660.340(18)	E_{11}	2.090
E_2	0.	E_{10}	1.632
E_M	−4943.241		

With available fine structure parameters and hyperfine structure parameters, the

hyperfine structure can be obtained by diagonalizing the complete matrix of fine and hyperfine interaction in the basis set of 1s3p ^{1}P and 1s3p ^{3}P states. Our calculations show that the mixing between hyperfine states of 3P with different J but the same F of ^{3}He plays an important role in the hyperfine structure and hyperfine transition strength. As for the 2S state, this hyperfine mixing is also important in hyperfine structure, as shown by Riis *et al.* [60], but its contribution to the transition strength is negligible in the present work.

Due to the hyperfine interaction, the true eigenstates $|3\,^3\mathrm{P}(J,F)\rangle_{\mathrm{ture}}$ and $|2\,^3\mathrm{S}(J,F)\rangle_{\mathrm{ture}}$ can be expressed in terms of the pure eigenstates (without mixing):

$$\begin{aligned}|3\,^3\mathrm{P}(J,F)\rangle_{\mathrm{true}} &= c_1|3\,^1\mathrm{P}_1\,1/2\rangle + c_2|3\,^1\mathrm{P}_1\,3/2\rangle + c_3|3\,^3\mathrm{P}_0\,1/2\rangle + \\ &\quad c_4|3\,^3\mathrm{P}_1\,1/2\rangle + c_5|3\,^3\mathrm{P}_1\,3/2\rangle + c_6|3\,^3\mathrm{P}_2\,3/2\rangle + \\ &\quad c_7|3\,^3\mathrm{P}_2\,5/2\rangle \end{aligned} \tag{123}$$

$$|2\,^3\mathrm{S}(J,F)\rangle_{\mathrm{true}} = d_1|2\,^1\mathrm{S}(0,1/2)\rangle + d_2|2\,^3\mathrm{S}(1,1/2)\rangle + d_3|2\,^3\mathrm{S}(1,3/2)\rangle \tag{124}$$

All expansion coefficients are determined by diagonalization of the complete Hamiltonian matrix and summarized in Table 10 and Table 11.

The line strengths of electric dipole transitions between the hyperfine states of 2S and 3P are of the form

$$S = |\langle 2\,^3\mathrm{S}(J,F)||\vec{r_1}+\vec{r_2}||3\,^3\mathrm{P}(J',F')\rangle_{\mathrm{true}}|^2 \tag{125}$$

Consequently, each transition line strength reduces to:

$$S(2\,^3\mathrm{S}_1\,1/2 \rightarrow 3\,^3\mathrm{P}_0\,1/2)_{\mathrm{true}} = 0.4806|\langle 2\,^3\mathrm{S}||\vec{r_1}+\vec{r_2}||3\,^3\mathrm{P}\rangle|^2 \tag{126}$$

Table 10: The expansion coefficients for the 3P state. Numbers in brackets represent powers of 10.

coefficient	$^1P_1, F = \frac{1}{2}$	$^1P_1, F = \frac{3}{2}$	$^3P_0, F = \frac{1}{2}$	$^3P_1, F = \frac{1}{2}$
c_1	0.999 9999	0	0.000 0636	0.000 1339
c_2	0	0.999 9999	0	0
c_3	-0.000 1107	0	0.921 5456	0.388 2676
c_4	-0.000 0987	0	-0.388 2676	0.921 5467
c_5	0	-0.000 3340	0	0
c_6	0	0.000 1753	0	0
c_7	0	0	0	0

coeffcient	$^3P_2, F = \frac{3}{2}$	$^3P_1, F = \frac{3}{2}$	$^3P_2, F = \frac{5}{2}$
c_1	0	0	0
c_2	0.000 2214	-0.000 3054	0
c_3	0	0	0
c_4	0	0	0
c_5	0.895 9965	-0.444 0609	0
c_6	0.444 0610	0.895 9966	0
c_7	0	0	1

Table 11: The expansion coefficients for the 2S state. Numbers in brackets represent powers of 10.

coefficient	$^1S_0, F = \frac{1}{2}$	$^3S_1, F = \frac{1}{2}$	$^3S_1, F = \frac{3}{2}$
d_1	0.999 9999	-0.000 0177	0
d_2	0.000 1774	0.999 9999	0
d_3	0	0	1

$$S(2\,^3S_1\,1/2 \to 3\,^3P_1\,1/2)_{\text{true}} = 0.1860|\langle 2\,^3S||\vec{r_1} + \vec{r_2}||3\,^3P\rangle|^2 \tag{127}$$

$$S(2\,^3S_1\,1/2 \to 3\,^3P_1\,3/2)_{\text{true}} = 0.1331|\langle 2\,^3S||\vec{r_1} + \vec{r_2}||3\,^3P\rangle|^2 \tag{128}$$

$$S(2\,^3S_1\,1/2 \to 3\,^3P_2\,3/2)_{\text{true}} = 0.0021|\langle 2\,^3S||\vec{r_1} + \vec{r_2}||3\,^3P\rangle|^2 \tag{129}$$

$$S(2\,^3S_1\,1/2 \to 3\,^3P_2\,5/2)_{\text{true}} = 0 \tag{130}$$

$$S(2\,^3S_1\,3/2 \to 3\,^3P_0\,1/2)_{\text{true}} = 0.1860|\langle 2\,^3S||\vec{r_1} + \vec{r_2}||3\,^3P\rangle|^2 \tag{131}$$

$$S(2\,^3S_1\,3/2 \to 3\,^3P_1\,1/2)_{\text{true}} = 0.4806|\langle 2\,^3S||\vec{r_1} + \vec{r_2}||3\,^3P\rangle|^2 \tag{132}$$

$$S(2\,^3S_1\,3/2 \to 3\,^3P_1\,3/2)_{\text{true}} = 0.0021|\langle 2\,^3S||\vec{r_1} + \vec{r_2}||3\,^3P\rangle|^2 \tag{133}$$

$$S(2\,^3S_1\,3/2 \to 3\,^3P_2\,3/2)_{\text{true}} = 0.1331|\langle 2\,^3S||\vec{r_1} + \vec{r_2}||3\,^3P\rangle|^2 \tag{134}$$

$$S(2\,^3S_1\,3/2 \rightarrow 3\,^3P_2\,5/2)_{\text{true}} = 2.0|\langle 2\,^3S||\vec{r_1} + \vec{r_2}||3\,^3P\rangle|^2 \quad (135)$$

The final results are shown in Table 12. Comparison of all theoretical calculations and experiment are shown in Figure 6 and Figure 7. Importantly, it shows that there is excellent agreement between the theory of exact diagonalization and experiment.

Table 12: Relative transitions strengths for all E1 allowed transitions between the 2^3S_1 and 3^3P_J manifolds. All values are normalized with respect to the $2^3S_1, F = \frac{3}{2} \rightarrow 3^3P_2, F = \frac{5}{2}$. Values in red indicate suppressed transitions.

Initial state $2^3S_J(J,F)$	Final state $3^3P_J(J,F)$	Experiment [5]	Pure LSJ	IS	Exact diag.
(1,3/2)	(2,5/2)	1	1	1	1
	(2,3/2)	0.693(42)	0.1111	0.6666	0.6672
	(1,1/2)	0.267(44)	0.1111	0.3333	0.2409
	(1,3/2)	0.0012(6)	0.5555	0	0.0010
	(0,1/2)	0.098(59)	0.2222	0	0.0932
(1,1/2)	(2,3/2)	0.0011(4)	0.5555	0	0.0010
	(1,1/2)	0.088(28)	0.2222	0	0.0932
	(1,3/2)	0.654(40)	0.1111	0.6666	0.6672
	(0,1/2)	0.276(45)	0.1111	0.3333	0.2409

Figure 6: Relative line strengths of the transition: $2\ ^3S_1, 3/2 \rightarrow 3\ ^3P_J, F$ (experiment and theory).

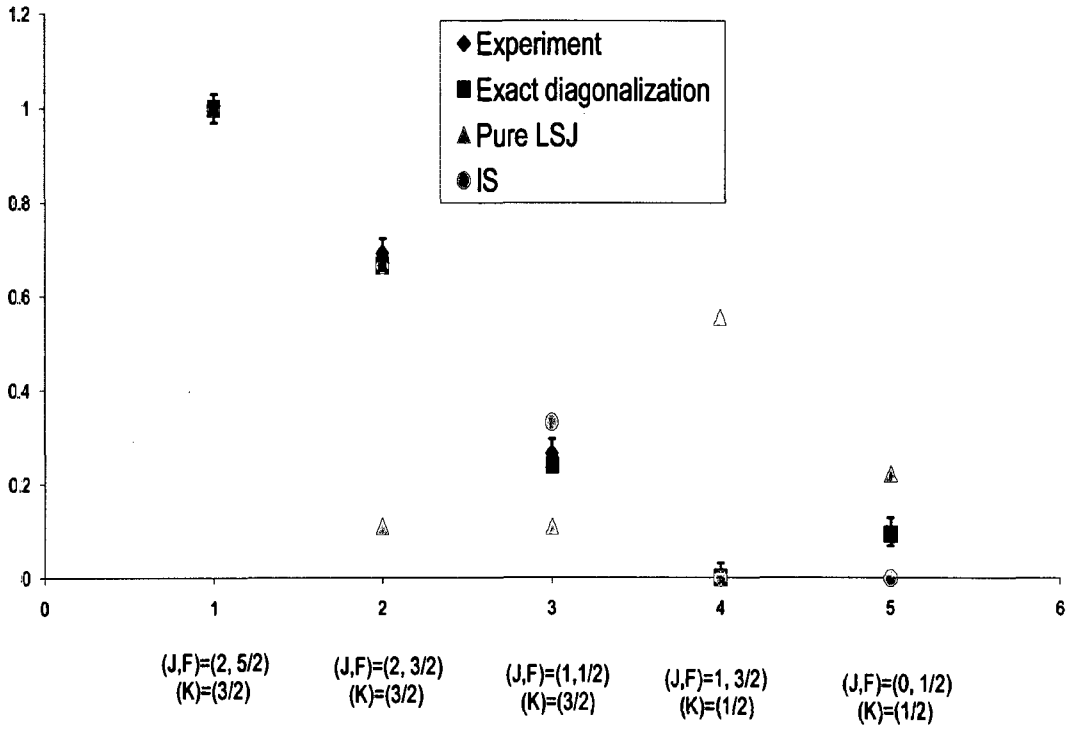

Figure 7: Relative line strengths of the transition: $2\ ^3\mathrm{S}_1, 1/2 \rightarrow 3\ ^3\mathrm{P}_J, F$ (experiment and theory).

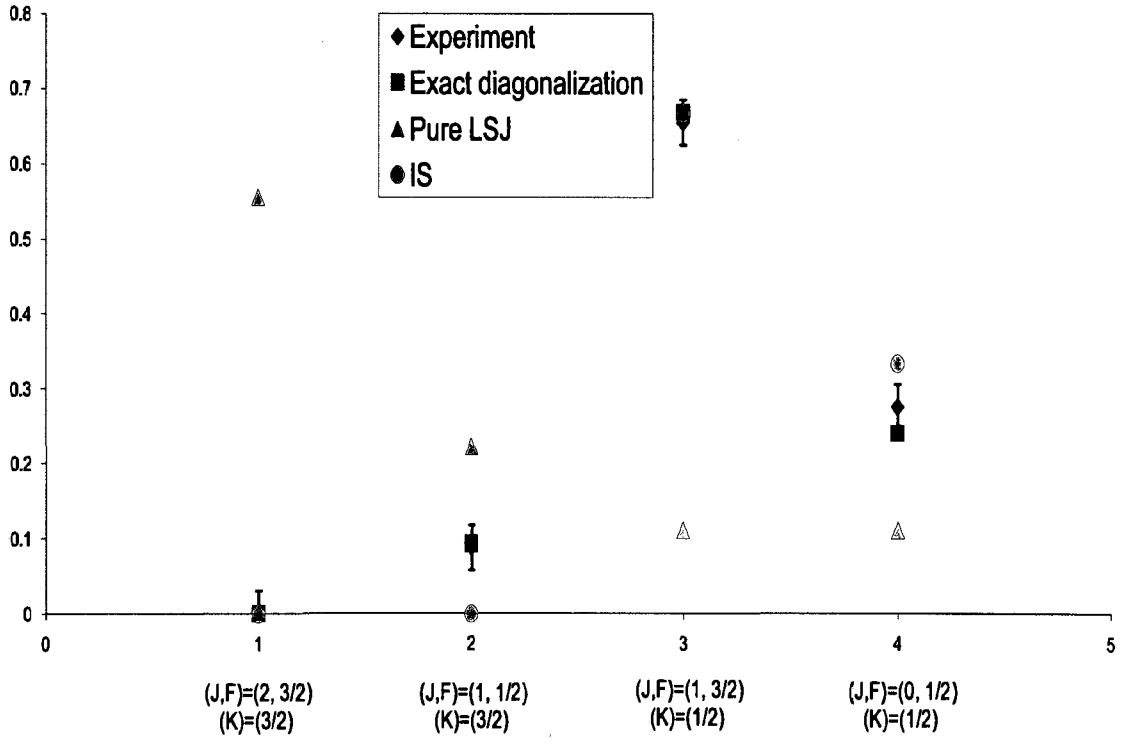

4.5 Discussion of the IS Coupling Model

Even though the IS coupling model provides a good qualitative explanation of the experimentally observed suppression of hyperfine transitions, slight deviations still exist. The deviations mainly result from the mixing between $3\,^3\mathrm{P}$ hyperfine states with different K but the same F in ^{3}He. This mixing is due to the fine-structure interactions including all the one-body spin-orbit (H_{so}), the two-body spin-spin (H_{ss}) and the spin-other-orbit (H_{soo}) interactions. In fact, all three interactions H_{so}, H_{ss}, and H_{soo} are comparable in magnitude. The effect is equally dramatic on the energy levels themselves. However, the IS coupling model only accounts for the contribution from H_{so}, which cannot by itself be responsible for the necessary K mixing in the 3P manifold. This is the reason why the transition from $2\,^3\mathrm{S}_1, F = \frac{3}{2}\,(K = \frac{3}{2})$ to $3\,^3\mathrm{P}_0, F = \frac{1}{2}\,(K = \frac{1}{2})$ is experimentally allowed, in violation of the K-selection rule in electric dipole transitions. All contributions from H_{so}, H_{ss}, and H_{soo} are clearly shown in Figures 8-10. However, with increasing principal quantum number n of the second electron of ^{3}He, the IS coupling model should rapidly become more accurate because the fine structure interactions decrease in proportion to $1/n^3$, while the hyperfine interactions tend to a constant at the series limit $^3\mathrm{He}^+$. In this limit, K will be such a good quantum number that the transition from $2\,^3\mathrm{S}_1 F = \frac{3}{2}\,(K = \frac{3}{2})$ to $n\,^3\mathrm{P}_0 F = \frac{1}{2}\,(K = \frac{1}{2})$ will be strongly suppressed.

Figure 8: Line strengths of transition $2\,^3S_1$ to $3\,^3P_J$ as tuning the spin-orbit interaction strength but turning off the spin-spin and the spin-other-orbit interaction strengths.

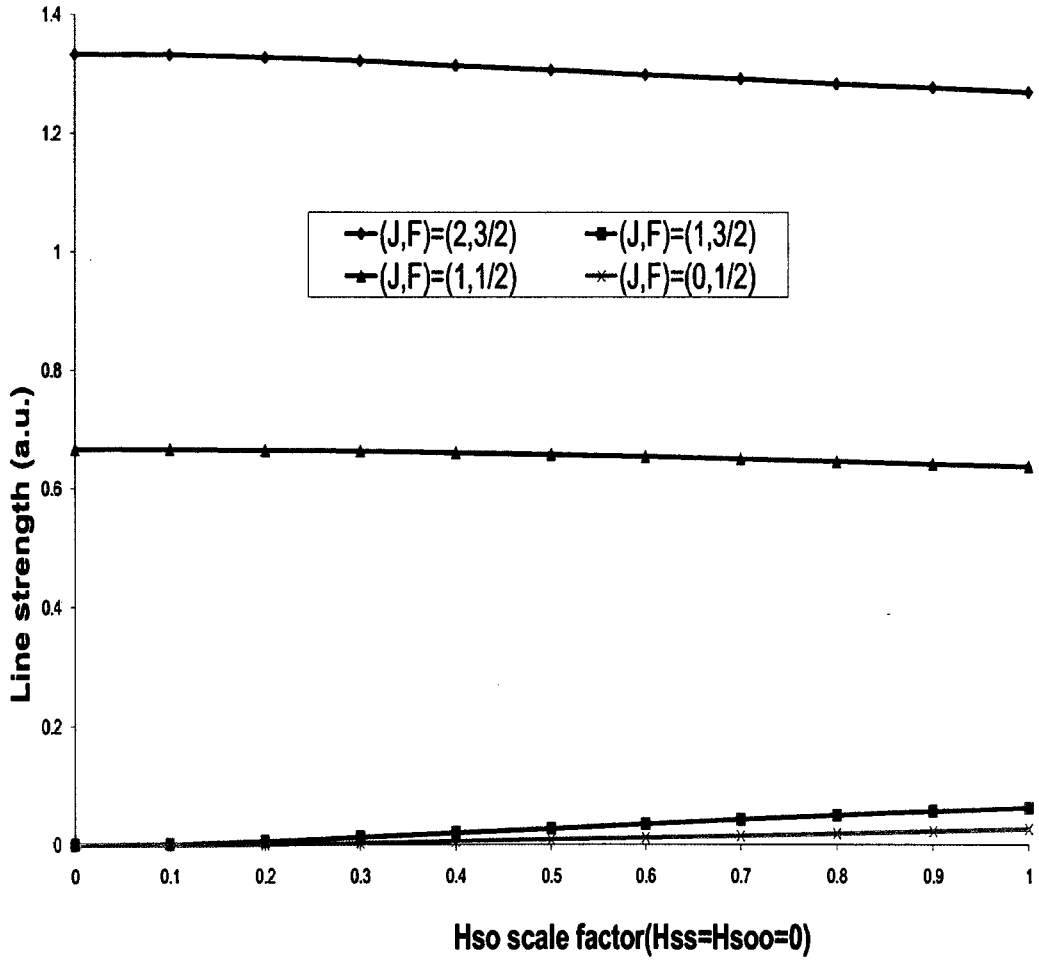

Figure 9: Line strengths of transition $2\,^3S_1$ to $3\,^3P_J$ as tuning the spin-spin and the spin-other-orbit interaction strengths but keeping the spin-orbit interaction strength at full value.

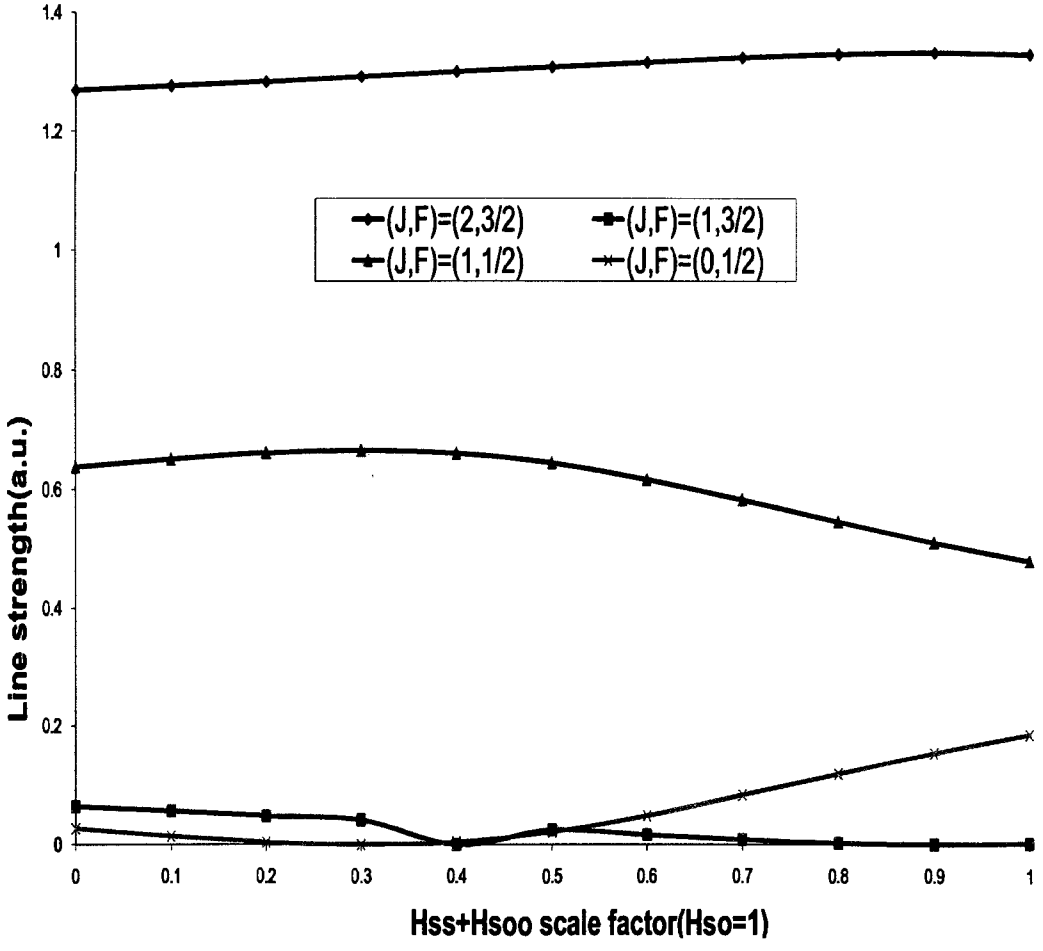

Figure 10: Line strengths of transition $2\,^3S_1$ to $3\,^3P_J$ as tuning the spin-orbit interaction strength but keeping the spin-spin and the spin-other-orbit interaction strengths at their full values.

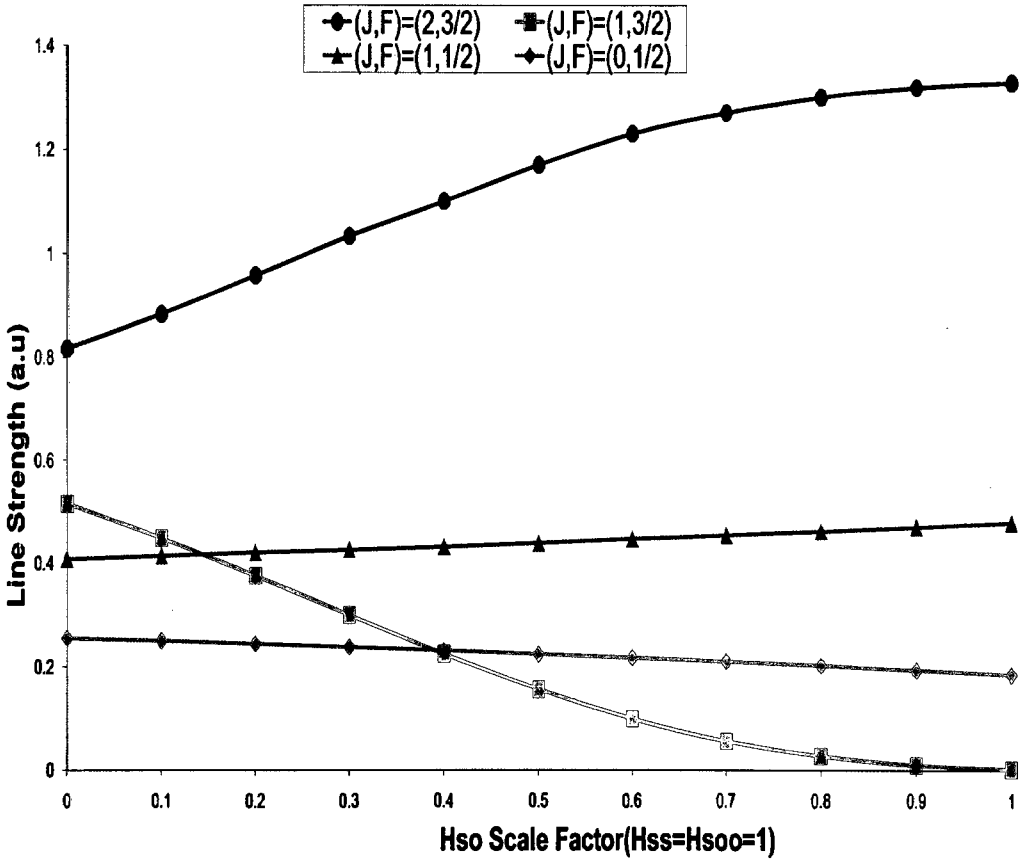

4.6 Magnetic Field Dependence of Line Strengths

Since the effect of the magnetic field of the nucleus could be considered as being similar to an external magnetic field applied to the atomic electrons, it is necessary to check the influence of an external magnetic field on the line strength. This will provide an additional test of the hyperfine suppression phenomenon.

The total Hamiltonian of the ^{3}He atom in an applied magnetic field is

$$H = H_{\rm NR} + H_{\rm Rel} + H_{\rm QED} + H_{\rm hfs} + H_{\rm Z}, \tag{136}$$

where $H_{\rm NR}$, $H_{\rm Rel}$, $H_{\rm QED}$, and $H_{\rm hfs}$ have the same significance as in Section 3, while the Zeeman term $H_{\rm Z}$ represents the linear interactions of the two electrons and nuclear spin with a low applied magnetic field. As for high magnetic field, diamagnetic terms and α^2 order relativistic corrections should be added, as shown in Section 3.

$$H_Z = \mu_B B[g_L L_Z + g_S S_Z + g_I I_Z] \tag{137}$$

The matrix element of $H_{\rm Z}$ in pure hyperfine states is:

$$\langle L'S'J'IF'M'_F|H_Z|LSJIFM_F\rangle = \langle H_Z(L)\rangle + \langle H_Z(S)\rangle + \langle H_Z(I)\rangle, \tag{138}$$

where

$$\begin{aligned}\langle H_Z(L)\rangle = \mu_B B g_L \cdot [(2F+1)(2F'+1)(2J+1)(2J'+1)L(L+1)]^{\frac{1}{2}} \\ (2L+1)^{\frac{1}{2}} \begin{pmatrix} F' & 1 & F \\ -M'_F & 0 & M_F \end{pmatrix} \begin{Bmatrix} J' & F' & I \\ F & J & 1 \end{Bmatrix} \begin{Bmatrix} L' & J' & S \\ J & L & 1 \end{Bmatrix} \\ (-1)^{F+F'+J+J'+I+L'+S'-M_F} \delta_{M_F,M'_F} \delta_{S,S'} \delta_{L,L'}\end{aligned} \tag{139}$$

$$\langle H_Z(S)\rangle = \mu_B B g_S \cdot [(2F+1)(2F'+1)(2J+1)(2J'+1)S(S+1)]^{\frac{1}{2}}$$
$$(2S+1)^{\frac{1}{2}} \begin{pmatrix} F' & 1 & F \\ -M'_F & 0 & M_F \end{pmatrix} \begin{Bmatrix} J' & F' & I \\ F & J & 1 \end{Bmatrix} \begin{Bmatrix} S' & J' & L' \\ J & S & 1 \end{Bmatrix}$$
$$(-1)^{F+F'+2J'+I+L'+S-M_F} \delta_{M_F,M'_F} \delta_{S,S'} \tag{138}$$

$$\langle H_Z(I)\rangle = \mu_B B g_I (-1)^{2F'+J'+I+1-M_F} \cdot [(2F+1)(2F'+1)I(I+1)]^{\frac{1}{2}}$$
$$(2I+1)^{\frac{1}{2}} \begin{pmatrix} F' & 1 & F \\ -M'_F & 0 & M_F \end{pmatrix} \begin{Bmatrix} I & F' & J' \\ F & J & 1 \end{Bmatrix} \delta_{M_F,M'_F} \delta_{J,J'} \tag{139}$$

where g_L, g_S and g_I have the same significance as in Section 3.

The hyperfine structure of 3P and 2S states in an external magnetic field can be obtained by similarly diagonalizing the total Hamiltonian in Equation (134) in the basis set of 1s3p ^{1}P, 1s3p ^{3}P and 1s2s ^{1}S, 1s2s ^{3}S states, respectively. Also, the true hyperfine states $|3\ ^3\mathrm{P}(J,F,M_F)\rangle_{\mathrm{true}}$ and $|2\ ^3\mathrm{S}(J,F,M_F)\rangle_{\mathrm{true}}$ can be expressed in terms of the pure eigenstates (without mixing):

$$\begin{aligned} |3\ ^3\mathrm{P}(J,F,M_F)\rangle_{\mathrm{true}} \;=\; & c_1|3\ ^1\mathrm{P}_1\, 1/2\, M_F\rangle + c_2|3\ ^1\mathrm{P}_1\, 3/2\, M_F\rangle + \\ & c_3|3\ ^3\mathrm{P}_0\, 1/2\, M_F\rangle + c_4|3\ ^3\mathrm{P}_1\, 1/2\, M_F\rangle + \\ & c_5|3\ ^3\mathrm{P}_1\, 3/2\, M_F\rangle + c_6|3\ ^3\mathrm{P}_2\, 3/2\, M_F\rangle + \\ & c_7|3\ ^3\mathrm{P}_2\, 5/2\, M_F\rangle \end{aligned} \tag{140}$$

$$\begin{aligned} |2\ ^3\mathrm{S}(J,F,M_F)\rangle_{\mathrm{true}} \;=\; & d_1|2\ ^1\mathrm{S}(0,1/2,M_F)\rangle + d_2|2\ ^3\mathrm{S}(1,1/2,M_F)\rangle + \\ & d_3|2\ ^3\mathrm{S}(1,3/2,M_F)\rangle \end{aligned} \tag{141}$$

All expansion coefficients are magnetic field dependent and can be numerically calculated through the diagonalization of the above total Hamiltonian matrix. Tables 13-17 summarizes these coefficients for three typical states $|3\ ^3\mathrm{P}_1, F = \frac{1}{2}, M_F = \frac{1}{2}\rangle_{\mathrm{true}}$, $|3\ ^3\mathrm{P}_1, F = \frac{1}{2}, M_F = -\frac{1}{2}\rangle_{\mathrm{true}}$, $|3\ ^3\mathrm{P}_1, F = \frac{3}{2}, M_F = \frac{1}{2}\rangle_{\mathrm{true}}$,

$|3\ ^3\mathrm{P}_1, F = \frac{3}{2}, M_F = -\frac{1}{2}\rangle_{\mathrm{true}}$ and $|3\ ^3\mathrm{P}_1, F = \frac{3}{2}, M_F = \frac{3}{2}\rangle_{\mathrm{true}}$ at selected values of the magnetic field up to 200 Gauss.

The electric dipole transition probability between the two hyperfine states of 2S and 3P in an applied magnetic field is of the form:

$$a \propto |\langle 2\ ^3\mathrm{S}(J, F, M_F)|\vec{r_1} + \vec{r_2}|3\ ^3\mathrm{P}(J', F', M'_F)\rangle_{\mathrm{true}}|^2 \tag{142}$$

which reduces to

$$a \propto \begin{pmatrix} F' & 1 & F \\ -M'_F & q & M_F \end{pmatrix}^2 |\langle 2\ ^3\mathrm{S}(J, F)||\vec{r_1}+\vec{r_2}||3\ ^3\mathrm{P}(J', F')\rangle|^2_{\mathrm{true}},\ q = 0, \pm 1 \tag{143}$$

The above $3J$ symbol yields the electric dipole selection rule:

$$\Delta M_F = 0, \pm 1 \tag{144}$$

The possible electric dipole transitions between hyperfine Zeeman levels of $3\,^3\mathrm{P}_J\,F$ and $2\,^3\mathrm{S}_{J'}\,F'$ which satisfies Equation (144) are shown in Tables 18-21.

The magnetic field dependence of line strengths are numerically shown in Table 22 to Table 24, in which three different $\sigma^+(\Delta M = +1)$ transitions of $2\,^3\mathrm{S}_1$, $F = \frac{3}{2}$ to $3\,^3\mathrm{P}_1$, $F = \frac{3}{2}$ are successfully observed in experiment by Sulai [61](Numbers 8, 11, and 14 represent transition sequence as shown in Table 18).

- $8 : 2\,^3\mathrm{S}_1, F = \frac{3}{2}, M_F = \frac{1}{2}$ to $3\,^3\mathrm{P}_1, F = \frac{3}{2}, M_F = \frac{3}{2}$

- $11 : 2\,^3\mathrm{S}_1, F = \frac{3}{2}, M_F = -\frac{1}{2}$ to $3\,^3\mathrm{P}_1, F = \frac{3}{2}, M_F = \frac{1}{2}$

- $14 : 2\,^3\mathrm{S}_1, F = \frac{3}{2}, M_F = -\frac{3}{2}$ to $3\,^3\mathrm{P}_1, F = \frac{3}{2}, M_F = -\frac{1}{2}$

Comparison of theory and experiment is shown in Figure 11, which suggests that the agreement is satisfactory. Theoretical calculations also show that two maximum suppressions of transitions occur as shown in Figure 12 for the Zeeman component $2\,^3\mathrm{S}_1, F = \frac{3}{2}, M_F = -\frac{1}{2}$ to $3\,^3\mathrm{P}_1, F = \frac{3}{2}, M_F = -\frac{1}{2}$ at 65 gauss and $2\,^3\mathrm{S}_1, F = \frac{3}{2}, M_F = \frac{3}{2}$ to $3\,^3\mathrm{P}_1, F = \frac{3}{2}, M_F = \frac{1}{2}$ at 120 gauss.

Table 13: The field dependence of expansion coefficients for $3\,^3\mathrm{P}_1\ F = \frac{1}{2}, M_F = \frac{1}{2}$ state. Unit of magnetic field strength B is Gauss. Numbers in brackets represent powers of 10.

B	c_1	c_2	c_3	c_4	c_5	c_6	c_7
0	0.1339(-3)	0	0.3882	0.9215	0	0	0
20	0.1339(-3)	0	0.3883	0.9215	-0.1559(-2)	0.5838(-2)	0.3866(-4)
40	0.1339(-3)	0	0.3883	0.9214	-0.3129(-2)	0.1171(-1)	0.1545(-3)
60	0.1339(-3)	0	0.3884	0.9213	-0.4707(-2)	0.1763(-1)	0.3472(-3)
80	0.1339(-3)	0	0.3884	0.9211	-0.6291(-2)	0.2358(-1)	0.6065(-3)
100	0.1339(-3)	0	0.3883	0.9210	-0.7881(-2)	0.2956(-1)	0.9621(-3)
120	0.1339(-3)	0	0.3882	0.9208	-0.9474(-2)	0.3557(-1)	0.1383(-2)
140	0.1338(-3)	-0.1099(-4)	0.3881	0.9206	-0.1107(-2)	0.4160(-1)	0.1879(-2)
160	0.1338(-3)	-0.1258(-4)	0.3879	0.9204	-0.1266(-2)	0.4765(-1)	0.2451(-2)
180	0.1337(-3)	-0.1418(-4)	0.3878	0.9201	-0.1426(-2)	0.5373(-1)	0.3096(-2)
200	0.1337(-3)	-0.1578(-4)	0.3876	0.9198	-0.1585(-2)	0.5981(-1)	0.3814(-2)

Table 14: The field dependence of expansion coefficients for $3\,^3\mathrm{P}_1\, F = \frac{1}{2}, M_F = -\frac{1}{2}$ state. Unit of magnetic field strength B is Gauss. Numbers in brackets represent powers of 10.

B	c_1	c_2	c_3	c_4	c_5	c_6	c_7
0	0.1339(-3)	0	0.3882	0.9215	0	0	0
20	0.1339(-3)	0	0.3881	0.9215	-0.1548(-2)	0.5796(-2)	0.3872(-4)
40	0.1339(-3)	0	0.3880	0.9215	-0.3084(-2)	0.1154(-1)	0.1550(-3)
60	0.1339(-3)	0	0.3878	0.9215	-0.4606(-2)	0.1725(-1)	0.3489(-3)
80	0.1339(-3)	0	0.3877	0.9214	-0.6111(-2)	0.2290(-1)	0.6205(-3)
100	0.1339(-3)	0	0.3875	0.9213	-0.7599(-2)	0.2850(-1)	0.9698(-3)
120	0.1338(-3)	0	0.3873	0.9213	-0.9070(-2)	0.3405(-1)	0.1397(-2)
140	0.1337(-3)	-0.1044(-4)	0.3870	0.9212	-0.1052(-2)	0.3955(-1)	0.1901(-2)
160	0.1337(-3)	-0.1187(-4)	0.3867	0.9210	-0.1195(-2)	0.4497(-1)	0.2483(-2)
180	0.1336(-3)	-0.1328(-4)	0.3864	0.9208	-0.1336(-2)	0.5034(-1)	0.3142(-2)
200	0.1336(-3)	-0.1468(-4)	0.3861	0.9206	-0.1474(-2)	0.5565(-1)	0.3878(-2)

Table 15: The field dependence of expansion coefficients for $3\,^3\mathrm{P}_1\, F = \frac{3}{2}, M_F = \frac{1}{2}$ state. Unit of magnetic field strength B is Gauss. Numbers in brackets represent powers of 10.

B	c_1	c_2	c_3	c_4	c_5	c_6	c_7
0	0	-0.3054(-3)	0	0	-0.4440	0.8959	0
20	0	-0.3051(-3)	-0.4970(-2)	-0.4335(-2)	-0.4432	0.8963	0.3820(-2)
40	0	-0.3049(-3)	-0.9977(-2)	-0.8701(-2)	-0.4423	0.8967	0.7633(-2)
60	0	-0.3047(-3)	-0.1502(-1)	-0.1309(-1)	-0.4413	0.8970	0.1143(-1)
80	0	-0.3044(-3)	-0.2010(-1)	-0.1751(-1)	-0.4404	0.8972	0.1523(-1)
100	0	-0.3041(-3)	-0.2521(-1)	-0.2195(-1)	-0.4394	0.8974	0.1901(-1)
120	0	-0.3018(-3)	-0.3036(-1)	-0.2641(-1)	-0.4384	0.8975	0.2278(-1)
140	0	-0.3034(-3)	-0.3554(-1)	-0.3089(-1)	-0.4373	0.8976	0.2653(-1)
160	0	-0.3031(-3)	-0.4075(-1)	-0.3538(-1)	-0.4363	0.8977	0.3028(-1)
180	0	-0.3027(-3)	-0.4600(-1)	-0.3988(-1)	-0.4352	0.8976	0.3400(-1)
200	0	-0.3023(-3)	-0.5127(-1)	-0.4439(-1)	-0.4340	0.8975	0.3771(-1)

Table 16: The field dependence of expansion coefficients for $3\,^3\mathrm{P}_1\ F = \frac{3}{2}, M_F = -\frac{1}{2}$ state. Unit of magnetic field strength B is Gauss. Numbers in brackets represent powers of 10.

B	c_1	c_2	c_3	c_4	c_5	c_6	c_7
0	0	-0.3054(-3)	0	0	-0.4440	0.8959	0
20	0	-0.3056(-3)	-0.4932(-2)	-0.4303(-2)	-0.4448	0.8955	0.3827(-2)
40	0	-0.3057(-3)	-0.9826(-2)	-0.8571(-2)	-0.4456	0.8950	0.7659(-2)
60	0	-0.3059(-3)	-0.1468(-1)	-0.1280(-1)	-0.4464	0.8945	0.1149(-1)
80	0	-0.3061(-3)	-0.1949(-1)	-0.1699(-1)	-0.4472	0.8939	0.1533(-1)
100	0	-0.3062(-3)	-0.2426(-1)	-0.2114(-1)	-0.4479	0.8932	0.1917(-1)
120	0	-0.3063(-3)	-0.2900(-1)	-0.2525(-1)	-0.4486	0.8926	0.2301(-1)
140	0	-0.3064(-3)	-0.3369(-1)	-0.2931(-1)	-0.4492	0.8918	0.2686(-1)
160	0	-0.3065(-3)	-0.3834(-1)	-0.3333(-1)	-0.4498	0.8911	0.3070(-1)
180	0	-0.3065(-3)	-0.4295(-1)	-0.3730(-1)	-0.4504	0.8902	0.3453(-1)
200	0	-0.3066(-3)	-0.4752(-1)	-0.4122(-1)	-0.4511	0.8894	0.3837(-1)

Table 17: The field dependence of expansion coefficients for $3\,^3\mathrm{P}_1\, F = \frac{3}{2}, M_F = \frac{3}{2}$ state. Unit of magnetic field strength B is Gauss. Numbers in brackets represent powers of 10.

B	c_1	c_2	c_3	c_4	c_5	c_6	c_7
0	0	-0.3054(-3)	0	0	-0.4440	0.8959	0
20	0	-0.3047(-3)	0	0	-0.4415	0.8972	0.3114(-2)
40	0	-0.3041(-3)	0	0	-0.4389	0.8984	0.6211(-2)
60	0	-0.3035(-3)	0	0	-0.4364	0.8996	0.9292(-1)
80	0	-0.3028(-3)	0	0	-0.4339	0.9008	0.1235(-1)
100	0	-0.3022(-3)	0	0	-0.4314	0.9020	0.1540(-1)
120	0	-0.3016(-3)	0	0	-0.4289	0.9031	0.1843(-1)
140	0	-0.3009(-3)	0	0	-0.4264	0.9042	0.2144(-1)
160	0	-0.3003(-3)	0	0	-0.4239	0.9053	0.2443(-1)
180	0	-0.2997(-3)	0	0	-0.4214	0.9064	0.2741(-1)
200	0	-0.2991(-3)	0	0	-0.4189	0.9074	0.3036(-1)

Table 18: Possible electric dipole transitions between states $3\,^3\mathrm{P}_J, F$ and $2\,^3\mathrm{S}_1, F'$.

	final	initial		final	initial
	$3\,^3\mathrm{P}_1, 1/2$	$2\,^3\mathrm{S}_1, 3/2$		$3\,^3\mathrm{P}_1, 3/2$	$2\,^3\mathrm{S}_1, 3/2$
sequence	M_F	M'_F	sequence	M_F	M'_F
1	$1/2$	$3/2$	7	$3/2$	$3/2$
2	$1/2$	$1/2$	8	$3/2$	$1/2$
3	$1/2$	$-1/2$	9	$1/2$	$3/2$
4	$-1/2$	$1/2$	10	$1/2$	$1/2$
5	$-1/2$	$-1/2$	11	$1/2$	$-1/2$
6	$-1/2$	$-3/2$	12	$-1/2$	$1/2$
			13	$-1/2$	$-1/2$
			14	$-1/2$	$-3/2$
			15	$-3/2$	$-1/2$
			16	$-3/2$	$-3/2$

Table 19: Possible electric dipole transitions between states $3\,^3\mathrm{P}_J, F$ and $2\,^3\mathrm{S}_1, F'$.

	final	initial		final	initial
	$3\,^3\mathrm{P}_0, 1/2$	$2\,^3\mathrm{S}_1, 3/2$		$3\,^3\mathrm{P}_2, 3/2$	$2\,^3\mathrm{S}_1, 3/2$
sequence	M_F	M'_F	sequence	M_F	M'_F
1	$1/2$	$3/2$	7	$3/2$	$3/2$
2	$1/2$	$1/2$	8	$3/2$	$1/2$
3	$1/2$	$-1/2$	9	$1/2$	$3/2$
4	$-1/2$	$1/2$	10	$1/2$	$1/2$
5	$-1/2$	$-1/2$	11	$1/2$	$-1/2$
6	$-1/2$	$-3/2$	12	$-1/2$	$1/2$
			13	$-1/2$	$-1/2$
			14	$-1/2$	$-3/2$
			15	$-3/2$	$-1/2$
			16	$-3/2$	$-3/2$

Table 20: Possible electric dipole transitions between states $3\,^3\mathrm{P}_J, F$ and $2\,^3\mathrm{S}_1, F'$.

	final	initial		final	initial
	$3\,^3\mathrm{P}_2, 5/2$	$2\,^3\mathrm{S}_1, 3/2$		$3\,^3\mathrm{P}_0, 1/2$	$2\,^3\mathrm{S}_1, 1/2$
sequence	M_F	M'_F	sequence	M_F	M'_F
7	3/2	3/2	2	1/2	1/2
8	3/2	1/2	3	1/2	−1/2
9	1/2	3/2	4	−1/2	1/2
10	1/2	1/2	5	−1/2	−1/2
11	1/2	−1/2		$^3\mathrm{P}_2, 3/2$	$^3\mathrm{S}_1, 1/2$
12	−1/2	1/2	sequence	M_F	M'_F
13	−1/2	−1/2	8	3/2	1/2
14	−1/2	−3/2	10	1/2	1/2
15	−3/2	−1/2	11	1/2	−1/2
16	−3/2	−3/2	12	−1/2	1/2
17	5/2	3/2	13	−1/2	−1/2
18	−5/2	−3/2	15	−3/2	−1/2

Table 21: Possible electric dipole transitions between states $3\,^3\mathrm{P}_J, F$ and $2\,^3\mathrm{S}_1, F'$.

	final	initial		final	initial
	$3\,^3\mathrm{P}_1, 1/2$	$2\,^3\mathrm{S}_1, 1/2$			
sequence	M_F	M'_F			
2	1/2	1/2			
3	1/2	−1/2			
4	−1/2	1/2			
5	−1/2	−1/2			
	$^3\mathrm{P}_1, 3/2$	$^3\mathrm{S}_1, 1/2$		$^3\mathrm{P}_2, 3/2$	$^3\mathrm{S}_1, 1/2$
sequence	M_F	M'_F	sequence	M_F	M'_F
8	3/2	1/2	8	3/2	1/2
10	1/2	1/2	10	1/2	1/2
11	1/2	−1/2	11	1/2	−1/2
12	-1/2	1/2	12	−1/2	1/2
13	-1/2	−1/2	13	−1/2	−1/2
15	-3/2	−1/2	15	−3/2	−1/2

Table 22: Field dependence of relative transition strength from $3\,^3P_1, F = 1/2$ to $2\,^3S_1, F = 3/2$. Numbers in brackets represent powers of 10.

B(G)	1	2	3	4	5	6
0	0.1202	0.8010(-1)	0.4005(-1)	0.4005(-1)	0.8010(-1)	0.1202
20	0.1199	0.7880(-1)	0.3983(-1)	0.4028(-1)	0.8040(-1)	0.1204
40	0.1197	0.7947(-1)	0.3960(-1)	0.4050(-1)	0.8068(-1)	0.1206
60	0.1195	0.7914(-1)	0.3937(-1)	0.4072(-1)	0.8094(-1)	0.1208
80	0.1192	0.7879(-1)	0.3914(-1)	0.4094(-1)	0.8120(-1)	0.1210
100	0.1190	0.7843(-1)	0.3891(-1)	0.4116(-1)	0.8143(-1)	0.1213
120	0.1187	0.7806(-1)	0.3867(-1)	0.4137(-1)	0.8166(-1)	0.1215
140	0.1185	0.7767(-1)	0.3843(-1)	0.4159(-1)	0.8187(-1)	0.1217
160	0.1182	0.7727(-1)	0.3819(-1)	0.4181(-1)	0.8207(-1)	0.1219
180	0.1179	0.7686(-1)	0.3795(-1)	0.4202(-1)	0.8225(-1)	0.1221
200	0.1177	0.7644(-1)	0.3771(-1)	0.4224(-1)	0.8242(-1)	0.1224

Table 23: Field dependence of relative transition strength from $3\ ^3P_1, F = 1/2$ to $2\ ^3S_1, F = 3/2$. Numbers in brackets represent powers of 10.

B(G)	7	8	9	10	11	12
0	0.3133(-3)	0.2089(-3)	0.2089(-3)	0.3481(-4)	0.2785(-3)	0.2785(-3)
20	0.3089(-3)	0.2040(-3)	0.1470(-3)	0.6107(-4)	0.3217(-3)	0.2390(-3)
40	0.3045(-3)	0.1991(-3)	0.9557(-4)	0.9504(-4)	0.3685(-3)	0.2029(-3)
60	0.3002(-3)	0.1943(-3)	0.5481(-4)	0.1369(-3)	0.4191(-3)	0.1702(-3)
80	0.2958(-3)	0.1896(-3)	0.2509(-4)	0.1876(-4)	0.4735(-3)	0.1408(-3)
100	0.2915(-3)	0.1849(-3)	0.6721(-5)	0.2453(-3)	0.5319(-3)	0.1145(-3)
120	0.2873(-3)	0.1803(-3)	0.2429(-7)	0.3121(-3)	0.5944(-3)	0.9125(-4)
140	0.2830(-3)	0.1757(-3)	0.5293(-5)	0.3876(-3)	0.6610(-3)	0.7094(-4)
160	0.2788(-3)	0.1712(-3)	0.2281(-4)	0.4719(-3)	0.7317(-3)	0.5345(-4)
180	0.2747(-3)	0.1668(-3)	0.5286(-4)	0.5651(-3)	0.8068(-3)	0.3865(-4)
200	0.2706(-3)	0.1624(-3)	0.9568(-4)	0.6673(-3)	0.8861(-3)	0.2643(-4)

Table 24: Field dependence of relative transition strength from $3\ ^3P_1, F = 1/2$ to $2\ ^3S_1, F = 3/2$. Numbers in brackets represent powers of 10.

B(G)	13	14	15	16
0	0.3481(-4)	0.2089(-3)	0.2089(-3)	0.3133(-3)
20	0.1606(-4)	0.2808(-3)	0.2138(-3)	0.3178(-3)
40	0.4559(-5)	0.3623(-3)	0.2188(-3)	0.3223(-3)
60	0.8174(-7)	0.4531(-3)	0.2239(-3)	0.3267(-3)
80	0.2372(-5)	0.5529(-3)	0.2289(-3)	0.3313(-3)
100	0.1117(-4)	0.6613(-3)	0.2341(-3)	0.3358(-3)
120	0.2621(-4)	0.7778(-3)	0.2392(-3)	0.3404(-3)
140	0.4722(-4)	0.9022(-3)	0.2443(-3)	0.3449(-3)
160	0.7392(-4)	0.1034(-2)	0.2496(-3)	0.3495(-3)
180	0.1060(-3)	0.1173(-2)	0.2548(-3)	0.3541(-3)
200	0.1433(-3)	0.1319(-2)	0.2601(-3)	0.3588(-3)

Figure 11: Magnetic field dependence of the individual σ^+ transitions. The points with error bar indicate experimental data. The dashed lines indicate theoretical calculations. Numbers 8, 11, and 14 represent transition sequence.

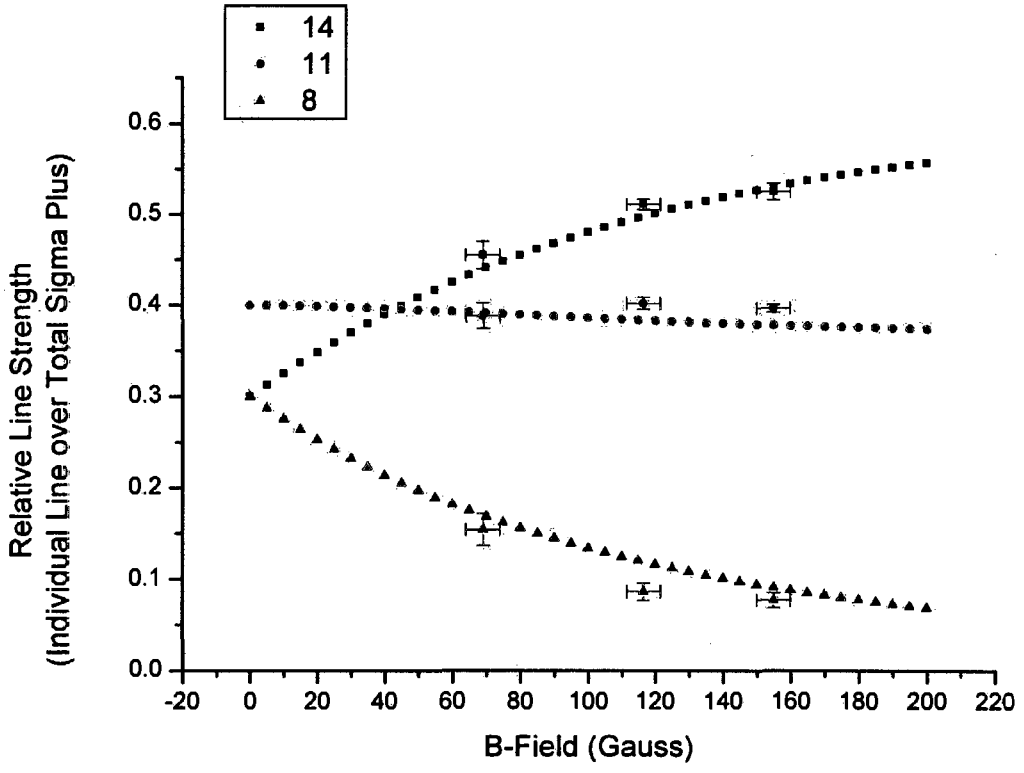

Figure 12: Maximum suppressions in Sequence 9: $^3P_1(F = 3/2, M_F = 1/2) - {}^3S_1(F = 3/2, M_F = 3/2)$ and in Sequence 13: $^3P_1(F = 3/2, M_F = 1/2) - {}^3S_1(F = 3/2, M_F = 1/2)$.

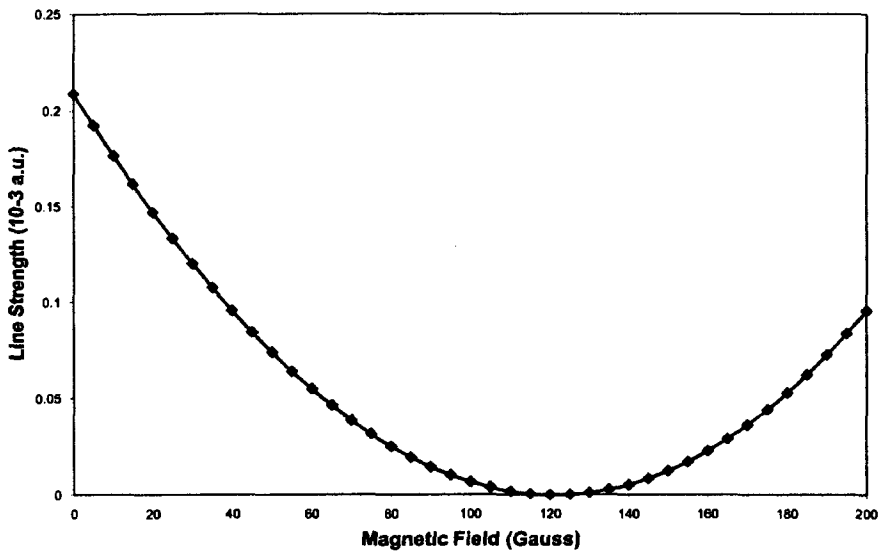

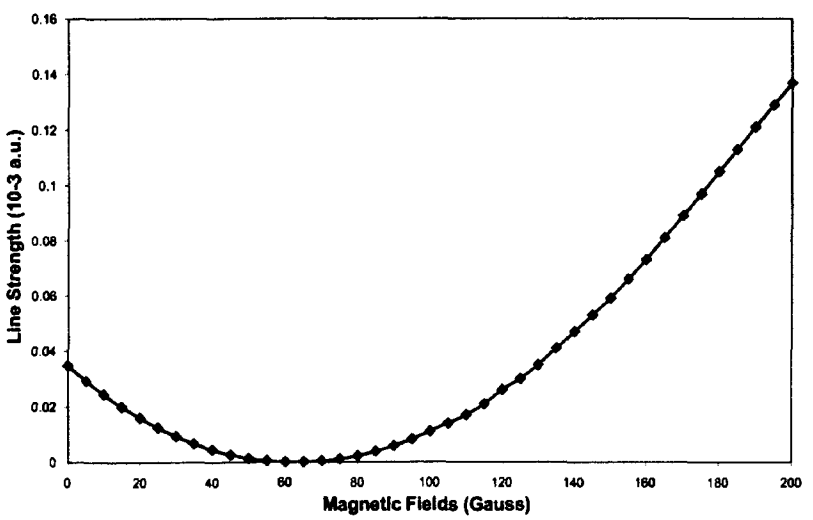

4.7 Strong Hyperfine Interaction Limit and Asymptotic Selection Rules

From the above calculations and discussions, it is concluded that hyperfine suppressions of $2\,^3\mathrm{S}(1,3/2)$ to $3\,^3\mathrm{P}(1,3/2)$ and $2\,^3\mathrm{S}(1,1/2)$ to $3\,^3\mathrm{P}(2,3/2)$ radiative transitions in ^{3}He are caused mainly by strong hyperfine mixing and accidental cancellation between two hyperfine states with the same quantum number F but different quantum number J. A physical picture of these hyperfine transitions can also be extracted by studying the selection rules in the limit of strong hyperfine interaction, which is equivalent to increasing the Fermi contact parameter C of the hyperfine interaction for a certain atomic state such as 3P (discussed here), or by investigating the P states with higher principal quantum number n (details follow in the next section).

As shown in Table 10, the true hyperfine state $|3^3\mathrm{P}_0, 1/2\rangle_{\mathrm{true}}$ is mainly formed from the mixing of two pure hyperfine states $|3^3\mathrm{P}_0, 1/2\rangle$ and $|3^3\mathrm{P}_1, 1/2\rangle$. The mixing from the singlet state $|3^1\mathrm{P}_0, 1/2\rangle$ is so small that it can be ignored at this stage. Similarly, the true hyperfine state $|3^3\mathrm{P}_1, 3/2\rangle_{\mathrm{true}}$ is mainly formed from the mixing of two pure hyperfine states $|3^3\mathrm{P}_1, 3/2\rangle$ and $|3^3\mathrm{P}_2, 3/2\rangle$. The following equations show this approximation.

$$|3\,^3\mathrm{P}(0,1/2)\rangle_{\mathrm{true}} = \alpha|3\,^3\mathrm{P}_0\,\frac{1}{2}\rangle + \beta|3\,^3\mathrm{P}_1\,\frac{1}{2}\rangle \tag{147}$$

$$|3\,^3\mathrm{P}(1,3/2)\rangle_{\mathrm{true}} = \alpha'|3\,^3\mathrm{P}_1\,\frac{3}{2}\rangle + \beta'|3\,^3\mathrm{P}_2\,\frac{3}{2}\rangle \tag{148}$$

In order to extract the selection rules for hyperfine transitions of the 3P state in the strong hyperfine interactions limit, the hyperfine Fermi contact parameter C is

artificially varied from zero (This indicates the main hyperfine Fermi contact interaction is zero) to an extremely high value (1000 times the real value of C). The expansion coefficients $\alpha(\alpha')$ and $\beta(\beta')$ are calculated through the diagonalization of total Hamiltonian with increasing Fermi contact parameter C. Final results are shown in Table 25. As a result, the Fermi contact parameter C-dependence of the line strength is obtained and shown in Figures 13 to 16. The two pure hyperfine states $|^3P_1, 1/2\rangle$ and $|^3P_2, 3/2\rangle$ may be considered as two bent states where the nuclear spin $\vec{I}$ and total angular momentum of electrons $\vec{J}$ point in opposite directions. In contrast, the two pure hyperfine states $|^3P_0, 1/2\rangle$ and $|^3P_1, 3/2\rangle$ may be considered as two stretched states where the nuclear spin $\vec{I}$ and total angular momentum of electrons $\vec{J}$ point in the same direction. Similarly, $|^3S_1, 1/2\rangle$ is a bent state but $|^3S_1, 3/2\rangle$ a stretched state. The electric dipole transition can occur between stretched P state and stretched S state; or between bent P state and bent S state, since the electric dipole operator does not depend in any way on the nuclear spin $\vec{I}$, the component of the nuclear spin $\vec{I}$ in the direction of quantisation remains unaltered within the dipole radiation. However, as shown in Table 25, the strong hyperfine interaction causes such strong mixing of two pure hyperfine states that the component of $|^3P_1, 1/2\rangle$ dominates the component of $|^3P_0, 1/2\rangle$ in the true hyperfine state $|^3P_0, 1/2\rangle_{\text{true}}$, and the component of $|^3P_2, 3/2\rangle$ dominates the component of $|^3P_1, 3/2\rangle$ in the true hyperfine state $|^3P_1, 3/2\rangle_{\text{true}}$ at the strong hyperfine limit with large value of Fermi contact parameter C. Hence, the asymptotic form of the selection rules between the two true hyperfine states $|^3P_J, F\rangle_{\text{true}}$ and $|^3S_{J'}, F'\rangle_{\text{true}}$ are found to be that stretched states turn into bent states, or bent states turn into stretched states:

$$
\begin{array}{ccc}
 & 3P & 2S \\
F = J + I & \rightarrow & F' = J' - I \\
\text{(stretched)} & \rightarrow & \text{(bent)}
\end{array}
\tag{149}
$$

$$
\begin{array}{ccc}
F = J - I & \rightarrow & F' = J' + I \\
\text{(bent)} & \rightarrow & \text{(stretched)}
\end{array}
\tag{150}
$$

Table 25: The Fermi contact parameter C dependence of expansion Coefficient α and β

C	α	β	α'	β'	C	α	β	α'	β'
0	1	0	-1	0					
0.1	0.9992	-0.0385	-0.8443	0.5358	10	0.6262	-0.7795	-0.4117	0.9113
0.2	0.9968	-0.0787	-0.6295	0.7769	15	0.6098	-0.7925	-0.4105	0.9118
0.3	0.9927	-0.1200	-0.5466	0.8373	20	0.6016	-0.7987	-0.4099	0.9120
0.4	0.9868	-0.1617	-0.5079	0.8614	30	0.5935	-0.8048	-0.4094	0.9123
0.5	0.9791	-0.2033	-0.4858	0.8740	40	0.5894	-0.8077	-0.4091	0.9124
0.6	0.9697	-0.2444	-0.4717	0.8817	50	0.5870	-0.8095	-0.4089	0.9125
0.7	0.9590	-0.2833	-0.4619	0.8868	100	0.5821	-0.8130	-0.4085	0.9127
0.8	0.9471	-0.3207	-0.4578	0.8905	200	0.5797	-0.8147	-0.4084	0.9128
0.9	0.9345	-0.3558	-0.4492	0.8933	500	0.5783	-0.8158	-0.4083	0.9128
1	0.9214	-0.3885	-0.4449	0.8955	1000	0.5778	-0.8161	-0.4082	0.9129
2	0.8052	-0.5930	-0.4260	0.9046					
3	0.7378	-0.6749	-0.4200	0.9075					
4	0.6994	-0.7146	-0.4170	0.9088					
5	0.6754	-0.7374	-0.4152	0.9097					
6	0.6591	-0.7519	-0.4140	0.9102					
7	0.6474	-0.7621	-0.4132	0.9106					
8	0.6386	-0.7695	-0.4126	0.9109					
9	0.6317	-0.7751	-0.4121	0.9111					

Figure 13: The Fermi contact parameter C dependence of line strength of transition $2\ ^3S_1, 3/2$ to $3\ ^3P_J, F$

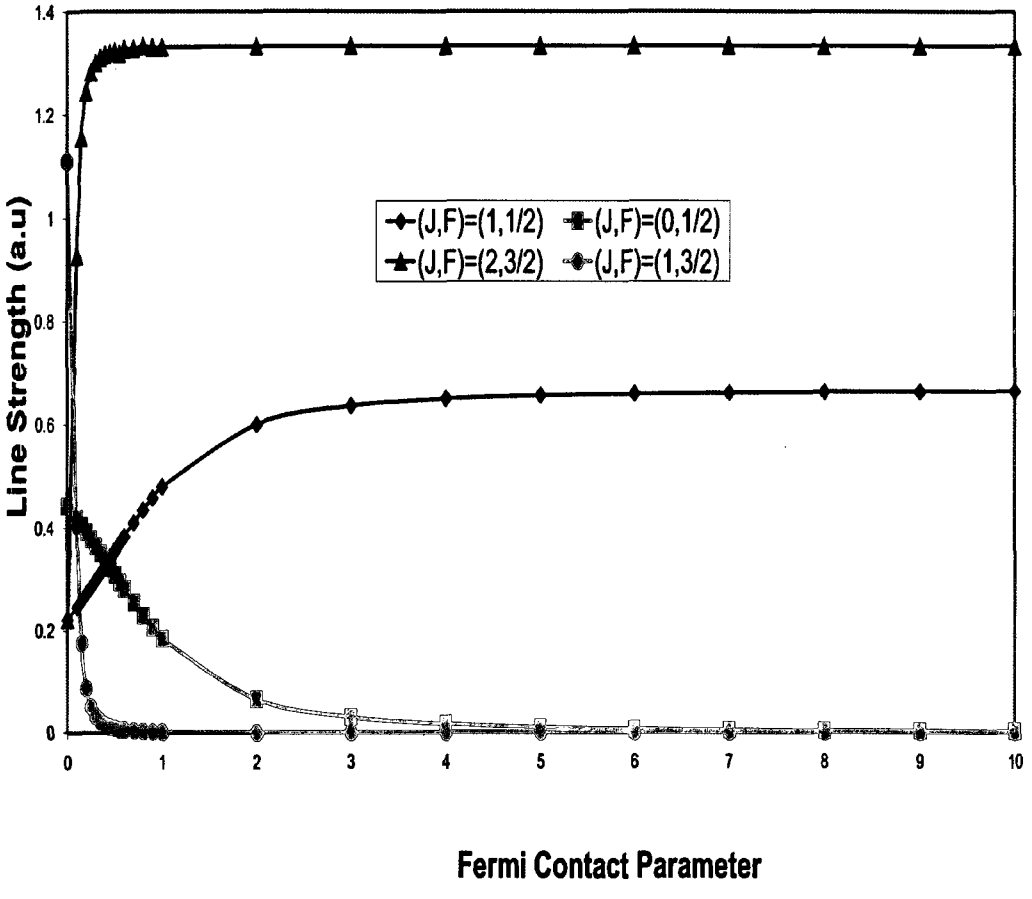

Figure 14: The Fermi contact parameter C dependence of line strength of transition $2\ ^3\mathrm{S}_1, 3/2$ to $3\ ^3\mathrm{P}_J, F$

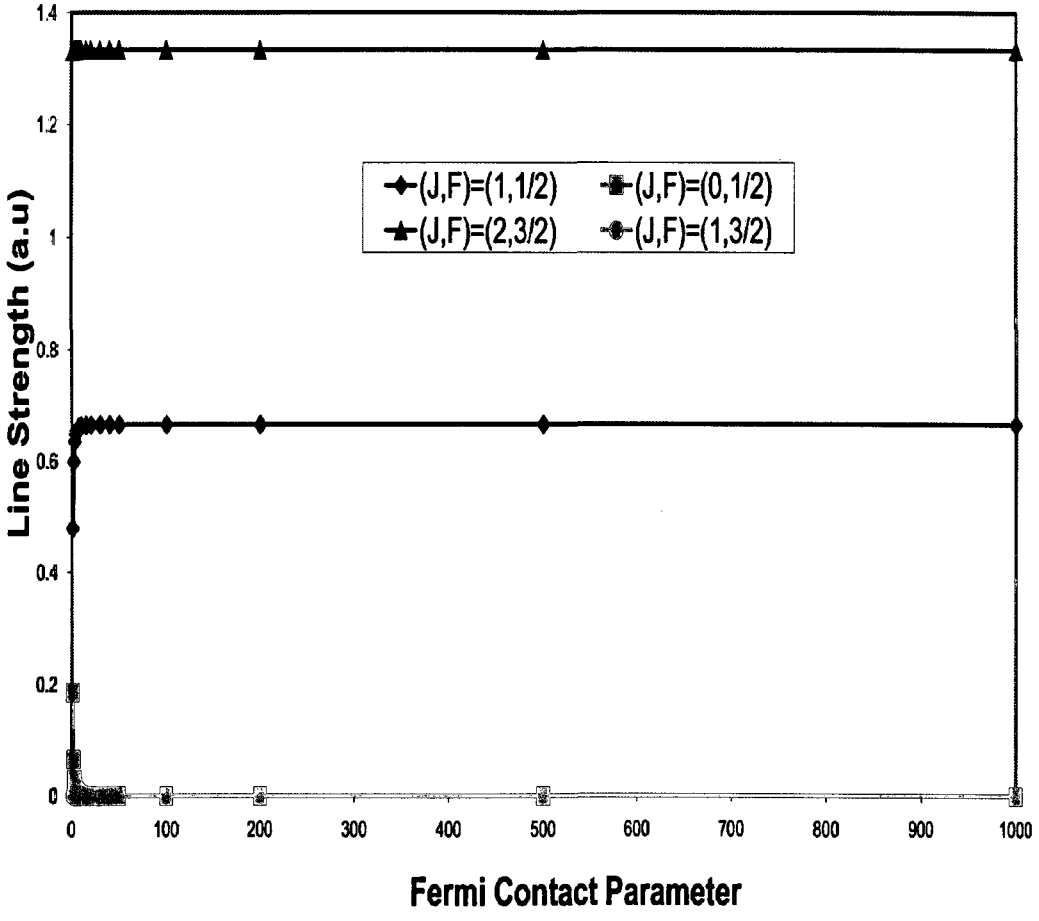

Figure 15: The Fermi contact parameter C dependence of line strength of transition $2\,^3\mathrm{S}_1, 1/2$ to $3\,^3\mathrm{P}_J, F$

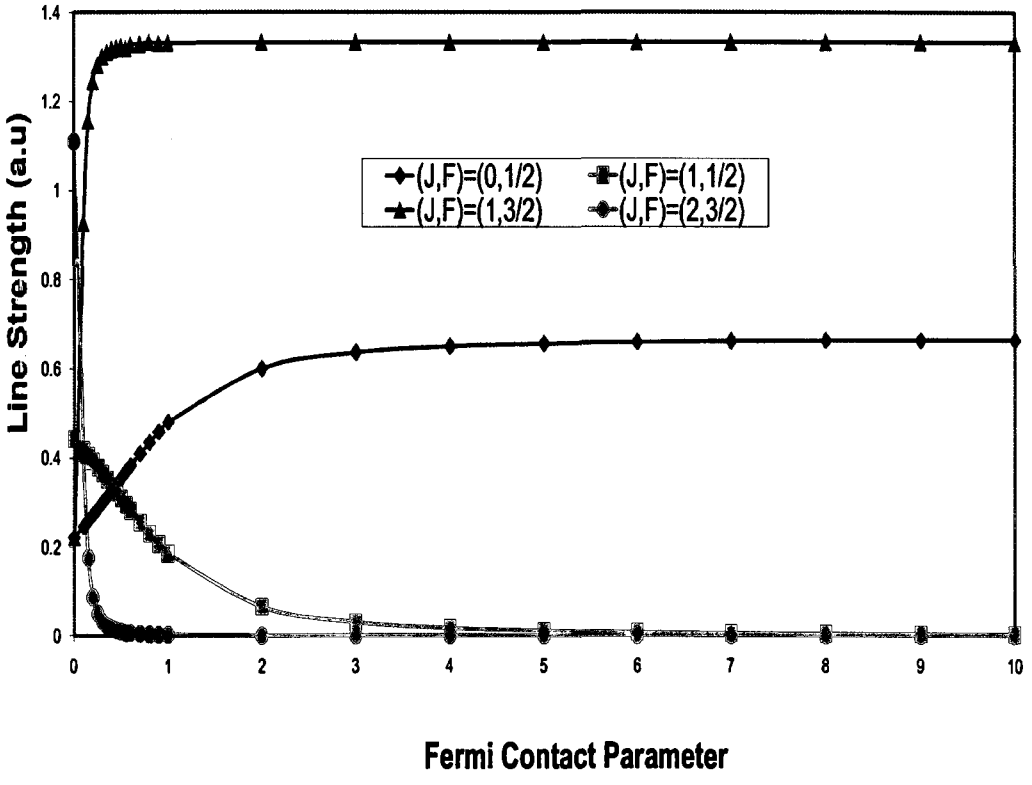

Figure 16: The Fermi contact parameter C dependence of line strength of transition $2\ ^3S_1, 1/2$ to $3\ ^3P_J, F$

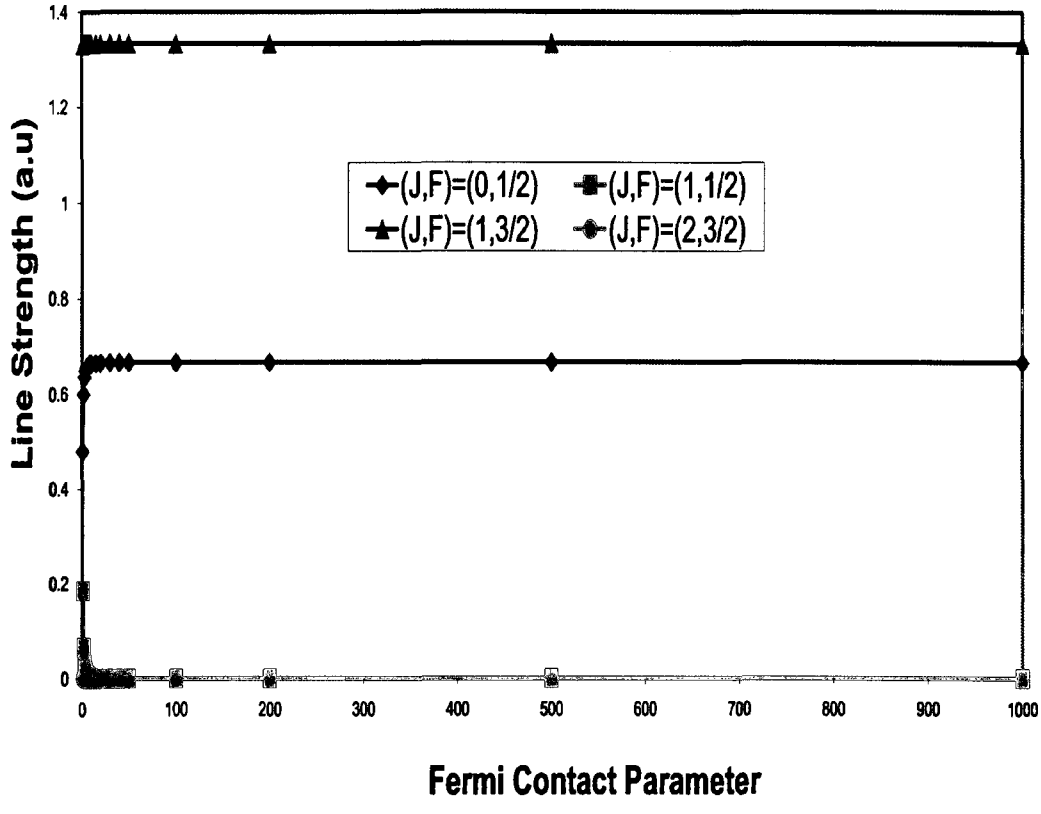

4.8 Hyperfine Suppression of $2\,^3S_1$ to $n\,^3P_J$ Radiative Transition in ^{3}He

Sections 4.1 to 4.7 discuss hyperfine suppression of the $2\,^3S_1$ to $3\,^3P_J$ radiative transition in ^{3}He in theory and experiment. It is interesting to extend this theory to transitions of $2\,^3S_1$ to $n\,^3P_J$, $n = 2$ to 10, which will lead to a deeper understanding of hyperfine suppression of ^{3}He. For transitions 2S to nP instead of the 2S to 3P transition , no extra technique is needed to calculate hyperfine transitions, except for using different double basis set wave functions of Drake to calculate fine structure and hyperfine structure parameters and coefficients of expansion with respect to a particular P state. The final results for the line strengths of hyperfine transitions are tabulated in Appendix A (weak intercombination transitions between singlet state and triplet state are included). However, in order to understand the strong hyperfine interaction limit as described in the previous section, special attention is paid here to hyperfine transitions between triplet states $2\,^3S_1$ and $n\,^3P_J$. The state dependence of the line strength of electric dipole transitions is shown in Figure 17 and Figure 18. The variation of line strength with principal quantum number n of the excited electron of ^{3}He as shown in Figures 17-18 has the same trend as the variation of line strength with Fermi contact parameter as shown previously in Figures 13-14. It is not a surprise since the fine structure interaction decreases as $1/n^3$, but the hyperfine structure interaction on the other hand, for large n tends to a constant at the series limit. Figures 13-14 keep the fine structure interaction constant for 3P state but artificially increase hyperfine interaction mainly specified by Fermi contact parameter C. Figures 17-18 show decreasing the fine structure interaction because of $1/n^3$ law, but keeping hyperfine structure interaction tending to series limit ($C = -4283.850$MHz for 2P state, $C = -4332.467$MHz for 10P state, and $C = -4332.825$MHz for $^3He^+$ as calculated in previous work [62]). Both are physically equivalent to each other. In addition, the variation of line strength with higher principal quantum number n calculated

in Appendix A and shown in Figure 17 numerically verifies our early prediction in section 4.5 that the IS coupling model should rapidly become more accurate with increasing n.

Figure 17: State dependence of the line strength of hyperfine transitions $2\ ^3S_1, 3/2$ to $n\ ^3P_1, 3/2$ and $2\ ^3S_1, 3/2$ to $n\ ^3P_0, 1/2$, where n is the principal quantum number used to specify the excited electron of ^3He.

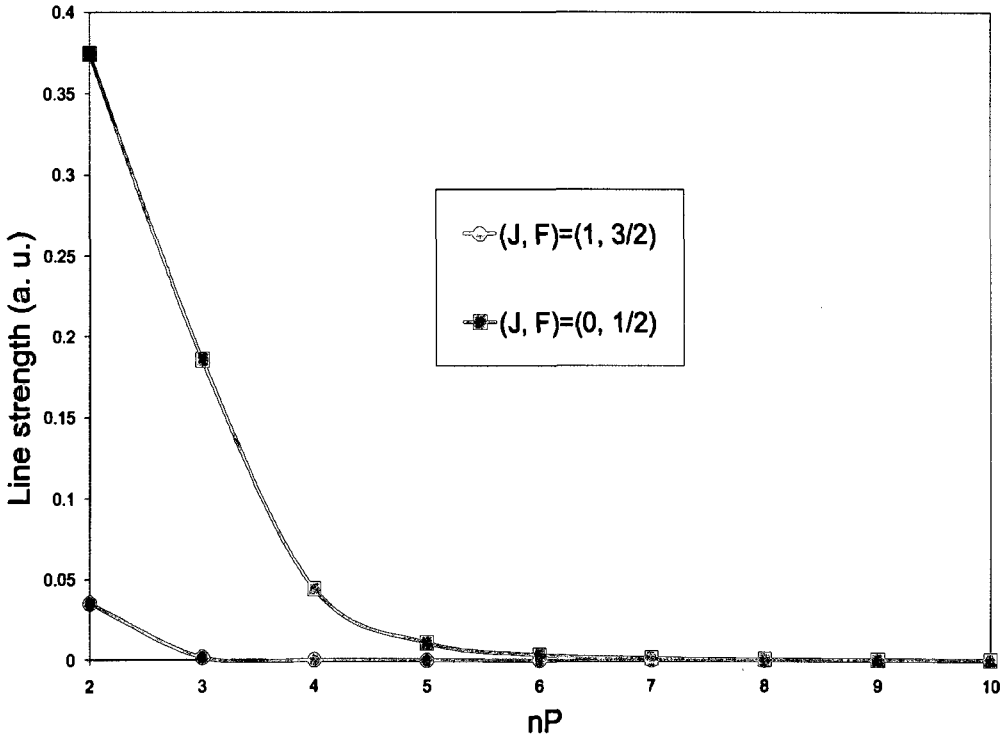

Figure 18: State dependence of the line strength of hyperfine transitions $2\ ^3S_1, 3/2$ to $n\ ^3P_1, 1/2$ and $2\ ^3S_1, 3/2$ to $n\ ^3P_2, 3/2$, where n is the principal quantum number used to specify the excited electron of ^3He.

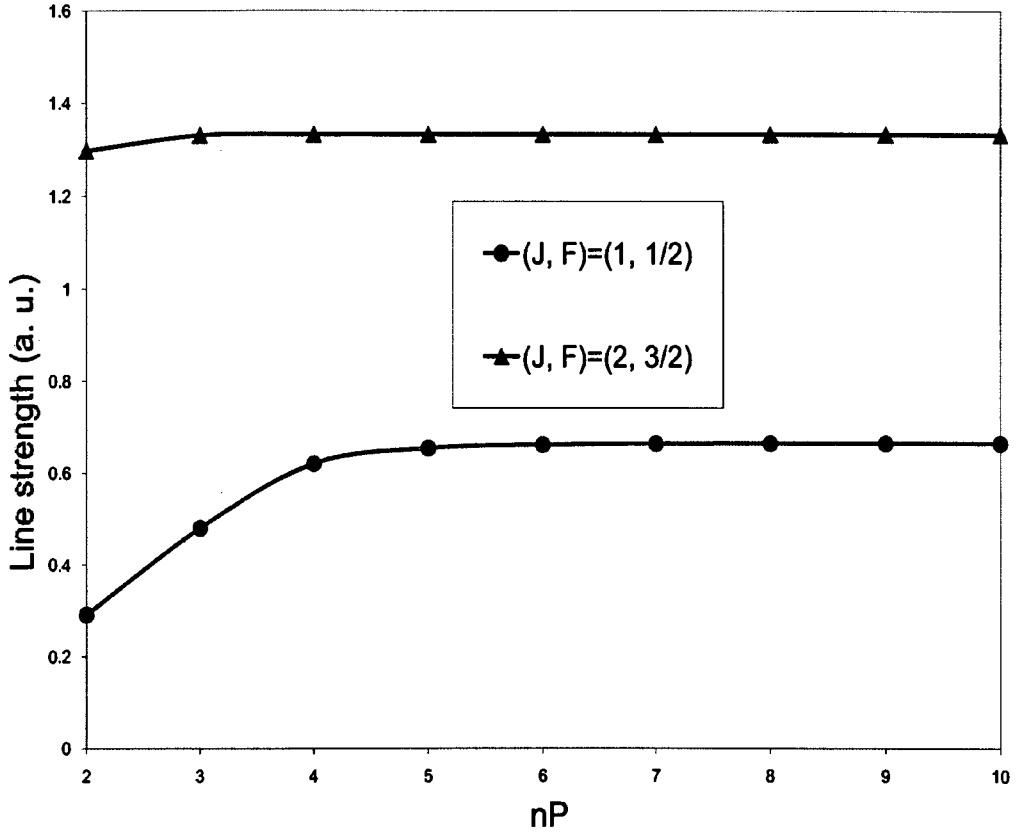

5 Hyperfine Induced Transition $n\,^{1,3}\mathrm{D}$ to $2\,^{1,3}\mathrm{P}$ in $^3\mathrm{He}$

5.1 Transition Operator and Transition Rate

Based on the definition of Fisher [63], the electric and magnetic transition operator $O_q^{(K)}$ as a spherical tensor of rank K can be expressed as

- Electric transition operator with parity of $(-1)^K$

$$E_q^{(K)} = \sum_{i=1}^{N} r_i^K C(i)_q^{(K)} \tag{151}$$

where N is the total number of electrons in the atomic system. r_i is radial coordinate of the ith electron, and $C_q^{(K)}$ is a rank-K spherical harmonic function.

- Magnetic transition operator with parity of $(-1)^{(K-1)}$

$$M_q^{(K)} = \alpha\,[K(2K-1)]^{\frac{1}{2}} \left[\frac{1}{K+1} MA_q^{(K)} + \frac{1}{2} g_s MB_q^{(K)}\right] \tag{152}$$

where α is the fine structure constant, g_s is g factor of electron, and $MA_q^{(K)}$ and $MB_q^{(K)}$ are

$$MA_q^{(K)} = \sum_{i=1}^{N} r_i^{(K-1)} \left[C(i)^{(K-1)} \bigotimes l_i^{(1)}\right]_q^{(K)} \tag{153}$$

$$MB_q^{(K)} = \sum_{i=1}^{N} r_i^{(K-1)} \left[C(i)^{(K-1)} \bigotimes s_i^{(1)}\right]_q^{(K)} \tag{154}$$

and l_i and s_i represent orbital and spin angular momentum, respectively. The coupling tensor operators are

$$\left[C^{(K-1)} \bigotimes l^{(1)}\right]_q^{(K)} = \sum_{q_1,q_2} \langle K-1,1,q_1,q_2|K-1,1,K,q\rangle C_{q_1}^{(K-1)} l_{q_2}^{(1)} \tag{155}$$

$$\left[C^{(K-1)} \bigotimes s^{(1)}\right]_q^{(K)} = \sum_{q_1,q_2} \langle K-1,1,q_1,q_2|K-1,1,K,q\rangle C_{q_1}^{(K-1)} s_{q_2}^{(1)} \tag{156}$$

The transition rate for emission from upper energy level $E_{\gamma' J'}$ to lower energy level $E_{\gamma J}$ is

$$A^{(K)}(\gamma' J';\gamma J) = 2C_K \left[\alpha(E_{\gamma' J'} - E_{\gamma J})\right]^{(2K+1)} \frac{S^{(K)}(\gamma' J';\gamma J)}{g_{J'}} \tag{157}$$

where

$$g_{J'} = 2J' + 1 \tag{158}$$

$$C_K = \frac{(2K+1)(K+1)}{K[(2K+1)!!]^2} \tag{159}$$

and

$$S^{(K)}(\gamma' J';\gamma J) = |\langle \gamma J||O^{(K)}||\gamma' J'\rangle|^2 \tag{160}$$

representing the line strength of the transition from $E_{\gamma' J'}$ to $E_{\gamma J}$. By the Wigner-Eckart theorem, the relation between the matrix element and the reduced matrix element is

$$\langle \gamma' J', M'_{J'}|O_q^k|\gamma J, M_J\rangle = (-1)^{J'-M'_{J'}} \begin{pmatrix} J' & K & J \\ -M'_{J'} & q & M_J \end{pmatrix} \langle \gamma' J'\|O^k\|\gamma J\rangle \tag{161}$$

It follows from Equation (157) that

$$A^{(K)}(E) \propto \alpha^{2K+1} \tag{162}$$

$$A^{(K)}(M) \propto \alpha^{2K+3}, \tag{163}$$

which gives the relative size of the rate for the different multipole transitions. It is clear that the largest transition rate will, in general, be for electric dipole (E1) radiation, dominating by at least a factor $\frac{1}{\alpha^2}$ over other types of transitions ($E^{(2)}$ and $M^{(1)}$ have the same order of magnitude α^5).

5.2 Selection Rules

According to standard angular momentum theory, the reduced matrix elements of transition operator may be expressed as (notation $[a, b, c...] = (2a+1)(2b+1)(2c+1)...$ is used here).

$$\begin{aligned}\langle \gamma LSJ||E^{(K)}||\gamma' L'S'J'\rangle &= \delta_{S,S'}(-1)^{L+S+J'+K}[J,J']^{\frac{1}{2}} \left\{ \begin{array}{ccc} L & S & J \\ J' & K & L \end{array} \right\} \\ &\quad \langle \gamma L||E^{(K)}||\gamma' L'\rangle \end{aligned} \tag{164}$$

$$\begin{aligned}\langle \gamma LSJ||MA^{(K)}||\gamma' L'S'J'\rangle &= \delta_{S,S'}(-1)^{L+S+J'+K}[J,J']^{\frac{1}{2}} \left\{ \begin{array}{ccc} L & S & J \\ J' & K & L \end{array} \right\} \\ &\quad \langle \gamma L||MA^{(K)}||\gamma' L'\rangle \end{aligned} \tag{165}$$

$$\begin{aligned}\langle \gamma LSJ||MB^{(K)}||\gamma' L'S'J'\rangle &= \sum_{i=1}^{N}[J,K,J']^{\frac{1}{2}} \left\{ \begin{array}{ccc} L & S & J \\ L' & S' & J' \\ K-1 & 1 & K \end{array} \right\} \\ &\quad \langle \gamma L||r_i^{K-1}C(i)^{(K)}||\gamma' L'\rangle \langle S||s_i^{(1)}||S'\rangle \end{aligned} \tag{166}$$

where $\left\{ \begin{array}{ccc} L & S & J \\ J' & K & L \end{array} \right\}$ is the $6j$ symbol. $\left\{ \begin{array}{ccc} L & S & J \\ L' & S' & J' \\ K-1 & 1 & K \end{array} \right\}$ is the $9j$ symbol.

The selection rules for E1, M1 and E2 may be obtained from the properties of the $6j$ symbol in Equations (164)-(165), the $9j$ symbol in Equation (166) and parities of transition operators $E^{(K)}$ and $M^{(K)}$:

- E1

$\triangle S = 0 \quad \triangle L = \pm 1 \quad \triangle J = 0, \pm 1 \; (J + J' \geq 1)$

- M1

$\triangle S = 0, \pm 1 \quad \triangle L = 0 \quad \triangle J = 0, \pm 1 \; (J + J' \geq 1)$

- E2

$\triangle S = 0 \quad \triangle L = 0, \pm 2 \quad \triangle J = 0, \pm 1, \pm 2 \; (J + J' \geq 2)$

5.3 Hyperfine-induced Transition (HFI)

5.3.1 Review of Literature

Historically, in atomic spectroscopy, all transitions which violate the rigorous selection rules for electric dipole radiation in free atoms are termed forbidden transitions [64]. This category includes all magnetic dipole and electric quadrupole transitions, two-photon processes, electric dipole radiation enforced by perturbation external to the atom and electric dipole radiation caused by the atomic nuclei. Among the early discoveries of forbidden transitions were two lines of Hg I. Rayleigh [65] observed the line $6s^2\,{}^1S_0 - 6s6p\,{}^3P_2$ and Fukuda [66] observed $6s^2\,{}^1S_0 - 6s6p\,{}^3P_0$. The former line is rigorously forbidden for electric dipole and magnetic dipole ra-

diation because $\Delta J = 2$, and for electric quadrupole radiation by the parity rule. The second line is forbidden for all types of radiation from $J = 0$ to $J' = 0$. In Ref. [67], Bowen first suggested that a nuclear interaction with the outer electrons was responsible. Many nuclei have magnetic moments, and these interact with the magnetic fields produced by the orbit motion of the electrons. Bowen's suggestion was confirmed by Mrozowski [68]. Detailed discussions of these forbidden transitions in Mg, Zn, Cd, and Hg have been given by Garstang [69]. For those isotopes with nonzero nuclear spin, the hyperfine interactions mix the states with different total angular momentum of electron J, which opens a new decay channel and shortens the lifetimes of certain states. This phenomenon in atomic physics is often referred to as *hyperfine quenching* [70]. Since the pioneering works of Mohr [71], who studied hyperfine quenching of the $2\ ^3P_0$ state in heliumlike ions ($Z = 9$ to 29) by means of a Z^{-1} expansion calculation, hyperfine quenching has been a important subject for theoretical and experimental investigations in atomic physics. Experimentally, hyperfine quenching in heliumlike ions was first observed by Gould, Marrus and Mohr [72], who found that hyperfine effects contributed appreciably to the decay rates of the $2\ ^3P_2$ level in V^{21+}. Dunford [73] directly observed hyperfine quenching of the $2\ ^3P_0$ level in heliumlike $^{61}N_i^{26+}$. Marrus [74] and Bruce [75] even determined the absolute value of the fine structure splitting $2\ ^3P_0 - 2\ ^3P_1$ from the hyperfine-quenched lifetime of the $2\ ^3P_0$ state of heliumlike ion Ag^{45+}. More accurate lifetimes allowing experimental verification were repeated by Engstrom [77]. These experiments with those of Denne [78] and Livingston and Hinterlong [79] for Al^{11+} and P^{13+} respectively all confirmed the theoretical predictions of Mohr [71]. Theoretically, Indelicato [80] used the multiconfiguration Dirac-Fock method to extensively calculate hyperfine quenching rates of $2\ ^3P_0$ and $2\ ^3P_1$ for heliumlike ions from $Z = 45$ to $Z = 71$. Aboussaid [81] investigated the hyperfine quenching of the $2\ ^3P_0$ for the heliumlike ions $^{19}F^{7+}$, $^{23}Na^{9+}$ and $^{27}Al^{11+}$ in the multiconfiguration-Hartree-Fock-Breit-Pauli scheme. More recently, Johnson [82]

used a radiation damping formalism to calculate extensively hyperfine quenching rates of $2\,^3P_0$ state for all stable isotopes in the range $Z = 6$ to 92.

For clarity, the basic ideas behind hyperfine quenching for the $2\,^3P_0$ state in heliumlike ion is briefly presented here. Details may be found in Refs. [81, 82]. The lifetime of the $2\,^3P_0$ state, which normally decays to the $2\,^3S_1$ state by an allowed electric dipole transition E1, is shortened by the new decay channel $2\,^3P_0 \rightarrow 1\,^1S_0$. Two kinds of mixing are considered in the calculation of hyperfine quenching of the $2\,^3P_0$ state. They are (i) direct hyperfine mixing with the $2\,^1P_1$ state and (ii) hyperfine mixing with the $2\,^3P_1$ state combined with fine structure interaction mixing of $2\,^3P_1$ and $2\,^1P_1$ (so-called intercombination transition(IC) or spin-forbidden transition). Figure 19 shows the transitions of E1, E1(HFI), and E1(IC).

The following equations demonstrate both kinds of mixing:

- Mixing due to fine structure interaction:

$$|2\,^1P_1\rangle_{\text{true}} = a|2\,^1P_1\rangle + b|2\,^3P_1\rangle \tag{167}$$

$$|2\,^3P_1\rangle_{\text{true}} = -b|2\,^1P_1\rangle + a|2\,^3P_1\rangle \tag{168}$$

- Mixing due to hyperfine structure interaction:

$$\begin{aligned} |2\,^3P_0 IF\rangle_{\text{true}} &= \alpha|2\,^1P_1 IF\rangle + \beta|2\,^3P_0 IF\rangle + \gamma|2\,^3P_1 IF\rangle \\ &\quad +\delta|2\,^3P_2 IF\rangle \end{aligned} \tag{169}$$

Figure 19: Energy level diagram of 1S, 2S, and 2P multiplicity in heliumlike ions. The level position is not drawn to scale. Electric dipole transitions E1, E1(HFI), and E1(IC) are shown in the diagram. The dashed line shows the hyperfine-induced transition of $2\ ^3P_0 - 1\ ^1S_0$ due to hyperfine mixing between the $2\ ^3P_0$ and $2\ ^3P_1$ states.

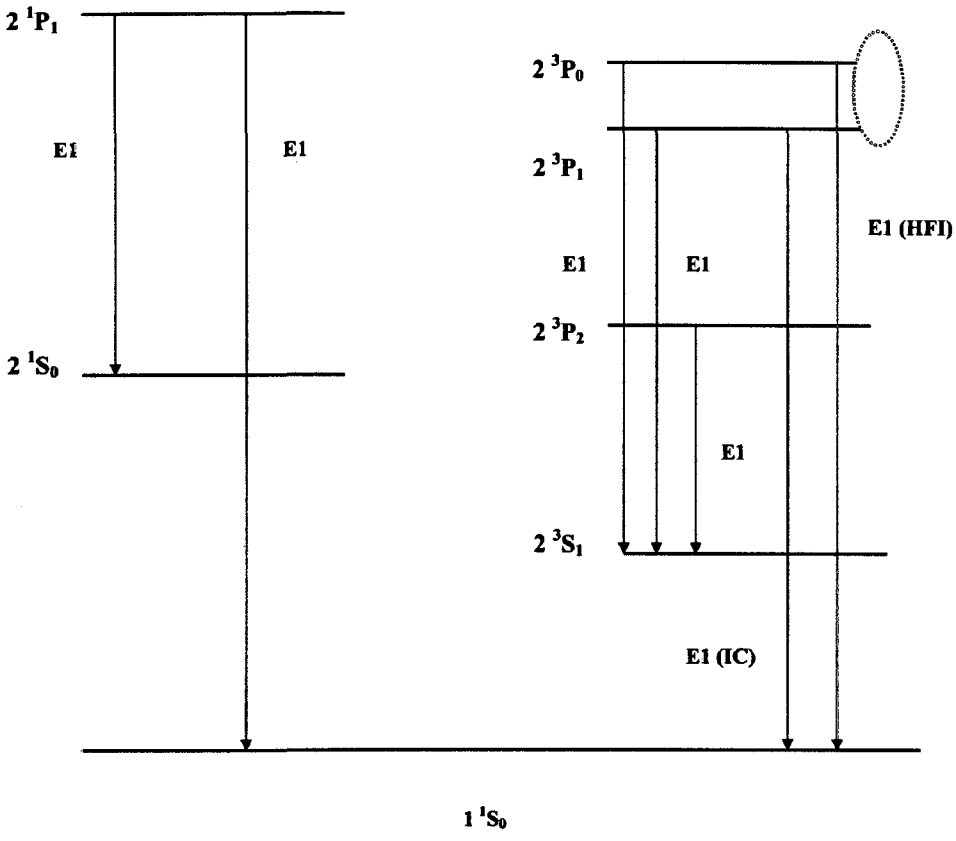

where a and b are expansion coefficients due to the fine structure interaction, and α, β, γ and δ are expansion coefficients due to the hyperfine structure interaction. I is nuclear spin and F is total angular momentum.

Finally, the hyperfine quenching rate of $2\ ^3\mathrm{P}_0$ state is obtained by the following equation:

$$A(\mathrm{HFI}) \propto |\langle 1\ ^1S_0 IF||D^{(1)}||2\ ^3P_0 IF\rangle_{\mathrm{true}}|^2 \tag{170}$$

where $D^{(1)} = e\vec{r}_1 + e\vec{r}_2$ represents the rank-one tensor of electric dipole operator of helium or heliumlike ion. F in Equations (169) to (170) satisfies $F = I$ since $J = 0$.

In the literature, however, all the theory and experiment concerning hyperfine quenching in heliumlike ions treated only the more highly charged cases (Mohr for $Z = 9$ to 29 [71]; Indelicato for $Z = 45$ to 71 [80]; Johnson for $Z = 6$ to 92 [82]), since the singlet-triplet mixing caused by fine and hyperfine interactions is so small for low-Z ions that hyperfine-induced transition $2\ ^3\mathrm{P}_0 - 1\ ^1\mathrm{S}_0$ is difficult to observe. This is clearly demonstrated by Johnson's calculation [82]. Table 26 shows their calculated hyperfine quenching rates $A(hf)$ of the $2\ ^3\mathrm{P}_0$ state of heliumlike ions in the range $Z = 6$ to 50 and comparison with decay rates A_0 for allowed E1 transition in $2\ ^3\mathrm{P}_0 - 2\ ^3\mathrm{S}_1$.

Table 26: Hyperfine quenching of 2 $^3P_0$ state of heliumlike ions with nuclear charges in the range $Z = 6$ to 50. A_{hf} shows the values of the hyperfine-induced 2 $^3P_0 - 1\ ^1S_0$ transition rate. A_0 is the normal 2 $^3P_0 - 2\ ^3S_1$ E1 transition rate (from Johnson [82]).

Ion	Z	I	$A_0(\mathrm{ns}^{-1})$	$A_{hf}(\mathrm{ns}^{-1})$
^{13}C	6	$\frac{1}{2}$	0.05652	0.00011
^{14}N	7	1	0.06770	0.00086
^{15}N	7	$\frac{1}{2}$	0.06770	0.00054
^{17}O	8	$\frac{5}{2}$	0.07902	0.00260
^{19}F	9	$\frac{1}{2}$	0.09054	0.01391
^{21}Ne	10	$\frac{3}{2}$	0.01023	0.0006
^{41}Ca	20	$\frac{7}{2}$	0.02412	0.3095
^{67}Zn	30	$\frac{5}{2}$	0.4493	4.373
^{91}Zr	40	$\frac{5}{2}$	0.7884	561.6
^{115}Sn	50	$\frac{1}{2}$	1.363	4554

5.3.2 Hyperfine-induced Transition from $n\ ^{1,3}$D to 2 ^{1,3}P in ^{3}He

As described previously, the hyperfine-induced transition rate for 2 $^3P_0 - 1\ ^1S_0$ is very weak compared with normal E1 transition 2 $^3P_0 - 2\ ^3S_1$ for low-Z heliumlike ions. The same is expected to be true when extended to ^{3}He ($Z = 2$). However, the present work has found theoretically that even for ^{3}He, the hyperfine-induced transitions in $n\ ^3D - 2\ ^1P$ and $n\ ^1D - 2\ ^3P$ with higher n (9 or 10) have comparable intensities to normal E1 transition between two hyperfine states.

Equations (53) to (63) in Section 3 are still applicable to hyperfine structure calculations for D states. For the sake of comparison, fine structure parameters and hyperfine structure parameters for nD (n = 3, 9, 10) are precisely calculated by using the double basis wave function in Hylleraas coordinates. The calculated values of parameters are listed in Tables 27 to 29.

Table 27: Δ', E_0, and E_1' are the 3 $^1D_2$–3 $^3D_3$, 3 $^3D_1$–3 $^3D_3$ and 3 $^3D_2$–3 $^3D_3$ energy level separation before diagonalization, respectively. E_M is the off-diagonal matrix element. $C_{S,S'}$, D_S, and $E_{S,S'}$ are the hyperfine structure parameters. Units are MHz.

fine structure parameter		hyperfine structure parameter	
Δ'	102 433.57	C_{11}	−4332.241
E_0	1400.246	C_{10}	−4332.294
E_1'	100.277	D_1	−2.276
E_2	0.	D_0	−2.266
E_M	−1599.180	E_{11}	0.239
		E_{10}	0.316

Table 28: Δ', E_0, and E_1' are the 9 $^1D_2$–9 $^3D_3$, 9 $^3D_1$–9 $^3D_3$ and 9 $^3D_2$–9 $^3D_3$ energy level separation before diagonalization, respectively. E_M is the off-diagonal matrix element. $C_{S,S'}$, D_S, and $E_{S,S'}$ are the hyperfine structure parameters. Units are MHz.

fine structure parameter		hyperfine structure parameter	
Δ'	6655.992	C_{11}	−4332.793
E_0	51.906	C_{10}	−4332.797
E_1'	3.963	D_1	−0.085
E_2	0.	D_0	−0.084
E_M	−59.107	E_{11}	0.009
		E_{10}	0.012

Table 29: Δ', E_0, and E_1' are the 10 $^1D_2$–10 $^3D_3$, 10 $^3D_1$–10 $^3D_3$ and 10 $^3D_2$–10 $^3D_3$ energy level separation before diagonalization, respectively. E_M is the off-diagonal matrix element. $C_{S,S'}$, D_S, and $E_{S,S'}$ are the hyperfine structure parameters. Units are MHz.

fine structure parameter		hyperfine structure parameter	
Δ'	4902.197	C_{11}	−4332.805
E_0	37.837	C_{10}	−4332.804
E_1'	2.893	D_1	−0.062
E_2	0.	D_0	−0.061
E_M	−43.084	E_{11}	0.007
		E_{10}	0.009

With available fine structure parameters and hyperfine structure parameters, the hyperfine structure can be obtained by diagonalizing the complete matrix of fine and hyperfine interactions in the basis set of $1snd\ ^1\mathrm{D}$ and $1snd\ ^3\mathrm{D}$ states. Our calculations show that the mixing between hyperfine states (including singlet and triplet states) of nD with different J but the same F of ^{3}He plays an important role in hyperfine structure and hyperfine transition strength.

The line strength of electric dipole transitions between hyperfine states of nD and 2P are the form:

$$S = |\langle 2\ ^{1,3}\mathrm{P}(J,F)\|{r_1}^{(1)} + {r_2}^{(1)}\|n\ \mathrm{D}^{1,3}(J',F')\rangle_{\mathrm{true}}|^2 \tag{171}$$

where the two true hyperfine states are:

$$\begin{aligned} |2\ ^{1,3}\mathrm{P(J,F)}\rangle_{\mathrm{true}} &= c_1|2\ ^1\mathrm{P}_1\ 1/2\rangle + c_2|2\ ^1\mathrm{P}_1\ 3/2\rangle + c_3|2\ ^3\mathrm{P}_0\ 1/2\rangle + \\ &\quad c_4|2\ ^3\mathrm{P}_1\ 1/2\rangle + c_5|2\ ^3\mathrm{P}_1\ 3/2\rangle + c_6|2\ ^3\mathrm{P}_2\ 3/2\rangle + \\ &\quad c_7|2\ ^3\mathrm{P}_2\ 5/2\rangle \end{aligned} \tag{172}$$

$$\begin{aligned} |n\ ^{1,3}\mathrm{D}(J,F)\rangle_{\mathrm{true}} &= c_1|n\ ^1\mathrm{D}_2\ 3/2\rangle + c_2|n\ ^1\mathrm{D}_2\ 5/2\rangle + c_3|n\ ^3\mathrm{D}_1\ 1/2\rangle + \\ &\quad c_4|n\ ^3\mathrm{D}_1\ 3/2\rangle + c_5|n\ ^3\mathrm{D}_2\ 3/2\rangle + c_6|n\ ^3\mathrm{D}_2\ 5/2\rangle + \\ &\quad c_7|n\ ^3\mathrm{D}_3\ 5/2\rangle + c_8|n\ ^3\mathrm{D}_3\ 7/2\rangle \end{aligned} \tag{173}$$

All expansion coefficients are determined by diagonalization of the complete Hamiltonian matrix and summarized in Tables 30 to 33, and the induced matrix element S(IME) between any two pure hyperfine states can be calculated by the equation:

$$S(\mathrm{IME}) = |\langle \gamma LSJIF\|{r_1}^{(1)} + {r_2}^{(1)}\|\gamma' L'S'J'IF'\rangle|^2 \tag{174}$$

which leads to

$$S(\text{IME}) = [(2J+1)(2J'+1)(2F+1)(2F'+1)] \left\{ \begin{array}{ccc} J & F & I \\ F' & J' & 1 \end{array} \right\}^2 \left\{ \begin{array}{ccc} L & J & S \\ J' & L' & 1 \end{array} \right\}^2 \delta_{S,S'} |\langle \gamma L \| {r_1}^{(1)} + {r_2}^{(1)} \| \gamma' L' \rangle|^2 \quad (175)$$

where $|\langle \gamma L \| {r_1}^{(1)} + {r_2}^{(1)} \| \gamma' L' \rangle|^2$ is a common factor for a given transition line.

Table 30: The expansion coefficients for 2P state. Numbers in brackets represent powers of 10.

coefficient	$^1P_1, F = \frac{1}{2}$	$^1P_1, F = \frac{3}{2}$	$^3P_0, F = \frac{1}{2}$	$^3P_1, F = \frac{1}{2}$
c_1	0.999 9999	0	0.000 0099	0.000 2310
c_2	0	0.999 9999	0	0
c_3	–0.000 0347	0	0.994 2161	0.107 3972
c_4	–0.000 2286)	0	–0.107 3972	0.994 2161
c_5	0	–0.000 3028	0	0
c_6	0	0.000 0551	0	0
c_7	0	0	0	0

coefficient	$^3P_2, F = \frac{3}{2}$	$^3P_1, F = \frac{3}{2}$	$^3P_2, F = \frac{5}{2}$
c_1	0	0	0
c_2	0.000 2220	–0.000 2131	0
c_3	0	0	0
c_4	0	0	0
c_5	0.833 8454	–0.551 9979	0
c_6	0.551 9979	0.833 8454	0
c_7	0	0.	1

Table 31: The expansion coefficients for 3D state. Numbers in brackets represent powers of 10.

coefficient	$^1D_2, F = \frac{3}{2}$	$^1D_2, F = \frac{5}{2}$	$^3D_1, F = \frac{1}{2}$	$^3D_1, F = \frac{3}{2}$
c_1	0.999 5755	0	0	0.027 8879
c_2	0	0.998 8604	0	0
c_3	0	0	1	0
c_4	–0.026 8710	0	0	0.770 6077
c_5	0.011 2598	0	0	–0.636 6994
c_6	0	–0.033 4636	0	0
c_7	0	0.034 0320	0	0
c_8	0	0	0	0

coefficient	$^3D_2, F = \frac{3}{2}$	$^3D_2, F = \frac{5}{2}$	$^3D_3, F = \frac{5}{2}$	$^3D_3, F = \frac{7}{2}$
c_1	0.008 4319	0	0	0
c_2	0	0.013 6315	–0.045 7403	0
c_3	0	0	0	0
c_4	0.636 7431	0	0	0
c_5	0.771 0299	0	0	0
c_6	0	0.883 3543	–0.467 5098	0
c_7	0	0.468 5077	0.882 8037	0
c_8	0	0	0	1

Table 32: The expansion coefficients for 9D state. Numbers in brackets represent powers of 10.

coefficient	$^1D_2, F = \frac{3}{2}$	$^1D_2, F = \frac{5}{2}$	$^3D_1, F = \frac{1}{2}$	$^3D_1, F = \frac{3}{2}$
c_1	0.804 8208	0	0	0.593 5030
c_2	0	0.804 2489	0	0
c_3	0	0	1	0
c_4	–0.422 6029	0	0	0.568 0603
c_5	0.416 7377	0	0	–0.570 1418
c_6	0	–0.283 4036	0	0
c_7	0	0.522 3658	0	0
c_8	0	0	0	0

coefficient	$^3D_2, F = \frac{3}{2}$	$^3D_2, F = \frac{5}{2}$	$^3D_3, F = \frac{5}{2}$	$^3D_3, F = \frac{7}{2}$
c_1	0.004 2114	0	0	0
c_2	0	0.007 7339	–0.594 2422	0
c_3	0	0	0	0
c_4	0.706 1971	0	0	0
c_5	0.708 0028	0	0	0
c_6	0	0.883 8875	–0.372 0556	0
c_7	0	0.467 6357	0.713 0574	0
c_8	0	0	0	1

Table 33: The expansion coefficients for 10D state. Numbers in brackets represent powers of 10.

coefficient	$^1D_2, F = \frac{3}{2}$	$^1D_2, F = \frac{5}{2}$	$^3D_1, F = \frac{1}{2}$	$^3D_1, F = \frac{3}{2}$
c_1	0.732 6528	0	0	0.680 5899
c_2	0	0.733 2020	0	0
c_3	0	0	1	0
c_4	–0.483 5537	0	0	0.516 2211
c_5	0.478 9527	0	0	–0.519 9166
c_6	0	–0.322 9501	0	0
c_7	0	0.598 4297	0	0
c_8	0	0	0	0

coefficient	$^3D_2, F = \frac{3}{2}$	$^3D_2, F = \frac{5}{2}$	$^3D_3, F = \frac{5}{2}$	$^3D_3, F = \frac{7}{2}$
c_1	0.004 16209	0	0	0
c_2	0	0.007 6538	–0.679 9678	0
c_3	0	0	0	0
c_4	0.706 8887	0	0	0
c_5	0.707 3125	0	0	0
c_6	0	0.883 8931	–0.338 2843	0
c_7	0	0.467 6264	0.650 5440	0
c_8	0	0	0	1

Among all possible E1, and E1(HFI) transitions between two hyperfine states of nD and 2P, only those with dominant line strengths are shown in Figures 20 to 23. The calculated values of corresponding absolute line strengths are listed in Tables 34 to 37 (a common factor $|\langle \gamma L \| r_1{}^{(1)} + r_2{}^{(1)} \| \gamma' L' \rangle|^2$ in Equation (175) has been calculated and included for each line. A detailed list of common factors is in Appendix D). Our calculations show that hyperfine-induced transition in ^{1,3}D to 2 ^{1,3}P of ^{3}He is due to strong hyperfine mixing of singlet and triplet D states. In addition, the percentage of hyperfine-induced transitions in each group nD to $2P$ increases as the principle quantum number n increases. This is as expected since singlet-triplet mixing becomes stronger for higher Rydberg D states. All E1 and E1(HFI) of n ^{1,3}D to 2 ^{1,3}P (n=3-10) have been calculated and tabulated in Appendix B.

In summary, hyperfine-induced transitions from n ^{1,3}D to 2 ^{1,3}P in ^{3}He is first proposed and calculated by using the double basis set wave function in Hylleraas coordinates in this work. Comparable strengths of this hyperfine-induced transitions to normal E1 transition are theoretically obtained. We predict they will be observable in experiment. However, to our knowledge, no experiment so far for hyperfine-induced transitions n ^{1,3}D to 2 ^{1,3}P in ^{3}He has been published in the literature, except for Bloomfield *et al.* [83], who used Doppler-free ultraviolet-infrared double-resonance laser spectroscopy to observe the hyperfine transitions between 5 ^{3}P and 13 ^{1,3}D states, in which they found two strong components of the intercombination lines: 5 $^3P_1$, F = 3/2 to 13 $^1D_2$, F = 5/2 and 5 $^3P_0$, 1/2 to 13 $^1D_2$, 3/2. We expect that the present calculations will stimulate future experimental investigations.

Figure 20: Electric dipole transition E1 and E1(HFI) between hyperfine states $^1D_2, F = 3/2$ and $2\,^1P_1, F = 1/2$, $2\,^1P_1, F = 3/2$, $2\,^3P_0, F = 1/2$, $2\,^3P_1, F = 1/2$. The level position is not drawn to scale.

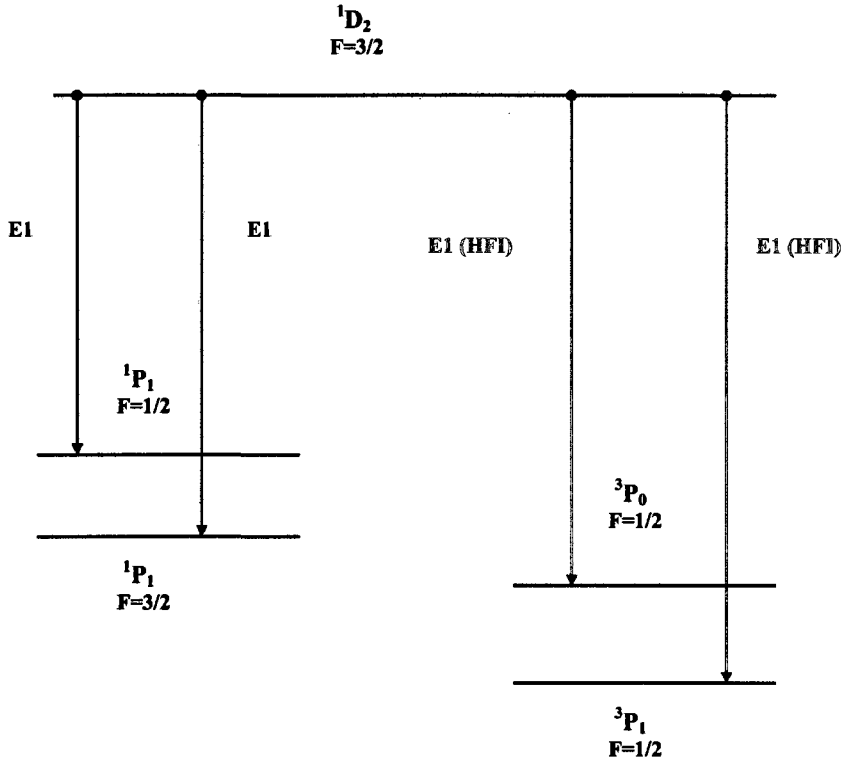

Figure 21: Electric dipole transition E1 and E1(HFI) between hyperfine states $^1D_2, F = 5/2$ and $2\,^1P_1, F = 3/2$, $2\,^3P_1, F = 3/2$. The level position is not drawn to scale.

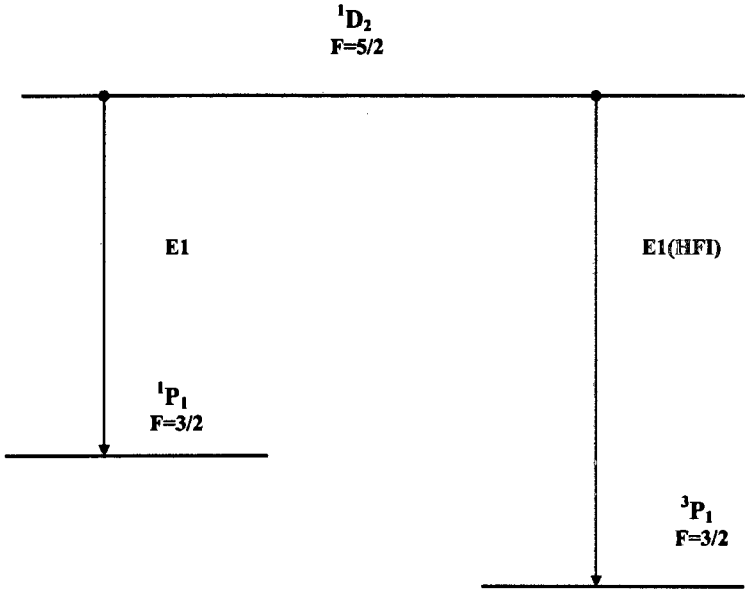

Figure 22: Electric dipole transition E1 and E1(HFI) between hyperfine states $^3D_1, F = 3/2$ and $2\ ^1P_1, F = 1/2$, $2\ ^1P_1, F = 3/2$, $2\ ^3P_{(0,1)}, F = (1/2, 3/2)$. The level position is not drawn to scale.

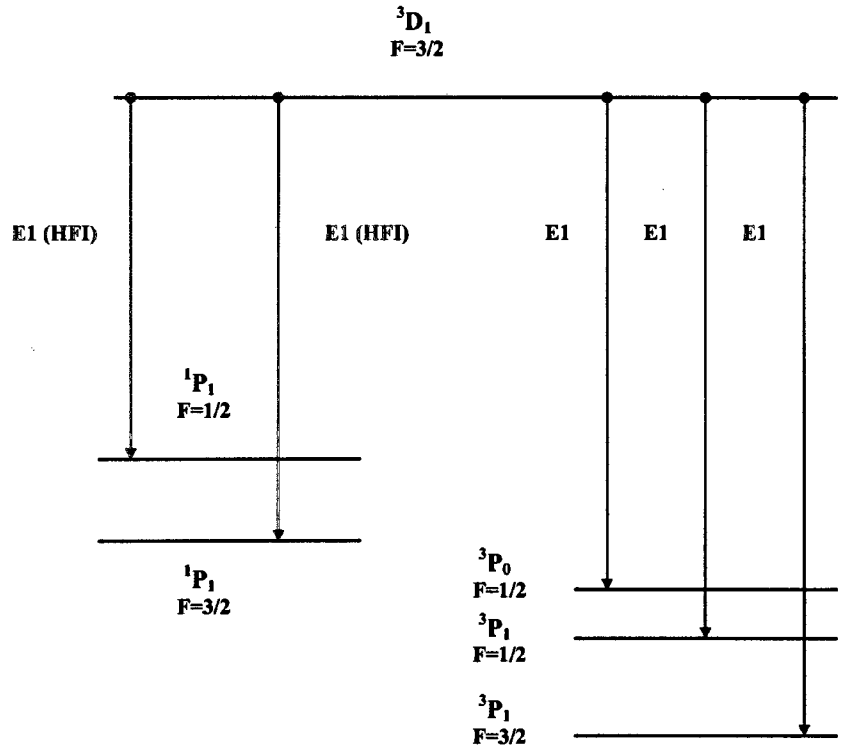

Figure 23: Electric dipole transition E1 and E1(HFI) between hyperfine states $^3D_2, F = 5/2$ and 2 $^1P_1, F = 3/2$, 2 $^3P_{1,2}, F = 3/2$. The level position is not drawn to scale.

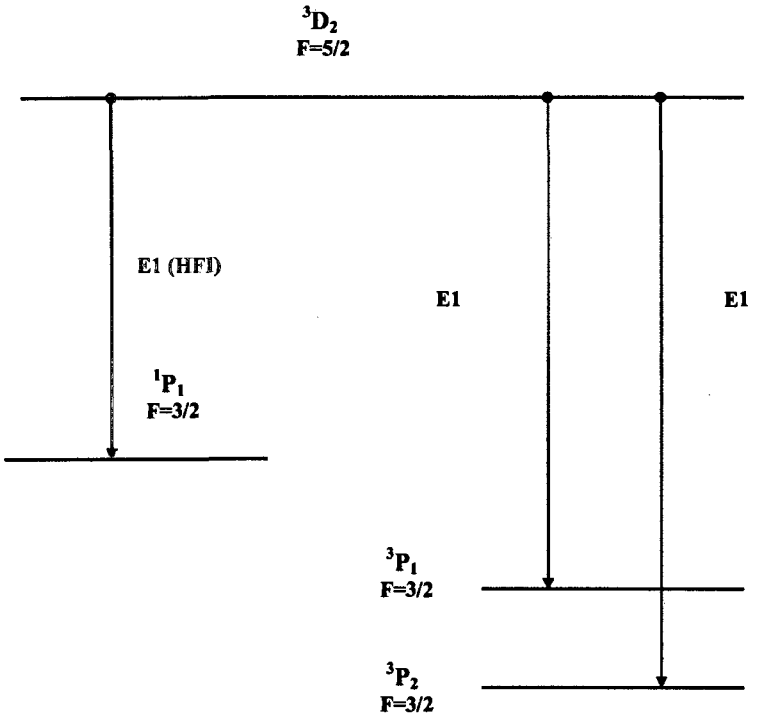

Table 34: Line strength of electric dipole transition E1 and E1(HFI) between hyperfine states $^1D_2, F = 3/2$ and $2\ ^1P_1, F = 1/2$, $2\ ^1P_1, F = 3/2$, $2\ ^3P_0, F = 1/2$, $2\ ^3P_1, F = 1/2$. The percentage of individual transition in each group nD to 2P is also indicated. Units are in a.u.

Initial state (D)	Final state (P)			
$^1D_2\ \frac{3}{2}$	$^1P_1\ \frac{1}{2}$	$^1P_1\ \frac{3}{2}$	$^3P_0\ \frac{1}{2}$ (HFI)	$^3P_1\ \frac{1}{2}$ (HFI)
3D	31.2001(83%)	6.2391(6%)	0.0175	0.0073
9D	0.0828 (56%)	0.0166 (11%)	0.0215(14%)	0.0270(19%)
10D	0.0478 (47%)	0.0096 (9%)	0.0198(19%)	0.0251(25%)

Table 35: Line strength of electric dipole transition E1 and E1(HFI) between hyperfine states $^1D_2, F = 5/2$ and $2\ ^1P_1, F = 3/2$, $2\ ^3P_1, F = 3/2$. The percentage of individual transition in each group nD to 2P is also indicated. Units are in a.u.

Initial state (D)	Final state (P)	
$^1D_2\ \frac{5}{2}$	$^1P_1\ \frac{3}{2}$	$^3P_1\ \frac{3}{2}$ (HFI)
3D	56.0675	0.0931
9D	0.1489 (64%)	0.0852(36%)
10D	0.0865 (52%)	0.0785(48%)

Table 36: Line strength of electric dipole transition E1 and E1(HFI) between hyperfine states $^3D_1, F = 3/2$ and $2\ ^1P_1, F = 1/2$, $2\ ^1P_1, F = 3/2$, $2\ ^3P_{(0,1)}, F = (1/2, 3/2)$. The percentage of individual transition in each group nD to 2P is also indicated. Units are in a.u.

Initial state (D)	Final state (P)				
$^3D_1\ \frac{3}{2}$	$^1P_1\ \frac{1}{2}$ (HFI)	$^1P_1\ \frac{3}{2}$ (HFI)	$^3P_0\ \frac{1}{2}$	$^3P_1\ \frac{1}{2}$	$^3P_1\ \frac{3}{2}$
3D	0.0246	0.0048	11.8586(42%)	11.6284(41%)	4.8136(17%)
9D	0.0451(28%)	0.0050 (6%)	0.0389(24%)	0.0502(31%)	0.0173(11%)
10D	0.0414(37%)	0.0089(7%)	0.0226(21%)	0.0294(26%)	0.0101(9%)

Table 37: Line strength of electric dipole transition E1 and E1(HFI) between hyperfine states $^3D_2, F = 5/2$ and $2\ ^1P_1, F = 3/2$, $2\ ^3P_{1,2}, F = 3/2$. The percentage of individual transition in each group nD to 2P is also indicated. Units are in a.u.

Initial state (D)	Final state (P)		
$^3D_2\ \frac{5}{2}$	$^1P_1\ \frac{3}{2}$ (HFI)	$^3P_1\ \frac{3}{2}$	$^3P_2\ \frac{3}{2}$
3D	0.1166	41.2289(97%)	1.1781(3%)
9D	0.0812(34%)	0.1555 (64%)	0.0047(2%)
10D	0.0744(44%)	0.0910(54%)	0.0028(2%)

6 Results and Conclusions

By using the double basis set wave functions, the hyperfine structure of ^{3}He without and with external magnetic field is investigated with high accuracy. In order to account for more and more precise experiments, still higher order corrections are necessary as shown in Section 3.3, which will be the subject of our future work.

This work has shown that hyperfine suppression of the $2\,^3S_1 - 3\,^3P_J$ radiative transition in ^{3}He can be qualitatively interpreted by an IS coupling model. This model will become more accurate as transitions occur between $2\,^3S_1$ and $n\,^3P_J$ with higher values of the principal quantum number n, because the fine structure interactions decrease in proportion to $1/n^3$, while the hyperfine interactions tend to a constant at the series limit $^3He^+$. In contrast, an exact diagonalization provides a comprehensive interpretation of the results across the complete range of hyperfine coupling strengths of ^{3}He. Our calculation shows that the suppression of the hyperfine transition $2\,^3S_1 - 3\,^3P_J$ is caused mainly by strong hyperfine mixing and accidental cancellation between two hyperfine states with the same F but different J. The investigation is also extended to hyperfine transitions of $2\,^3S_1$ to $n\,^3P_J$, $n = 2$ to 10. Our calculation of the state dependence of the line strength of hyperfine transitions numerically verifies the early prediction in Section 4.5 that the IS coupling model should rapidly become more accurate with increasing principal quantum number n. All of these will lead to a deeper understanding of the suppression of hyperfine transitions in ^{3}He.

In a related study, we have shown that hyperfine-induced transitions occur even for low-Z isotope ^{3}He. This originates from strong hyperfine mixing between singlet states and triplet states. The dominant line strengths due to normal electric dipole transition E1 and hyperfine-induced dipole transition E1 for $2\,^{1,3}P - n\,^{1,3}D$ are calculated. This calculation of hyperfine-induced transitions for low-Z isotope

^{3}He supplements previous studies for high-Z ions.

In astrophysics, ^{3}He is interesting because its spectral lines can be comparable in strength with ^{4}He in certain peculiar stars [13]. In present work, a table of extensively calculated line strengths of the hyperfine transitions for $n = 2$ to 10 and $L = 0$ to 2 is compiled.

Appendix A

The line strengths of electric dipole transitions between the hyperfine states of 2S and nP are the form:

$$S = |\langle 2\ ^{1,3}\mathrm{S}(J,F)||\vec{r}_1 + \vec{r}_2||n\ ^{1,3}\mathrm{P}(J',F')\rangle_{\mathrm{true}}|^2 \tag{176}$$

With the notations $2\ ^{2s+1}\mathrm{S}(J,F)$ and $n\ ^{2s+1}\mathrm{P}(J,F)$, the states are labeled: 1—$2\ ^3\mathrm{S}(0,1/2)$; 2—$2\ ^3\mathrm{S}(1,1/2)$; 3—$2\ ^3\mathrm{S}(1,3/2)$; and 1—$n\ ^1\mathrm{P}(1,\ 1/2)$; 2—$n\ ^1\mathrm{P}(1,\ 3/2)$; 3—$n\ ^3\mathrm{P}(0,\ 1/2)$; 4—$n\ ^3\mathrm{P}(1,\ 1/2)$; 5—$n\ ^3\mathrm{P}(2,\ 3/2)$; 6—$n\ ^3\mathrm{P}(1,\ 3/2)$; 7—$n\ ^3\mathrm{P}(2,\ 5/2)$ for $n = 2-4$, but 1—$n\ ^1\mathrm{P}(1,\ 1/2)$; 2—$n\ ^1\mathrm{P}(1,\ 3/2)$; 3—$n\ ^3\mathrm{P}(1,\ 1/2)$; 4—$n\ ^3\mathrm{P}(0,\ 1/2)$; 5—$n\ ^3\mathrm{P}(2,\ 3/2)$; 6—$n\ ^3\mathrm{P}(1,\ 3/2)$; 7—$n\ ^3\mathrm{P}(2,\ 5/2)$ for $n = 5-10$. In this labeling, adiabatic convention is using. All calculated values of line strength S are tabulated in following tables.

Table 38: Line strength of hyperfine transition of 2S to nP. Numbers in brackets represent powers of 10. Units are a. u.

S	P	2P	3P	4P	5P	6P
1	1	0.6667	0.6667	0.6667	0.6667	0.6667
2	1	0.2267(-7)	0.7905(-9)	0.3457(-7)	0.2857(-6)	0.1111(-5)
3	1	0.1714(-7)	0.1448(-7)	0.1382(-7)	0.1355(-7)	0.1342((-7)
1	2	0.1333(1)	0.1333(1)	0.1333(1)	0.1333(1)	0.1333(1)
2	2	0.3254(-7)	0.1035(-6)	0.3795(-6)	0.1222(-5)	0.3379(-5)
3	2	0.8599(-7)	0.7262(-7)	0.6924(-7)	0.6783(-7)	0.6708(-7)
1	3	0.2149(-11)	0.1576(-8)	0.4411(-7)	0.2192(-8)	0.1588(-8)
2	3	0.2919	0.4806	0.6219	0.1099(-1)	0.3440(-2)
3	3	0.3748	0.1860	0.4475(-1)	0.6557	0.6632
1	4	0.3982(-7)	0.1370(-7)	0.4272(-8)	0.2970(-6)	0.1122(-5)
2	4	0.3748	0.1860	0.4475(-1)	0.6557	0.6632
3	4	0.2919	0.4806	0.6219	0.1099(-1)	0.3440(-2)
1	5	0.6750(-7)	0.6581(-7)	0.6430(-7)	0.6353(-7)	0.6309(-7)
2	5	0.3564(-1)	0.2089(-2)	0.3187(-3)	0.7687(-4)	0.2420(-4)
3	5	0.1298(1)	0.1331(1)	0.1333(1)	0.1333(1)	0.1333(1)
1	6	0.5104(-7)	0.1103(-6)	0.3845(-6)	0.1227(-5)	0.3383(-5)
2	6	0.1298(1)	0.1331(1)	0.1333(1)	0.1333(1)	0.1333(1)
3	6	0.3564(-1)	0.2089(-2)	0.3187(-3)	0.7686(-4)	0.2420(-4)
1	7	0.	0.	0.	0.	0.
2	7	0.	0.	0.	0.	0.
3	7	0.2(1)	0.2(1)	0.2(1)	0.2(1)	0.2(1)

Table 39: Line strength of hyperfine transition of 2S to nP. Numbers in brackets represent powers of 10. Units are a. u.

S	P	7P	8P	9P	10P
1	1	0.6667	0.6667	0.6667	0.6667
2	1	0.3167(-5)	0.7552(-5)	0.1597(-4)	0.3092(-4)
3	1	0.1336(-7)	0.1332(-7)	0.1332(-7)	0.1332(-7)
1	2	0.1333(1)	0.1333(1)	0.1333(1)	0.1333(1)
2	2	0.8202(-5)	0.1792(-4)	0.3597(-4)	0.6741(-4)
3	2	0.6661(-7)	0.6627(-7)	0.6598(-7)	0.6572(-7)
1	3	0.1349(-8)	0.1234(-8)	0.1173(-8)	0.1137(-8)
2	3	0.1304(-2)	0.5685(-3)	0.2748(-3)	0.1439(-3)
3	3	0.6654	0.6661	0.6664)	0.6665
1	4	0.3179(-5)	0.7564(-5)	0.1598(-4)	0.3093(-4)
2	4	0.6654	0.6661	0.6664	0.6665
3	4	0.1304(-2)	0.5685(-3)	0.2748(-3)	0.1439(-3)
1	5	0.6287(-7)	0.6263(-7)	0.6251(-7)	0.6241(-7)
2	5	0.9054(-5)	0.3813(-5)	0.1745(-5)	0.8462(-6)
3	5	0.1333(1)	0.1333(1)	0.1333(1)	0.1333(1)
1	6	0.8206(-5)	0.1792(-4)	0.3597(-4)	0.6741(-4)
2	6	0.1333(1)(1)	0.1333(1)	0.1333(1)	0.1333(1)
3	6	0.9056(-5)	0.3809(-5)	0.1741(-5)	0.8429(-6)
1	7	0.	0.	0.	0.
2	7	0.	0.	0.	0.
3	7	0.2(1)	0.2(1)	0.2(1)	0.2(1)

Appendix B

The line strengths of electric dipole transitions between the hyperfine states of 2P and nD are the form:

$$S = |\langle 2\ ^{1,3}\mathrm{P}(J,F)||\vec{r}_1 + \vec{r}_2||n\ ^{1,3}\mathrm{D}(J',F')\rangle_{\mathrm{true}}|^2 \tag{177}$$

With the notations $2\ ^{2s+1}\mathrm{P}(J,F)$ and $n\ ^{2s+1}\mathrm{D}(J,F)$, the states are labeled: 1—2 ^{1}P(1, 1/2); 2—2 ^{1}P(1, 3/2); 3—2 ^{3}P(0, 1/2); 4—2 ^{3}P(1, 1/2); 5—2 ^{3}P(2, 3/2); 6—2 ^{3}P(1, 3/2); 7—2 ^{3}P(2, 5/2); and 1—n ^{1}D(2, 3/2); 2—n ^{1}D(2, 5/2); 3—n ^{3}D(1, 1/2); 4—n ^{3}D(1, 3/2); 5—n ^{3}D(2, 3/2); 6—n ^{3}P(3, 5/2); 7—n ^{3}D(2, 5/2); 8—n ^{3}D(3, 7/2) for $n = 3 - 10$. In this labeling, adiabatic convention is using. All calculated values of line strength S are tabulated in following tables.

Table 40: Line strength of hyperfine transition of 2P to nD. Numbers in brackets represent powers of 10. Units are a. u.

P	D	3D	4D	5D	6D
1	1	0.6661	0.6642	0.6576	0.6387
1	2	0.	0.	0.	0.
1	3	0.8572(-8)	0.8572(-8)	0.8572(-8)	
1	4	0.5243(-3)	0.2419(-2)	0.9030(-2)	0.2799(-1)
1	5	0.4596(-4)	0.2082(-4)	0.1540(-4)	0.1328(-4)
1	6	0.	0.	0.	0.
1	7	0.	0.	0.	0.
1	8	0.	0.	0.	0.
2	1	0.1332	0.1329	0.1315	0.1278
2	2	0.1197(1)	0.1193(1)	0.1180(1)	0.1144(1)
2	3	0.4300(-8)	0.4300(-8)	0.4300(-8)	0.4300(-8)
2	4	0.1021(-3)	0.4782(-3)	0.1795(-2)	0.5588(-2)
2	5	0.8525(-5)	0.3690(-5)	0.2666(-5)	0.2269(-5)
2	6	0.2161(-3)	0.1135(-3)	0.8880(-4)	0.7854(-4)
2	7	0.2492(-2)	0.6472(-2)	0.1967(-1)	0.5547(-1)
2	8	0.	0.	0.	0.
3	1	0.3739(-3)	0.1281(-2)	0.4328(-2)	0.1286(-1)
3	2	0.	0.	0.	0.
3	3	0.1847	01847	0.1847	0.1847
3	4	0.3348	0.3087	0.2963	0.2837

Table 41: Line strength of hyperfine transition of 2P to nD. Numbers in brackets represent powers of 10. Units are a. u.

P	D	3D	4D	5D	6D
3	5	0.1441	0.1693	0.1786	0.1828
3	6	0.	0.	0.	0.
3	7	0.	0.	0.	0.
3	8	0.	0.	0.	0.
4	1	0.1557(-3)	0.1138(-2)	0.4701(-2)	0.1513(-1)
4	2	0.	0.	0.	0.
4	3	0.1459	0.1459	0.1459	0.1459
4	4	0.3283	0.3550	0.3612	0.3550
4	5	0.1922	0.1645	0.1548	0.1506
4	6	0.	0.	0.	0.
4	7	0.	0.	0.	0.
4	8	0.	0.	0.	0.
5	1	0.2941(-4)	0.2338(-5)	0.6010(-5)	0.6572(-4)
5	2	0.1395(-4)	0.2215(-4)	0.2483(-3)	0.1040(-2)
5	3	0.6488(-1)	0.6488(-1)	0.6488(-1)	0.6488(-1)
5	4	0.2606(-5)	0.1200(-2)	0.2265(-2)	0.2786(-2)
5	5	0.4188	0.4176	0.4166	0.4160
5	6	0.8163	0.8163	0.8162	0.8162
5	7	0.3326(-1)	0.3327(-1)	0.3316(-1)	0.3243(-1)
5	8	0.	0.	0.	0.

Table 42: Line strength of hyperfine transition of 2P to nD. Numbers in brackets represent powers of 10. Units are a. u.

P	D	3D	4D	5D	6D
6	1	0.1169(-3)	0.4985(-3)	0.1807(-2)	0.5529(-2)
6	2	0.2628(-2)	0.630(-2)	0.1949(-1)	0.5449(-1)
6	3	0.1782(-2)	0.1782(-2)	0.1782(-2)	0.1782(-2)
6	4	0.1356	0.1321	0.1294	0.1250
6	5	0.5198(-2)	0.8582(-2)	0.9997(-2)	0.1065(-1)
6	6	0.2351(-1)	0.2360(-1)	0.2373(-1)	0.2380(-1)
6	7	0.1164(1)	0.1160(1)	0.1147((1)	0.1112(1)
6	8	0.	0.	0.	0.
7	1	0.4874(-5)	0.2858(-5)	0.2003(-5)	0.1693(-5)
7	2	0.6531(-4)	0.3553(-4)	0.2446(-4)	0.1881(-4)
7	3	0.	0.	0.	0.
7	4	0.3586(-3)	0.5973(-4)	0.1315(-4)	0.3058(-5)
7	5	0.3964(-1)	0.3994(-1)	0.3998(-1)	0.4000(-1)
7	6	0.3599	0.3600	0.3600	0.3600
7	7	0.5344(-5)	0.6455(-5)	0.9001(-5)	0.1204(-4)
7	8	0.1600(1)	0.1600(1)	0.1600(1)	0.1600(1)

Table 43: Line strength of hyperfine transition of 2P to nD. Numbers in brackets represent powers of 10. Units are a. u.

P	D	7D	8D	9D	10D
1	1	0.5946	0.5193	0.4317	0.3577
1	2	0.	0.	0.	0.
1	3	0.8572(-8)	0.8572(-8)	0.8572(-8)	
1	4	0.7208(-1)	0.1474	0.2349	0.3089
1	5	0.1221(-4)	0.1159(-4)	0.1119(-4)	0.1093(-4)
1	6	0.	0.	0.	0.
1	7	0.	0.	0.	0.
1	8	0.	0.	0.	0.
2	1	0.1189	0.1039	0.8639	0.7159
2	2	0.1064(1)	0.9307	0.7764	0.6453
2	3	0.4300(-8)	0.4300(-8)	0.4300(-8)	0.4300(-8)
2	4	0.1439(-1)	0.2944(-1)	0.4694(-1)	0.6174(-1)
2	5	0.2070(-5)	0.1955(-5)	0.1882(-5)	0.1833(-5)
2	6	0.7317(-4)	0.6996(-4)	0.6787(-4)	0.6644(-4)
2	7	0.1356	0.2692	0.4236	0.5546
2	8	0.	0.	0.	0.
3	1	0.3244(-1)	0.6561(-1)	0.1040	0.1362
3	2	0.	0.	0.	0.
3	3	0.1847	01847	0.1847	0.1847
3	4	0.2620	0.2276	0.1885	0.1558

Table 44: Line strength of hyperfine transition of 2P to nD. Numbers in brackets represent powers of 10. Units are a. u.

P	D	7D	8D	9D	10D
3	5	0.1849	0.1861	0.1868	0.1872
3	6	0.	0.	0.	0.
3	7	0.	0.	0.	0.
3	8	0.	0.	0.	0.
4	1	0.3965(-1)	0.8177(-1)	0.1310	0.1727
4	2	0.	0.	0.	0.
4	3	0.1459	0.1459	0.1459	0.1459
4	4	0.3326	0.2917	0.2432	0.2020
4	5	0.1485	0.1473	0.1465	0.1461
4	6	0.	0.	0.	0.
4	7	0.	0.	0.	0.
4	8	0.	0.	0.	0.
5	1	0.2524(-3)	0.6172(-3)	0.1077(-2)	0.1489(-2)
5	2	0.3014(-2)	0.6502(-2)	0.1067(-1)	0.1428(-1)
5	3	0.6488(-1)	0.6488(-1)	0.6488(-1)	0.6488(-1)
5	4	0.2919(-2)	0.2741(-2)	0.2396(-2)	0.2058(-2)
5	5	0.4157	0.4155	0.4154	0.4153
5	6	0.8161	0.8161	0.8161	0.8161
5	7	0.3048(-1)	0.2700(-1)	0.2284(-1)	0.1923(-1)
5	8	0.	0.	0.	0.

Table 45: Line strength of hyperfine transition of 2P to nD. Numbers in brackets represent powers of 10. Units are a. u.

P	D	7D	8D	9D	10D
6	1	0.1415(-1)	0.2883(-1)	0.4587(-1)	0.6025(-1)
6	2	0.1326	0.2628	0.4129	0.5404
6	3	0.1782(-2)	0.1782(-2)	0.1782(-2)	0.1782(-2)
6	4	0.1160	0.1012	0.8399(-1)	0.6954(-1)
6	5	0.1100(-1)	0.1119(-1)	0.1131(-1)	0.1138(-1)
6	6	0.2383(-1)	0.2384(-1)	0.2385(-1)	0.2385(-1)
6	7	0.1034(1)	0.9038	0.7536	0.6261
6	8	0.	0.	0.	0.
7	1	0.1396(-5)	0.1041(-5)	0.6880(-6)	0.4234(-6)
7	2	0.1360(-4)	0.8669(-5)	0.4909(-5)	0.264(-5)
7	3	0.	0.	0.	0.
7	4	0.5212(-6)	0.8683(-8)	0.8665(-7)	0.2731(-6)
7	5	0.4000(-1)	0.4000(-1)	0.4000(-1)	0.4000(-1)
7	6	0.3600	0.3600	0.3600	0.3600
7	7	0.1587(-4)	0.1995(-4)	0.2313(-4)	0.2498(-4)
7	8	0.1600(1)	0.1600(1)	0.1600(1)	0.1600(1)

Appendix C

The general integral needed for this work is derived by Drake [30]

$$I = \int\int d\vec{r_1} d\vec{r_2} R_{p'}(\alpha', \beta') Y^{M'}_{l_1' l_2' L'}(\hat{r}_1, \hat{r}_2) T^{Q}_{k_1 k_2 K} Y^{M}_{l_1 l_2 L}(\hat{r}_1, \hat{r}_2) R_p(\alpha, \beta) \tag{178}$$

where

$$R_p(\alpha, \beta) = r_1^i r_2^j r_{12}^k e^{-\alpha r_1 - \beta r_2} \tag{179}$$

$p = \{i\, j\, k\}$ represents a distinct combination of powers, and

$$T^{Q}_{k_1 k_2 K}(\hat{r}_1, \hat{r}_2) = \sum_{q_1, q_2} \langle k_1 k_2 q_1 q_2 | K Q \rangle Y^{q_1}_{k_1}(\hat{r}_1) Y^{q_2}_{k_2}(\hat{r}_2) \tag{180}$$

stands for tensor product.

In terms of $3-j$, $6-j$, and $9-j$ symbols, the general integral can be expressed as

$$I = (-)^{L'-M'} \begin{pmatrix} L' & K & L \\ -M' & Q & M \end{pmatrix} \sum_{\lambda_1, \lambda_2, \Lambda} X_{\lambda_1, \lambda_2, \Lambda} D_{\lambda_1, \lambda_2, \Lambda} I_\Lambda(R_{p'} R_P) \tag{181}$$

where notation $(a, b, ...) = (2a+1)(2b+1)...$ is used,

$$X_{\lambda_1, \lambda_2, \Lambda} = \frac{(-)^{l_1' + l_2' + L' + \Lambda}}{8\pi} (\lambda_1, \lambda_2, \Lambda)(l_1, k_1, l_1', l_2, k_2, l_2', L, L', K)^{1/2} \tag{182}$$

$$\begin{pmatrix} l_1 & k_1 & \lambda_1 \\ 0 & 0 & 0 \end{pmatrix} \begin{pmatrix} l_1' & \lambda_1 & \Lambda \\ 0 & 0 & 0 \end{pmatrix} \begin{pmatrix} l_2 & k_2 & \lambda_2 \\ 0 & 0 & 0 \end{pmatrix} \begin{pmatrix} l_2' & \lambda_2 & \Lambda \\ 0 & 0 & 0 \end{pmatrix}$$

$$D_{\lambda_1,\lambda_2,\Lambda} = \left\{ \begin{array}{ccc} L' & l_2' & l_1' \\ \Lambda & \lambda_1 & \lambda_2 \end{array} \right\} \left\{ \begin{array}{ccc} l_1 & l_2 & \mathrm{L} \\ k_1 & k_2 & K \\ \Lambda_1 & \lambda_2 & \mathrm{L}' \end{array} \right\} \tag{183}$$

and

$$I_\Lambda(R_{p'}R_P) = \int_0^\infty r_1 dr_1 \int_0^\infty r_2 dr_2 \int_{|r_1-r_2|}^{r_1+r_2} r_{12} dr_{12} R_{p'} R_p P_\Lambda(\cos\theta_{12}) \tag{184}$$

where $P_\Lambda(\cos\theta_{12})$ is an ordinary Legendre polynonmial, and $\cos\theta_{12}$ is a purely radial function defined by

$$\cos\theta_{12} = \frac{r_1^2 + r_2^2 - r_{12}^2}{2r_1 r_2} \tag{185}$$

The general integral can be further expressed in more compact form

$$I = \sum_\Lambda C_\Lambda I_\Lambda(R_{p'}R_P) \tag{186}$$

where the angular coefficients are

$$C_\Lambda = \sum_{\lambda_1,\lambda_2} (-)^{L'-M'} \begin{pmatrix} L' & K & L \\ -M' & Q & M \end{pmatrix} X_{\lambda_1,\lambda_2,\Lambda} D_{\lambda_1,\lambda_2,\Lambda} \tag{187}$$

and the radial integral in Equation (184) for higher values of Λ can be computed in terms of integral recurrence relations by Drake [30]

$$\begin{aligned} I_{\Lambda+1}(r_1^a, r_2^b, r_{12}^c) &= \frac{2\Lambda+1}{c+2} I_\Lambda(r_1^{a-1}, r_2^{b-1}, r_{12}^{c+2}) + I_{\Lambda-1}(r_1^a, r_2^b, r_{12}^c), \\ & \quad c \neq -2 \end{aligned} \tag{188}$$

$$I_{\Lambda+1}(r_1^a, r_2^b, r_{12}^{-2}) = (2\Lambda+1)c + 2I_\Lambda(r_1^{a-1}, r_2^{b-1}, \ln r) + \mathrm{I}_{\Lambda-1}(\mathrm{r}_1^{\mathrm{a}}, \mathrm{r}_2^{\mathrm{b}}, \mathrm{r}_{12}^{-2}),$$
$$c = -2 \tag{189}$$

The recurrence relation involving logarithmic integrals is

$$I_{\Lambda+1}(r_1^a, r_2^b, r_{12}^c \ln \mathrm{r}) = \frac{2\Lambda+1}{\mathrm{c}+2}\left[\mathrm{I}_\Lambda(\mathrm{r}_1^{\mathrm{a}-1}, \mathrm{r}_2^{\mathrm{b}-1}, \mathrm{r}_{12}^{\mathrm{c}+2} \ln \mathrm{r})\right] -$$
$$\frac{2\Lambda+1}{c+2}\left[\frac{1}{c+2} I_\Lambda(r_1^{a-1}, r_2^{b-1}, r_{12}^{c+2})\right] + I_{\Lambda-1}(r_1^a, r_2^b, r_{12}^c \ln \mathrm{r}),$$
$$c \neq -2 \tag{190}$$

The first and second integrals are

$$I_0(R_{p'} R_P) = \int_0^\infty r_1 dr_1 \int_0^\infty r_2 dr_2 \int_{|r_1 - r_2|}^{r_1 + r_2} r_{12} dr_{12} R_{p'} R_p \tag{191}$$

$$I_1(a,b,c) = \frac{1}{2}[I_0(a+1, b-1, c) + I_0(a-1, b+1, c)] -$$
$$\frac{1}{2} I_0(a-1, b-1, c+2) \tag{192}$$

Thus, the calculation of the integral $I_\Lambda(a,b,c)$ is reduced to evaluating $I_0(a,b,c)$ for a sufficient range of a, b, and c.

Appendix D

For the multipole transition integrals, the matrix element of $Y_k^q(\hat{r}_1) = \sqrt{4\pi}T^q_{k,0,k}(\hat{r}_1, \hat{r}_2)$ is involved (in this work, $k = 1$ is for dipole transition). The angular coefficients is defined by

$$C_\Lambda = \frac{(-)^{L'-M'}}{2(4\pi)^{1/2}} \begin{pmatrix} L' & k & L \\ -M' & q & M \end{pmatrix} (-)^{l_2'+L'+L+k}(l_1, l_1', l_2, l_2', L, L')^{1/2} \sum_\lambda (\lambda, \Lambda, k) \begin{pmatrix} l_1 & k & \lambda \\ 0 & 0 & 0 \end{pmatrix} \begin{pmatrix} l_1' & \lambda & \Lambda \\ 0 & 0 & 0 \end{pmatrix} \begin{pmatrix} l_2' & l_2 & \Lambda \\ 0 & 0 & 0 \end{pmatrix} \begin{Bmatrix} L' & \lambda & l_2 \\ \Lambda & l_2' & l_1' \end{Bmatrix} \begin{Bmatrix} L' & \lambda & l_2 \\ l_1 & L & k \end{Bmatrix} \tag{193}$$

Thus, by use of the general integral in Appendix C, the common factors of a given transition $|\langle 2\ ^{1,3}\mathrm{S}\|{r_1}^{(1)} + {r_2}^{(1)}\|n\ ^{1,3}\mathrm{P}\rangle|^2$ for $n = 2$ to 10 and $|\langle 2\ ^{1,3}\mathrm{P}\|{r_1}^{(1)} + {r_2}^{(1)}\|n\ ^{1,3}\mathrm{D}\rangle|^2$ for $n = 3$ to 10 are calculated. Final results are listed in following tables.

Table 46: Common factor $|\langle 2\ ^1\mathrm{S}\|r_1^{(1)}+r_2^{(1)}\|n\ ^1\mathrm{P}\rangle|^2$ and $|\langle 2\ ^1\mathrm{P}\|r_1^{(1)}+r_2^{(1)}\|n\ ^1\mathrm{D}\rangle|^2$ for a certain transition. Numbers in brackets represent powers of 10. Units are a. u.

	2P	3P	4P	5P	6P
2S	0.2552(2)	0.2499(1)	0.6417	0.2658	0.1377

	7P	8P	9P	10P
2S	0.8129(-1)	0.5224(-1)	0.3567(-1)	0.2549(-1)

	3D	4D	5D	6D	7D
2P	0.4684(2)	0.5847(1)	0.1874(1)	0.8574	0.4711

	8D	9D	10D
2P	0.2895	0.1918	0.1342

Table 47: Common factor $|\langle 2\ ^3\mathrm{S}\|r_1^{(1)}+r_2^{(1)}\|n\ ^3\mathrm{P}\rangle|^2$ and $|\langle 2\ ^3\mathrm{P}\|r_1^{(1)}+r_2^{(1)}\|n\ ^3\mathrm{D}\rangle|^2$ for a certain transition. Numbers in brackets represent powers of 10. Units are a. u.

	2P	3P	4P	5P	6P
2S	0.1922(2)	0.8253	0.2704	0.1211	0.6504(-1)

	7P	8P	9P	10P	
2S	0.3912(-1)	0.2543(-1)	0.1749(-1)	0.1255(-1)	

	3D	4D	5D	6D	7D
2P	0.3541(2)	0.5426(1)	0.1869(1)	0.8855	0.4964

	8D	9D	10D
2P	0.3089	0.2064	0.1452

References

[1] J. D. Prestage, E. A. Hinds, and F. M. J. Pichanick, Phys. Rev. Lett. **50**, 828 (1983)

[2] E. A. Hinds, J. D. Prestage, and F. M. J. Pichanick Phys. Rev. A **33**, 68 (1986)

[3] F. Marin, F. Minardi, F. S. Pavone, M. Inguscio, and G. W. F. Drake Z. Phys. D **32**, 285 (1995)

[4] P. C. Pastor *et al.*, Frequency measurements of ^{3}He 2 ^{3}P hyperfine structure. PSAS, Windsor, Ontario, Canada, 2008

[5] I. A. Sulai, Qixue Wu, M. Bishof, G. W. F. Drake, Z.-T. Lu, P. Mueller, R. Santra, Phys. Rev. Lett. **101**, 173001 (2008)

[6] G. W. F. Drake and D. C. Morton, Ap. J. Sup. Ser. **170**, 251 (2007)

[7] G. W. F. Drake, M. M. Cassar, and R. A. Nistor, Phys. Rev. A **65**, 054501 (2002)

[8] G. W. F. Drake, Nucl. Phys. A **790**, 151c (2007)

[9] G. W. F. Drake, Nucl. Phys. A **737**, 25 (2004)

[10] P. C. Pastor *et al.*, in *Laser Spectroscopy* edited by E. A. Hinds, A. Ferguson and E. Riis (World Scientific, 2005)

[11] L. B. Wang *et al.*, Phys. Rev. Lett. **93**, 142501 (2004)

[12] P. Mueller *et al.*, Phys. Rev. Lett. **99**, 252501 (2007)

[13] M. R. Hartoog and A. P. Cowley, Astrophys J. **228**, 229 (1979)

[14] D. C. Morton, Qixue Wu, and G. W. F. Drake, Can. J. Phys **84**, 83 (2006)

[15] G. W. F. Drake and D.C. Morton, Astrophys. J. Supp. Seri **170**, 251 (2007)

[16] E. A. Hylleraas and B. Undheim, Z. Phys. **65**, 759 (1930)

[17] J. K. L. MacDonald, Phys. Rev. **63**, 830 (1933)

[18] E. A. Hylleraas, Z. Phys. **48**, 469 (1928); **54**, 347 (1929)

[19] Y. Accad, C. L. Pekeris, and B. Schief, Phys. Rev. A **4**, 516 (1971)

[20] G. W. F. Drake *Long-Range Casimir Forces: Theory and Recent Experiments in Atomic Systems.* ed. by F. S. Levin and D. A. Micha (New York: Plenum, 1993)

[21] G. W. F. Drake in *Atomic, Molecular, and Optical Physics Handbook.* edited by G.W.F. Drake (Springer, New York, 2006)

[22] H. A. Bethe and E. E. Salpeter *Quantum Mechanics of One- and Two-Electron Atoms* (Berlin: Spring-Verlag, 1957)

[23] G. W. F. Drake, Adv. At. Mol. Opt. Phys. **32**, 93 (1994)

[24] A. P. Stron, Proc. Phys. Soc. London **77**, 786 (1961); **81**, 868 (1963)

[25] P. K. Kabir and E. E. Salpeter, Phys. Rev. **108**, 1256 (1957)

[26] H. Araki, Prog. Theo. Phys. **17**, 619 (1957); J. Sucher, Phys. Rev. **109**, 1010 (1958)

[27] D. C. Morton, Qixue Wu, and G. W. F. Drake, Phys. Rev. A **73**, 034502, (2006)

[28] L. B. Wang *et al.*, Phys. Rev. Lett. **93**, 142501 (2004)

[29] P. Mueller *et al.*, Phys. Rev. Lett. **99**, 252501 (2007)

[30] G. W. F. Drake, Phys. Rev. **A18**, 820 (1978)

[31] D. H. Yang, P. McNicholl, and H. Metcalf, Phys. Rev. A **33**, 1725 (1986)

[32] D. H. Yang and H. Metcalf, Phys. Rev. A **32**, 2249 (1985)

[33] F. D. Colegrove, P. A. Franken, R. R. Lewis, and R. H. Sands, Phys. Rev. Lett. **3**, 420 (1959)

[34] A. C. Tam, Phys. Rev. A**12**, 539 (1975)

[35] M. L. Derouard and R. Jost, J. Physique **41**, 819 (1980)

[36] R. Panock, R. R. Freeman, B. R. Zegarski, and T. A. Miller, Phys. Rev. A **25**, 869 (1982)

[37] K. R. German, Ph. D. thesis, University of Michigan, 1967 (Cited by Hinds in [2]).

[38] J. D. Prestage, C. E. Johnson, E. A. Hinds, and F. M. J. Pichanick, Phys. Rev. A **32**, 2712 (1985)

[39] E. A. Hinds, J. D. Prestage, and F. M. J. Pichanick, Phys. Rev. A **32**, 2615 (1985)

[40] L. Hambro, Phys. Rev. **175**, 31 (1965)

[41] E. Courtade, F. Marion, P. J. Nacher, G. Tastevin, K. Kiersnowski, and T. Dohnalik, Eur. Phys. J. D **21**, 25 (2002)

[42] K. Hijikata and K. Ohtsuki, J. Phys. Soc. Jpn. **57**, 4141 (1988)

[43] W. R. Johnson, K T. Cheng and D. R. Plante, Phys. Rev. A **55**, 2728 (1997)

[44] T. Zelevinsky, D. Farkas and G. Gabrielse, Phys. Rev. Lett. **95**, 203001 (2005)

[45] L. B. Wang *et al.*, Phys. Rev. Lett. **93**, 142501 (2004)

[46] G. Ewald *et al.*, Phys. Rev. Lett. **93**, 113002 (2004)

[47] G. Ewald *et al.*, Phys. Rev. Lett. **94**, 039901 (2005)

[48] E. Riis, A. G. Sinclair, O. Poulsen, G. W. F. Drake, W. R. C. Rowley and A. P. Levick, Phys. Rev. A **49**, 207 (1994)

[49] Z. C. Yan and G. W. F. Drake, Phys. Rev. A **50**, R1980 (1994)

[50] R. A. Hegstrom, Phys. Rev. A**7**, 451 (1973)

[51] Z. C. Yan, Phys. Rev. A**66**, 022502 (2002)

[52] W. Perl and V. W. Hughes, Phys. Rev. **91**, 842 (1953)

[53] S. A. Lewis, F. M. J. Pichanick, and V. W. Hughes, Phys. Rev. A **2**, 86 (1970)

[54] M. L. Lewis and V. W. Hughes, Phys. Rev. A **8**, 2845 (1973)

[55] R. A. Hegstrom, Phys. Rev. A **7**, 451 (1973)

[56] T. Kinoshita and D. R. Yennie, *Quantum Electrodynamics.* ed. by T. Kinoshita (Singapore: World Scientific, 1990)

[57] C. L'Huillier, J. P. Faroux, and N. Billy, J. Phys. (Paris) **37**, 335 (1976)

[58] K. Pachucki, J. Phys. B: At. Mol. Opt. Phys. **34**, 3357 (2001)

[59] P. Mueller *et al.* Phys. Rev. Lett. **94**, 133001 (2005).

[60] E. Riis, A. G. Sinclair, O. Poulsen, G. W. F. Drake, W. R. C. Rowley, and A. P. Levick, Phys. Rev. A **49**, 207 (1994).

[61] I. A. Sulai, Private Communication.

[62] Qixue Wu, M. Sc. Thesis, University of Windsor, 2004

[63] C. F. Fischer, T. Brage, P. Jonsson, *Computational Atomic Structure* (IOP, 1997)

[64] R. Garstang, in *Atomic and Molecular Processes*, edited by D. Bates (Academic, New York, 1962), pp 1-46

[65] L. Rayleigh, Proc. Roy. Soc. A**117**, 294 (1927)

[66] M. Fukuda, Sci. Pap. Inst. Phys. Chem. Res. (Tokyo) **4**, 171 (1926)

[67] L. D. Huff and W. V. Houston, Phys. Rev. **36**, 842 (1930)

[68] S. Mrozowski, Z. Phys **108**, 204 (1937)

[69] R. H. Garstang, J. Opt. Soc. Am. **52**, 845 (1962)

[70] R. Marrus and P. J. Mohr, Adv. At. Mol. Phys. **14**, 181 (1978)

[71] P. J. Mohr, in *Beam Foil Spectroscopy*, edited by I. Sellin Pegg, Vol. I, pp 97-103 (1976)

[72] H. Gould *et al.*, Phys. Rev. Letts. **33**, 676 (1974)

[73] R. W. Dunford *et al.*, Phys. Rev. A **44**, 764 (1991)

[74] R. Marrus *et al.*, **63**, 502 (1989)

[75] B. B. Bruce *et al.*, Phys. Rev. A **47**, R2454 (1993)

[76] J. Mowat *et al.*, Phys. Rev. A **11**, 2198 (1975)

[77] L. Engstrom *et al.*, J. Phys. B **13**, L143 (1980); Phys. Scr. **22**, 570 (1981)

[78] B. Denne *et al.*, Phys. Scr. **22**, 45 (1980)

[79] A. Livingston and S. Hinterlong, Nucl. Inst. Meth. **202**, 307 (1982)

[80] P. Indelicato *et al.*, Phys. Rev. A **40**, 3505 (1989)

[81] A. Aboussaid *et al.*, Phys. Rev. A **51**, 2031 (1995)

[82] W. R. Johnson *et al.*, Phys. Rev. A **55**, 2728 (1997)

[83] L. A. Bloomfield *et al.*, Phys. Rev. A **27**, 850 (1983)

Vita Auctoris

Qixue Wu graduated from Yunxiao High school in 1982. He obtained a B. Sc. Degree and a Master's Degree in Physics from the Fujian Normal University, China in 1986 and in 1989 respectively. He also received his Master's Degree in Physics from the University of Windsor in 2004. Wu entered the Ph.D. program in Physics at University of Windsor in October 2004 and expects to graduate in the spring of 2009.

Publications

[1] Sulai, I. A., **Wu, Qixue**, Bishof, M., Drake, G. W. F., Lu, Z.-T., Mueller, P., and Santra, R.(2008) Hyperfine suppression of $2\ ^3S_1 - 3\ ^3P_J$ transitions in ^{3}He. Physical Review Letters **101**, 173001.

[2] **Wu, Qixue**, Drake, G. W. F. (2007) Hyperfine structure in $2\ ^3P$ state of helium- 3 with and without external magnetic field. Journal of Physics B: Atomic, Molecular and Optical Physics **40**, 393-402.

[3] Morton, D. C., **Wu, Qixue**, and Drake, G. W. F. (2006) Nuclear charge radius for helium-3. Physical Review A **73**, 034502.

[4] **Wu, Qixue** (2006) Precision calculation of electronic g_J factors for $n\ ^3S_1$ states of helium and lithium ion. Journal of Physics B: Atomic, Molecular and Optical Physics **39**, 4213-4219.

[5] Morton, D. C., **Wu, Qixue**, and Drake, G. W. F. (2006) Energy levels for the stable isotopes of atomic helium (helium-4 and helium-3). Canadian Journal of Physics **84**, 83-105.